Nature Communications

https://doi.org/10.1038/s41467-026-71568-9

Article in Press

Convergent and selective representations of pain, appetitive processes, aversive processes, and cognitive control in the insula

Received: 17 February 2025

Accepted: 23 March 2026

Cite this article as: Kwon, M., Bo, K., Botvinik-Nezer, R. *et al.* Convergent and selective representations of pain, appetitive processes, aversive processes, and cognitive control in the insula. *Nat Commun* (2026). https://doi.org/10.1038/s41467-026-71568-9

Mijin Kwon, Ke Bo, Rotem Botvinik-Nezer, Philip A. Kragel, Lukas Van Oudenhove, Tor D. Wager & The Affective Neuroimaging Consortium

Convergent and selective representations of pain, appetitive processes, aversive processes, and cognitive control in the insula

Mijin Kwon[1*], Ke Bo[1], Rotem Botvinik-Nezer[1,2], Philip A. Kragel[3,4], Lukas Van Oudenhove[5], Tor D. Wager[1*], The Affective Neuroimaging Consortium[6]

[1] Department of Psychological and Brain Sciences, Dartmouth College, Hanover, NH, United States

[2] Department of Psychology, The Hebrew University of Jerusalem, Jerusalem, Israel

[3] Department of Psychology, Emory University, Atlanta, GA, United States

[4] Department of Psychiatry and Behavioral Sciences, Emory University, Atlanta, GA, United States

[5] Laboratory for Brain-Gut Axis Studies (LaBGAS), Translational Research in Gastrointestinal Disorders (TARGID), Department of Chronic Diseases and Metabolism (CHROMETA), University of Leuven, Leuven, Belgium

[6] A list of authors and their affiliations appears at the end of the paper.

* Corresponding authors

Correspondence to:

Tor D. Wager
Diana L. Taylor Distinguished Professor
Presidential Cluster in Neuroscience and
Department of Psychological and Brain Sciences
Dartmouth College
Email: tor.d.wager@dartmouth.edu

Mijin Kwon
Department of Psychological and Brain Sciences
Dartmouth College
Email: mijin.kwon.gr@dartmouth.edu

Abstract

Regions that respond to multiple types of information (“convergence zones”) are crucial for the brain to generate coherent experiences and behaviors. The insula, known for its functional diversity, has been hypothesized as a key convergence hub, yet empirical evidence remains incomplete. To address this gap, we analyzed functional convergence across four domains—pain, appetitive processes, aversive processes, and cognitive control—in a Bayesian mega-analysis of fMRI data (*n=540*, 36 study contrasts). Bayes Factor analyses identified both multi-domain convergent and single-domain selective zones, validated with independent datasets (*n=608*). Results revealed a hierarchical architecture, with a multi-domain convergence zone in bilateral dorsal anterior insula surrounded by progressively converging zones. Functional decoding and coactivation analyses further support the insula’s role as a convergence hub, while cytoarchitectonic and neurotransmitter profiling characterize the potential neuroanatomical basis of these zones. Here, we demonstrate a structured functional topography in the insula that bridges specialized and convergent processing, providing a potential neural basis for how diverse information streams combine into unified experiences.

Introduction

The human brain possesses an extraordinary ability to integrate a wide array of information from the body and environment into a seamless, unified subjective experience. The insula is central to this capacity, operating as a convergence zone—a region where diverse information streams are integrated—for a remarkably diverse range of interoceptive and exteroceptive processes, including visceral, autonomic, and homeostatic signals[1,2], along with information from somatosensory, olfactory, gustatory, and auditory sensory inputs[3–7].

Most empirical research has focused on identifying subregions specific to particular aspects of sensation, emotion, and cognition, documented by human neuroimaging[1–4,8–23], pathways in non-human animals[24–27], and human brain stimulation and electrophysiology[28–33]. In contrast, the concept of functional convergence zones in the insula has been largely theoretical[34,35].

Convergence zones are thought to exist at multiple levels throughout the brain, from modality-specific integration to higher-order multi-modal convergence[36,37]. Of particular interest are zones that integrate external sensory information with internal states, as this integration is thought to be fundamental for constructing the sense of self[34,38]. An influential theory by Bud Craig[38,39] posited that the anterior insula (AIns) constitutes a convergence zone contributing to subjective, conscious experience. This aligns with concepts of embodied cognition, where the integration of interoceptive states and sensorimotor capacities underlies cognitive and affective processes[40,41].

Several lines of evidence support this view. The insula is one of the most functionally diverse regions of the brain[42], integrating information at long time scales (several seconds or longer[43,44]), and coordinating functional relationships across brain networks[45]. Also, different insular neuronal populations encode diverse interoceptive and special sensory inputs, including viscerception[46,47], immune afferents[25,48–50], heartbeat perception[51–53], pain[54–57], and taste and smell[58,59]. Von Economo Neurons (VENs) located in AIns might provide a cellular substrate for rapid information integration[60,61].

Despite the prominence of Craig's theory, only a few studies have directly evaluated multi-modal convergence zones in AIns, and their precise locations have not been firmly established. Available research has relied on evidence of functional co-localization derived from Coordinate-Based Meta-Analyses (CBMAs)[4,19,20], including Kurth et al.[4], which identified partial overlap in AIns across functional domains. While informative, CBMA relies on smoothed peak coordinates with limited spatial precision[62], which can produce artificial convergence where none exists and cannot systematically evaluate functional specificity across domains or test effect sizes in an unbiased manner.

To provide a comprehensive test of convergent and functionally selective insular zones, we conducted a mega-analysis of participant-level fMRI contrast maps sampled from the Affective Neuroimaging Consortium (www.anic.science) database, focusing on four functional domains: somatic pain, non-somatic appetitive processes, non-somatic aversive processes, and cognitive control[63]. We systematically included three subdomains per domain (e.g., three distinct types of somatic pain), with three studies per subdomain and 15 participants per study (Supplementary Fig. 1; *k=36 study contrasts, n=540*). This design enabled us to test whether insular subregions encode domain

information in a generalizable way across studies, which is critical for construct validation[64]. For example, pain-selective regions should consistently respond to different types of pain (e.g., thermal, mechanical, and visceral pain), but not to non-nociceptive stimuli (e.g., non-somatic, emotionally arousing stimuli). We employed a two-part analytic strategy, examining: (1) global insular activation for domain differences in whole-insula activation, and (2) relative local patterns after z-score normalization to identify regions preferentially engaged by specific domains. We validated these patterns using cross-validated support vector machines (SVM). Bayes Factors[65] provided direct, voxel-wise tests for both presence and absence of domain-specific activation. This enabled systematic identification of insular subregions that: (1) activate across all domains ("domain-general"), indicating convergence zones, (2) activate selectively to specific functional domains ("domain-selective"), and (3) show gradients of cross-domain convergence. Global analyses revealed that pain produces significantly more widespread activation across the insula compared to other domains. The analysis of relative patterns identified both multi-domain convergence zones in bilateral dorsal anterior insula (dAIns) and domain-selective zones for each domain, which were validated with independent datasets (n=608). Domain-selective inputs, processed separately in distinct insular subregions, progressively converge toward multi-domain zones in bilateral dAIns. To further characterize these zones, we examined meta-analytic functional decoding[19,42], coactivation with extra-insular brain regions[66,67], cytoarchitectonic mapping[23,68–72], and neurotransmitter system profiling[73,74]. Together, these findings provide support for both considerable functional diversity and multi-modal convergence zones in specific parts of the insula, especially in dAIns.

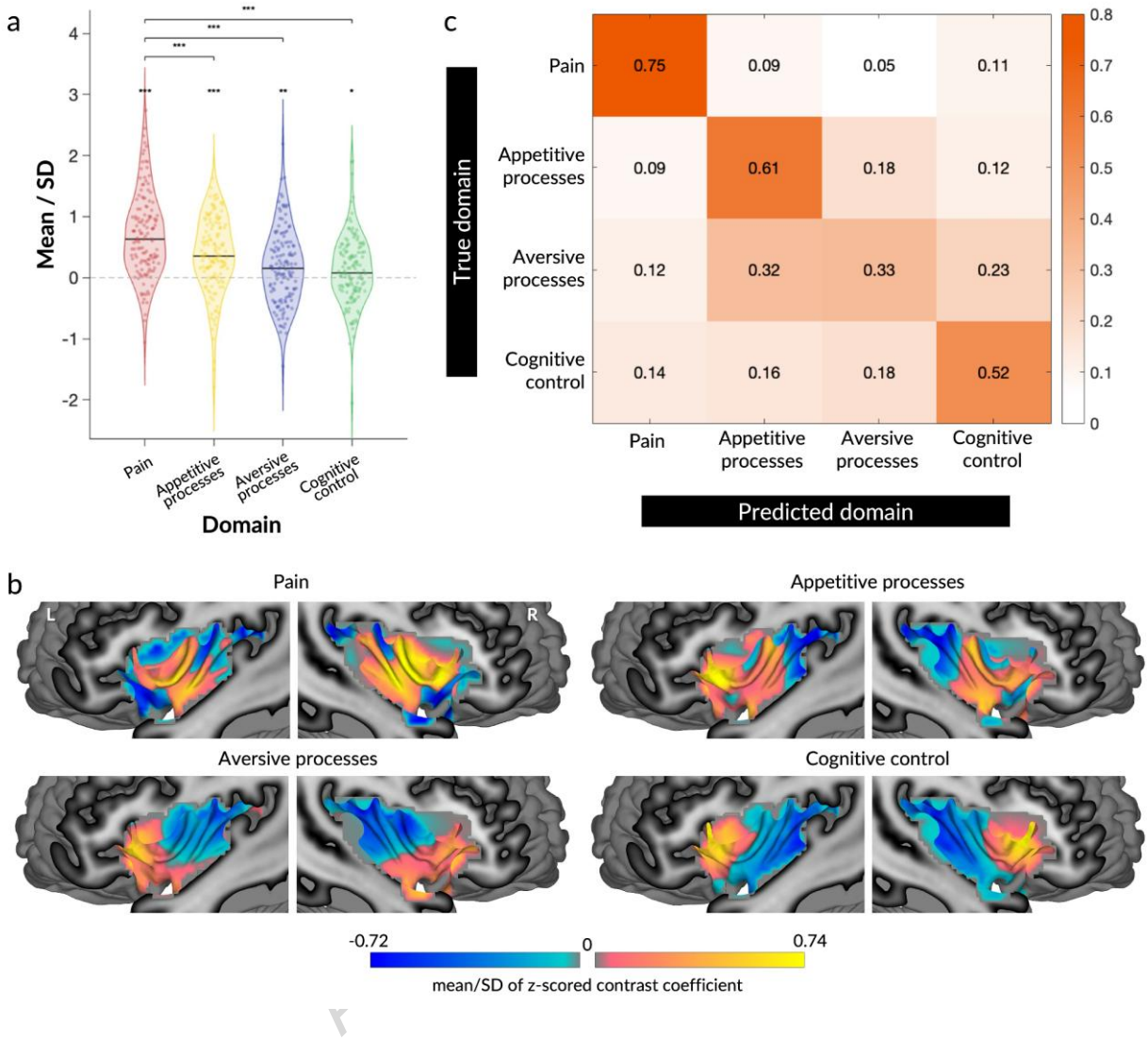

Figure 1. Global insular activation and multi-class SVM classification across four functional domains. a, *Global insular activation across four functional domains. Violin plots show the distribution of whole-insula activation values across participants (points; normalized by study-specific standard deviation). These values are removed when examining relative local patterns. All domains showed significant activation (all FDR-corrected q<0.05). Whole-insula activation was higher for pain than all other domains (all FDR-corrected q<0.001).* ***b,*** *Participant-level contrast images were z-scored for cross-study harmonization and subsequent analyses. Summary domain activation patterns (mean/SD) after normalization are shown here.* ***c,*** *Prediction accuracy for SVM classifiers trained to discriminate between domains using leave-one-study-out cross-validation. Accurate classification (see text) indicates separable, consistent neural representations for each domain. Source data are provided as a Source Data file.*

Results

Global insular activation across domains

Analysis of whole-insula activation revealed significant task-related activation compared to within-study controls (i.e., contrast values > 0) for each domain (Fig. 1a; Supplementary Fig. 2): Pain (*mean=0.70, t(134)=11.78, 95% CI [0.58, 0.82], Cohen's d = 1.02*); appetitive processes (*mean=0.36, t(134)=6.77, 95% CI [0.26, 0.47], Cohen's d = 0.59*); aversive processes (*mean=0.17, t(134)=3.38, 95% CI [0.07, 0.28], Cohen's d = 0.29*); and cognitive control (*mean=0.12, t(134)=2.50, 95% CI [0.03, 0.22], Cohen's d = 0.22; all FDR-corrected q<0.05*). Pain showed significantly higher whole-insula activation compared to all other domains: versus appetitive processes (*t(268)=4.22, 95% CI [0.18, 0.50], Cohen's d = 0.52), aversive processes (t(268)=6.60, 95% CI [0.37, 0.68], Cohen's d = 0.81), and cognitive control (t(268)=7.54, 95% CI [0.43, 0.73], Cohen's d = 0.92; all FDR-corrected q<0.001)*. These results indicate that pain elicits stronger widespread activations across the insula, consistent with its higher whole-insula activation, possibly due to its engagement of diffuse modulatory systems[75,76]. One consequence is that local posterior insular activity for pain, which was apparent in pre-normalized maps and alternative normalization methods that preserve global insular signals through magnitude scaling without mean centering (see Supplementary Fig. 3), was not significant after normalization.

Multivariate classification reveals distinct patterns across domains

We next examined relative activation patterns after accounting for the global differences described above (i.e., after normalization; Fig. 1b). We trained multiclass linear Support Vector Machine (SVM) classifiers to distinguish each domain from the others based on relative multivariate activation patterns in the insula (see Methods for details).

Domain-level classifiers achieved above-chance (>25%) prediction accuracy for three of the four domains: pain (74.71%; range: 40–100%), appetitive processes (60.73%; range: 40–80%), and cognitive control (52.00%; range: 17.78–75.56%; *all p<0.001*). Aversive processes showed lower accuracy (33.17%; range: 4.44–60%; *p=0.1327*). The confusion matrix (Fig. 1c) indicated that pain was most discriminable from all other domains. Aversive processes were confusable with appetitive processes, but less confusable with pain and cognitive control (see Supplementary Fig. 4 for pairwise predictive accuracy). Additional subdomain-level classification analyses revealed that some subdomains showed distinct neural patterns (Supplementary Fig. 5), especially responses to aversive sounds (a subtype of aversive processes) and working memory (a subtype of cognitive control; see Methods: Study design for subdomain descriptions).

These findings demonstrate that at the global level, domains differ markedly in their overall insular engagement, with pain showing particularly widespread activation. At the pattern level, pain, appetitive processes, and cognitive control domains show separable insular representations that generalize across studies. These patterns emerge despite substantial methodological variation in stimulus parameters (e.g., stimulus type, dynamics, and durations), task designs, and analytical choices (see Supplementary Table 4).

To localize domain-general and domain-selective patterns within the insula, we applied Bayes Factor analysis to the normalized images, identifying domain-general and domain-selective zones.

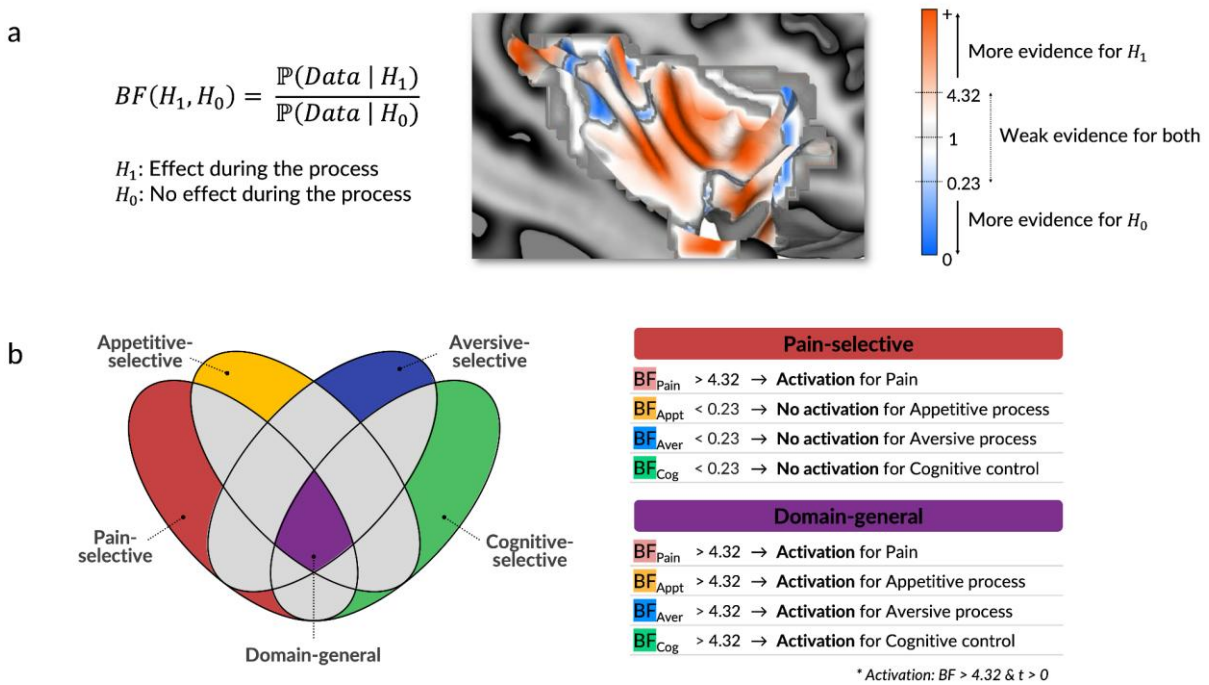

Figure 2. Identifying domain-general and domain-selective insular zones using Bayes Factors. *Bayes Factors (BFs) were calculated for each domain. BFs>1 indicate evidence favoring an effect, while BFs<1 indicate evidence favoring a null effect.* ***a,*** *An example map showing voxel-wise BFs for pain (red: favors effect; blue: favors null). Thresholds for sufficient evidence were set at 4.32 for effect (equivalent to FDR-corrected q<0.01) and 0.23 (the inverse of 4.32) for no effect.* ***b,*** *Definition of domain-general and domain-selective voxels. Voxels were considered activated only when BF>4.32 and t-statistics were positive, and not activated when BF<0.23 or BF>4.32 with negative t-statistics (i.e., significant deactivation). Domain-general voxels were defined as those showing activation in all domains. Domain-selective voxels showed activation in their designated domain and evidence favoring no activation in other domains.*

Domain-general and -selective zones identified using Bayes Factors

To identify insular zones encoding domain-general or domain-selective responses, we used Bayes Factors (BFs) to assess both presence and absence of domain-specific activation using a Bayes Factors one-sample t-test[65] (*n=135* per domain). We set a threshold of 4.32:1 odds favoring an effect versus no effect, corresponding to *q<0.01* FDR correction on average across domains (Fig. 2a; see Methods for details). Voxels were considered activated only when showing both *BF>4.32* and positive t-statistics. Evidence for no activation included cases of either more evidence for no effect (*BF<0.23*) or evidence for deactivation (*BF>4.32* with negative t-statistics). Based on these criteria, voxels activated in all four domains independently were classified as domain-general (Fig. 2b, purple), and voxels

activated in one domain and showing evidence favoring no activation in the other domains were classified as single domain-selective (Fig. 2b; pain in red, appetitive in yellow, aversive in blue, and cognitive in green). For brevity, we refer to zones selective for each domain as pain-selective, appetitive-selective, aversive-selective, and cognitive-selective throughout the paper. We note that fMRI selectivity at the voxel level should not be interpreted as homogeneous neuronal tuning, as individual voxels likely contain mixed neuronal populations responsive to multiple features.

Two specific regions within dAIns bilaterally were activated across all domains and therefore classified as domain-general (Fig. 3a, purple). These zones included 120 of 6012 insular voxels with relatively balanced bilateral distribution and spanned anterior short and inferior gyri[77]. This part of dAIns maps onto regions most frequently activated across task domains in the Neurosynth database[42] and highest along the principal cortical gradient identified by Margulies et al.[78], indicating transmodal (as opposed to unimodal) function.

We also identified zones selective to each domain. Pain-selective zones (320 voxels, red in Fig. 3a) included voxels clustered in mid-posterior insula bilaterally, spanning from middle short to posterior long gyrus. Appetitive-selective zones (14 voxels, yellow) were proximal to pain-selective zones in left dorsal and bilateral ventral mid-insula, spanning anterior and posterior long gyri. Aversive-selective zones (75 voxels, blue) were primarily located in the ventral-most portion of bilateral agranular insula, on anterior inferior gyrus. Cognitive-selective zones (142 voxels, green) were predominantly located in the anterior-most portion of dAIns and most dorsal frontal opercular border bilaterally and spanned anterior and middle short gyri. These activation patterns were consistent across subdomains and studies with few exceptions (Supplementary Fig. 6). Interestingly, these zones displayed distinct patterns of hemispheric asymmetry, with pain and cognitive control showing right hemispheric asymmetry (see Supplementary Table 1 for further information on each insular zone).

We further identified zones activated across two or three domains, surrounding domain-general zones activated across all domains (Fig. 3b). Coupled with the findings above, the topography of these zones demonstrated a spatial gradient of convergence, progressing from domain-selective zones (lightest purple) in posterior and ventral insular areas, through zones responsive to two or three domains, to full multi-domain convergence. This gradient showed bilateral symmetry, revealing a progression from specialized processing to multi-domain convergence.

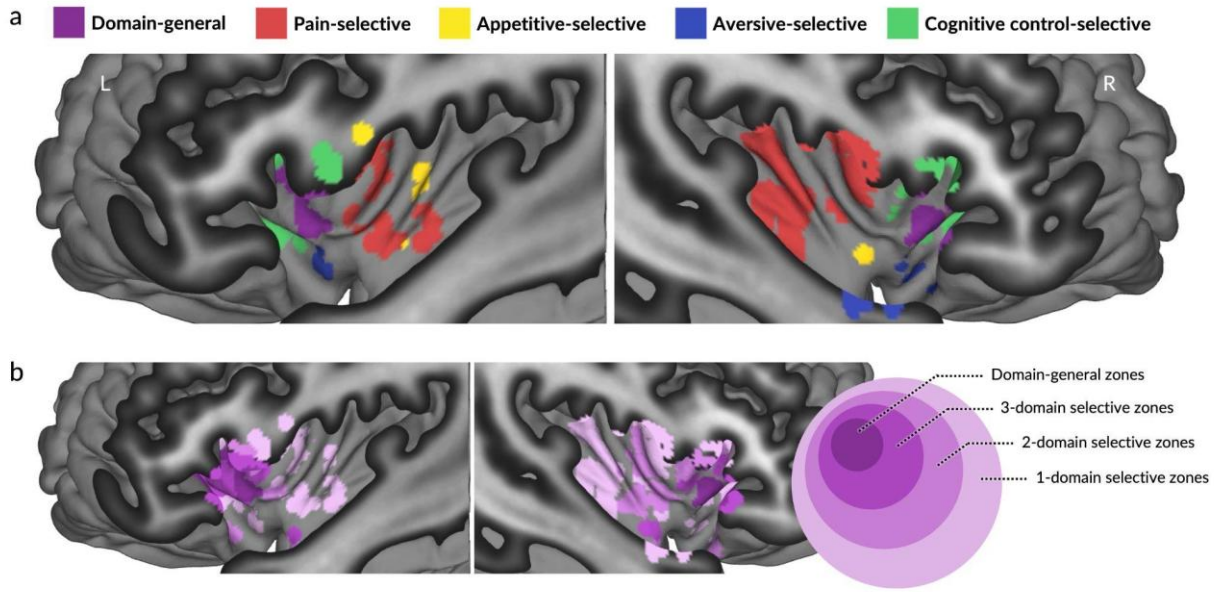

Figure 3. Domain-general and domain-selective zones in the insula. a, *Domain-general voxels (purple) were located in dorsal anterior insula, pain-selective voxels (red) in mid-posterior insula, appetitive-selective voxels (yellow) in mid-insula, aversive-selective voxels (blue) in ventral anterior insula, and cognitive-selective voxels (green) in dorsal anterior insula, anterior and dorsal to domain-general zones.* ***b,*** *Spatial gradient of functional convergence in the insula. Darker colors indicate greater generalization across domains (from lightest = 1 to darkest = 4 domains) and therefore higher functional convergence. Volumetric data were projected onto insular cutaway surfaces for visualization.*

Extended functional organization in adjacent opercular regions

While anatomically separable, the insula and operculum often function as an integrated system [38,79,80] via specific structural connections[81]. We therefore conducted supplementary analyses with an expanded mask including opercular parcels (OP3, 5, 7, and 9) from the Julich-Brain Cytoarchitectonic Atlas[68] (see Supplementary Methods for details). This revealed similar domain-general and domain-selective patterns in opercular areas with known structural connections to the insula (Supplementary Fig. 7). For example, pain-selective activation appeared primarily in OP5 and domain-general activation was found in OP7 and OP9, consistent with their connectivity to mid-posterior and dorsal anterior insula.

Validation with independent datasets

The distinct functional zones in the insula we identified may be limited to the particular studies and task contrasts included. To assess the generalizability of our findings, we validated the identified domain-general and domain-selective zones using 4 independent datasets not included in the primary analysis (total *n=608*): thermal pain stimulation for pain (*n=51*)[82], monetary reward anticipation for appetitive processes (*n=32*)[83], aversive image viewing for aversive processes (*n=160*)[84], and an n-back working memory task for cognitive control (*n=365*)[85] (see Methods for detailed task descriptions and contrasts).

We examined activation levels within all five functional zones to assess whether domain-selective zones showed preferential responses to their target domains and whether the domain-general zone responded to all domains.

The validation datasets replicated our primary findings regarding global insular activation, with pain showing the highest whole-insula activation (*mean/SD=0.66±0.44*), significantly exceeding all other validation datasets (*vs. appetitive: t(81)=3.93, d=0.89; aversive: t(209)=3.92, d=0.63; cognitive: t(414)=24.77, d=3.70; all p<0.001*).

All domain-selective zones showed significant domain selectivity, with higher activation for the hypothesized domain compared to pooled off-target domains (Supplementary Fig. 8). Pain-selective zones showed the strongest effect (*t(606)=6.98, p<0.001, d=1.02*), followed by cognitive-selective (*t(606)=6.86, p<0.001, d=0.57*), aversive-selective (*t(606)=4.32, p<0.001, d=0.40*), and appetitive-selective zones (*t(606)=2.04, p=0.042, d=0.37*). Activation in the domain-general convergence zones was significantly above zero for all test datasets: pain (*t(50)=6.01, p<0.001, d=0.84*), appetitive processes (*t(31)=4.32, p<0.001, d=0.76*), aversive processes (*t(159)=15.63, p<0.001, d=1.24*), and cognitive control (*t(364)=22.79, p<0.001, d=1.19)*. Some studies did show activation to non-target domains, potentially because some tasks can engage psychological processes related to multiple domains. Most notably, the validation task for the appetitive domain (Monetary Incentive Delay task[86]) also engaged cognitive-selective zones, likely because it involves reward processing but also performance under time pressure that is adaptively adjusted based on feedback.

Functional decoding using Neurosynth topic and term maps

To map the identified insular zones onto psychological topics, we employed meta-analytic functional decoding using Neurosynth[42]. We examined point-biserial correlations with 525 terms and 50 topics derived from 11,406 studies in the Neurosynth database and z-scoring correlations across topics (Fig. 4a-b; see Supplementary Table 2 for a full list of topics). Domain-general zones in dAIns demonstrated high correlations with diverse topics and terms, reflecting their hypothesized functional diversity. The strongest topic associations were with “response inhibition”, “pain processing”, and “task performance”. The convergence zones ranked in the top 5% of voxels in terms of functional diversity across Neurosynth topic maps (uniformity test maps across 50 topics), showing activation across the most heterogeneous set of topics.

In contrast, domain-selective zones showed associations matching their hypothesized domains. Pain-selective zones exhibited the strongest topic associations with “pain processing”, “somatosensory stimulation,” and “sensorimotor processing” (but also “food processing”). Among individual terms, the strongest were “pain”, “somatosensory”, “noxious”, and “stimulation” . Appetitive-selective zones were associated with “food processing”, “pain processing”, and “emotion processing” topics, and with appetitive processing-specific terms such as “cocaine”, “incentive”, and “reward”. Aversive-selective zones exhibited the strongest associations with topics “response inhibition”, “emotion processing”, “social cognition”, and terms “masked” (indicating priming), “automatic”, “pleasant”, and “conditioning”. Cognitive-selective zones showed the strongest associations with topics “task performance”, “cognitive

flexibility", "feedback-based learning", and "working memory", and terms "muscle", "task-related", "top-down", and "decision", indicating links with top-down control of motion and behaviors.

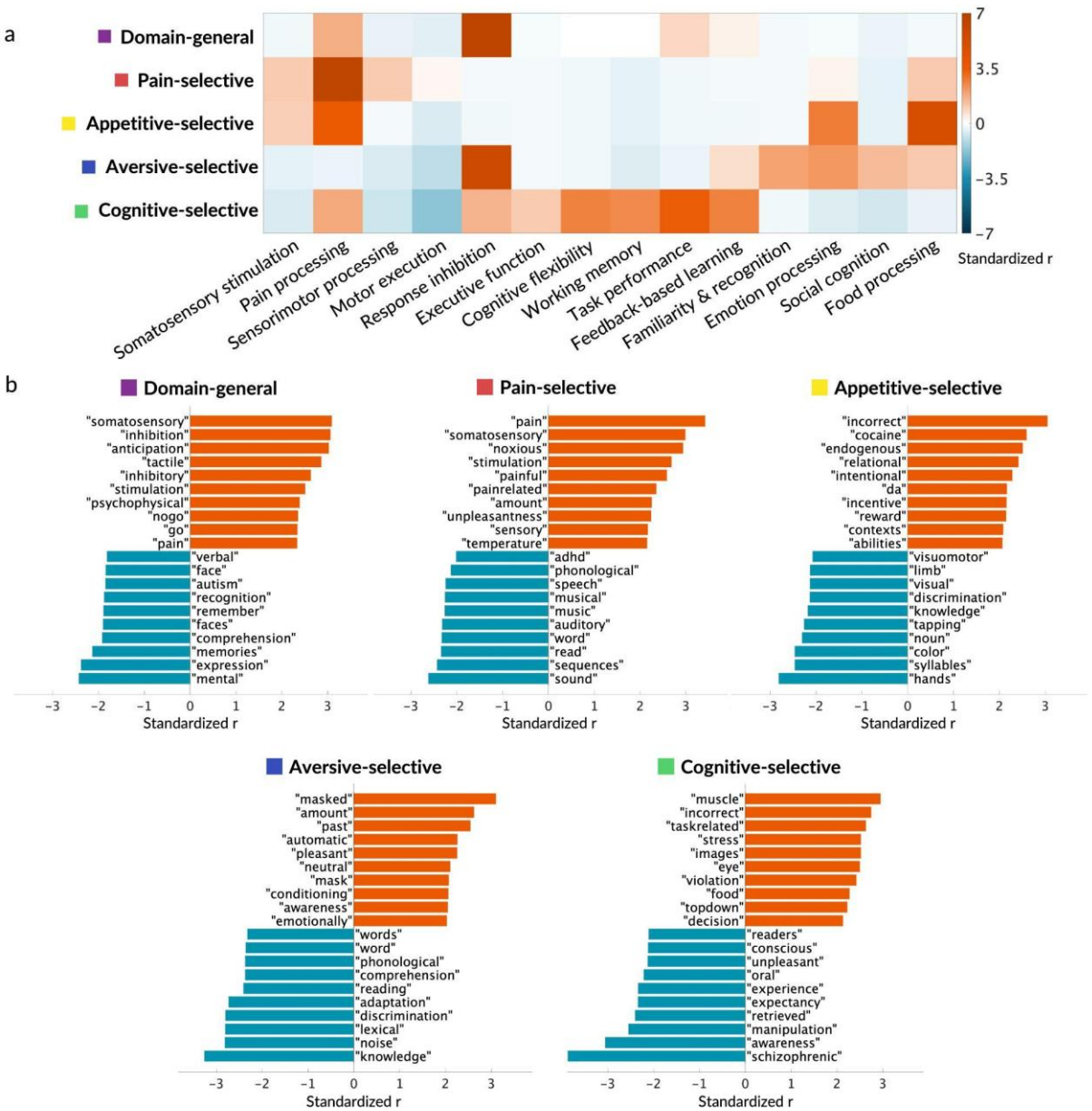

Figure 4. Meta-analytic functional decoding of domain-general and domain-selective insular zones using Neurosynth. a, *Topic-level decoding. Heatmap shows point-biserial correlations between domain-general and domain-selective zones and psychological topics registered in Neurosynth, z-scored across topics (Z(r)). Topics shown (x-axis)* have *Z(r)>1 for at least one domain (see Supplementary Fig. 9 for complete topic heatmap).* ***b,*** *Term-level decoding. Each subplot shows the top 10 highest and lowest correlating terms for each insular zone, selected from 525 psychological terms. da: Dopamine. Source data are provided as a Source Data file.*

Coactivation between insular zones and other brain systems

To better understand how these insular zones participate in brain-wide systems, we investigated their coactivation patterns with other regions across 27,072 contrast maps in the Neurosynth database. This approach provides a meta-analytic proxy of functional connectivity[19,66,67]. We also examined the relationship between each extra-insular coactivated system and seven canonical resting-state networks in cortical, subcortical, and cerebellar regions[87–89].

Domain-general zones showed high coactivation with other putative convergence zones across the brain (Fig. 5a), including bilateral rostrolateral (rlPFC), right ventrolateral (vlPFC), and right posterior dorsomedial prefrontal cortices (dmPFC), bilateral posterior temporal parietal junction (TPJp), and bilateral anterior midcingulate cortex (aMCC). No coactivated voxels were found in subcortical regions or thalamus. These regions lie at the transmodal end of the principal cortical gradient[78]. A majority of voxels coactivating with domain-general zones were located in frontoparietal (45.87%), ventral attention (27.08%), and default (20.30%) networks. These networks are also among the most transmodal networks across the brain.

Pain-selective insular zones showed high coactivation with brain regions involved in pain, somatosensory and somatomotor processing, including bilateral primary and secondary somatosensory cortices (S1 and S2), right premotor and primary (M1) and supplementary motor area (SMA), bilateral posterior operculum, bilateral anterior TPJ (TPJa), and bilateral posterior medial (pMCC) and dorsal posterior cingulate cortex (dPCC). Subcortical coactivation was observed in ventral posterior thalamus, including ventral posteromedial nucleus (VPM), as well as both posterior and anterior putamen, external and internal globus pallidus, subthalamic nucleus in basal ganglia, and the amygdalostriatal transition area and centromedial amygdala. Coactivated voxels were predominantly in somatomotor (58.88%) and ventral attention (31.36%) networks (Fig. 5b). This finding aligns with predictive models of pain[90,91], where most voxels with positive pain-predictive weights were located in somatomotor and ventral attention networks.

Appetitive-selective insular zones showed high coactivation with posterior putamen. These coactivated regions, predominantly located in dorsal attention network (47.22%), have been implicated in affective processing across multiple meta-analyses[92] and individual studies[93,94].

Aversive-selective insular zones showed the highest coactivation with bilateral orbitofrontal cortex (OFC), anterior medial wall—left ventromedial prefrontal cortex (vmPFC) and right posterior dmPFC, bilateral pregenual anterior cingulate cortices (pACC)—bilateral temporal pole, right superficial amygdala, and right nucleus accumbens (NAc). These regions have been broadly associated with regulation of affective and motivational processes in previous studies. The majority of coactivated voxels were in default mode (47.34%) and limbic (44.65%) networks. This contrasts with somatic pain, which involves different regions and networks despite also being aversive, helping to elucidate why pain and non-somatic negative affect have been strongly dissociable in prior studies[19,93].

Cognitive-selective zones showed greater coactivation with bilateral dorsolateral PFC (dlPFC), including inferior frontal junction (IFJ), and bilateral intraparietal sulcus (IPS) and superior parietal

lobule (SPL). Subcortical regions included thalamus (ventral anterior (VA), ventral lateral (VL), lateral dorsal (LD), mediodorsal (MD), ventromedial (VM) nuclei) and bilateral anterior striatum (putamen and caudate head). These regions have broadly been associated with cognitive control and goal-based action selection. A network including dlPFC, IFJ, and anterior insula has been proposed to select actions to execute via evidence accumulation[95,96]. The mid-caudate zone identified here has also been associated with executive control in a previous meta-analysis[97]. Coactivating voxels were distributed predominantly among frontoparietal (50.14%) and dorsal attention (35.14%) networks.

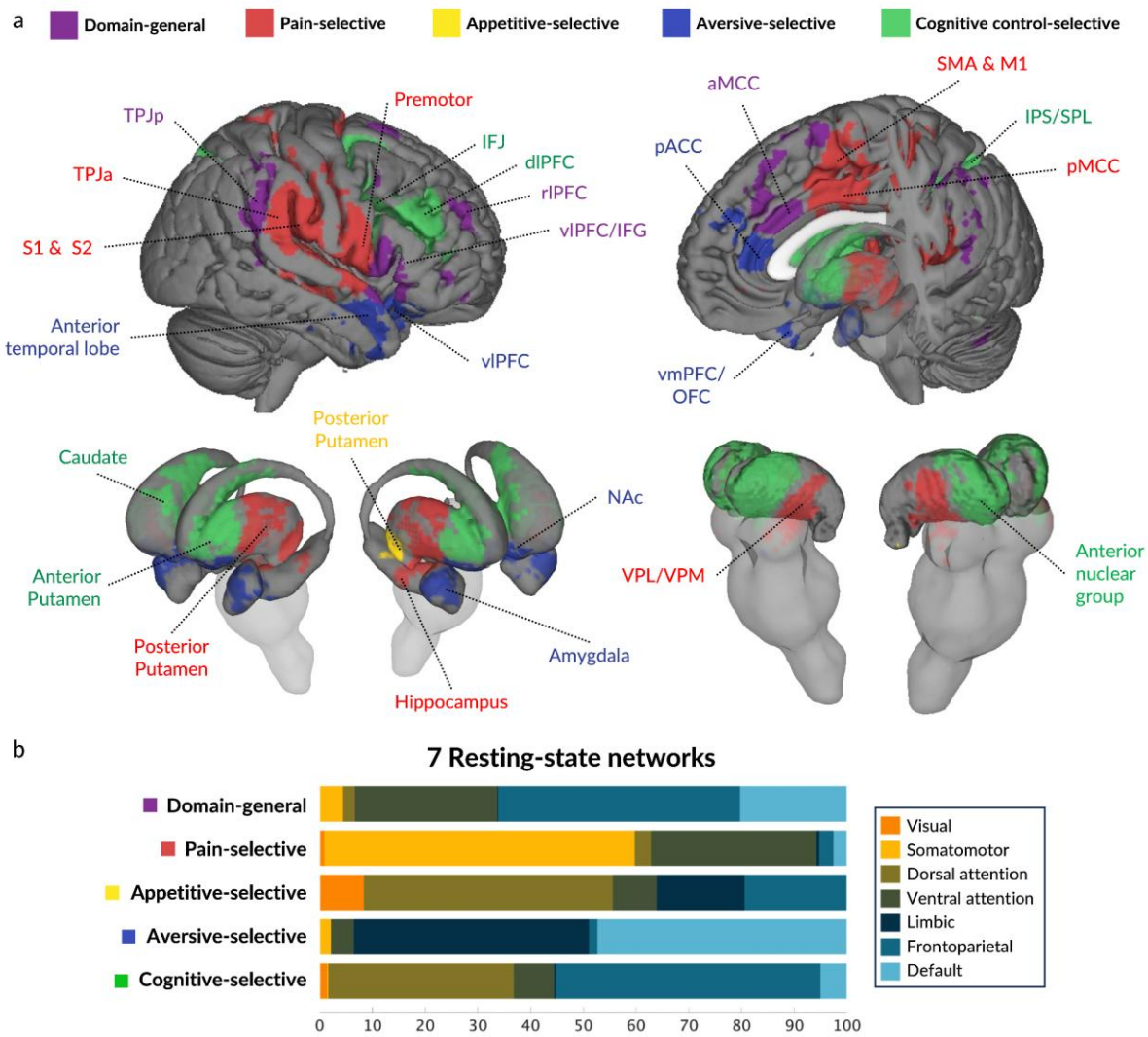

Figure 5. Brain-wide coactivation patterns and resting-state network affiliations of domain-general and domain-selective insular zones. a, *Meta-analytic coactivation patterns between insular zones and extra-insular regions. Coactivated voxels outside of the insula are assigned to the maximally correlated insular zone, requiring that maximum correlation to be at least 10% higher than the next highest correlation. aMCC: anterior midcingulate cortex; dlPFC: dorsolateral prefrontal cortex; IFJ: inferior frontal junction; IPS: intraparietal sulcus; SPL: superior parietal lobule; M1: primary motor cortex; NAc: nucleus accumbens; OFC: orbitofrontal cortex; pACC: pregenual anterior cingulate cortex;*

pMCC: posterior midcingulate cortex; rlPFC: rostrolateral prefrontal cortex; S1: primary somatosensory cortex; S2: secondary somatosensory cortex; SMA: supplementary motor area; TPJa: anterior temporoparietal junction; TPJp: posterior temporoparietal junction; vlPFC: ventrolateral prefrontal cortex; vmPFC: ventromedial prefrontal cortex; VPL: ventral posterolateral nucleus; VPM: ventral posteromedial nucleus. ***b,*** *Distribution of coactivated regions across seven resting-state networks[87–89]. Bar graph shows the percentage of coactivated voxels (FDR q<0.001) overlapping with each network across cortical, subcortical, and brainstem regions. Source data are provided as a Source Data file.*

Cytoarchitectonic characterization

To explore the cytoarchitectonic associations of the insular zones, we examined their overlap with the Julich-Brain Cytoarchitectonic Atlas[23,68], which parcellates the insula into 16 areas with varying cytoarchitectonic characteristics: Ig (granular), Id (dysgranular), and Ia (agranular) parcels (Fig. 6). Spatial overlap between each insular zone and atlas parcels was quantified using Dice coefficients, reporting parcels with coefficients>0.1.

Insular zones mapped onto different cytoarchitectonic regions, though the overlap was imperfect. Domain-general zones were contained predominantly within dysgranular areas, particularly left Id6 and right Id8. Cognitive-selective zones also demonstrated high overlap with bilateral Id7, dorsal and anterior to domain-general zones. In contrast, appetitive and aversive-selective zones were primarily in agranular, dysgranular, or dysgranular-agranular transitional areas: appetitive-selective zones overlapped most with left Id5 and right Ia3, and aversive-selective zones with Id10 bilaterally. Pain-selective zones showed the strongest associations with Id6, but also Id5 and Id3 (in a granular-dysgranular transitional area; see Supplementary Table 3).

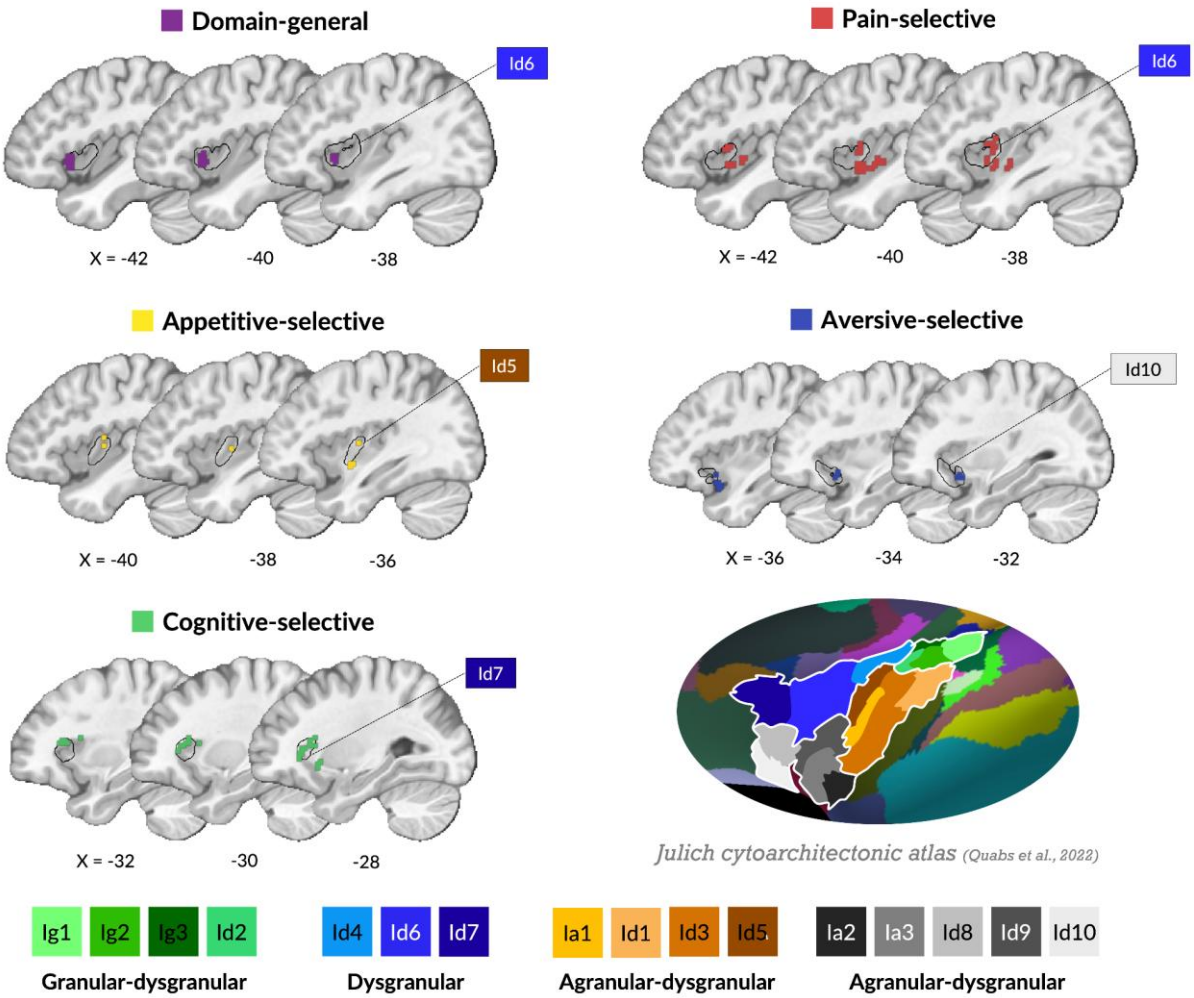

Figure 6. Cytoarchitectonic profiles of insular zones. *For each functional zone, only the best matching cytoarchitectonic parcels are shown from the Julich-Brain Cytoarchitectonic Atlas[23,68] (32 parcels across left and right insula). Inset illustrates the full cytoarchitectonic parcellation of the insula as defined by Quabs et al.[23] using the most up-to-date atlas.*

Neurochemical associations with functional insular zones

To characterize associations with neurotransmitter systems derived from human molecular imaging, we estimated spatial associations (point-biserial correlations) between insular zones and PET binding maps of 36 receptors and transporters across 8 neurotransmitter systems from Neuromaps[73,74]. Only associations replicated across at least two independent studies were interpreted[98].

Several neurotransmitter systems showed reliable associations with particular insular zones (Fig. 7a). Mu-opioid (MOR) and cannabinoid (CB1) receptor maps were positively associated with domain-general zones and all affective functional domains (appetitive, aversive, and pain-selective zones). Affective domains also had particularly strong associations with serotonin receptor (5-HT1a) and

transporter (5HTT) maps, whereas domain-general and cognitive-selective zones showed relatively stronger associations with serotonin 5-HT1b receptor. Both domain-general and pain-selective zones showed strong correlations with glutamate (mGluR5) receptors. Appetitive and cognitive-selective zones shared particularly strong associations with dopamine (D2) receptor distribution. Overall, these findings suggest that different neurotransmitter systems may be differentially involved in different functional domains.

Next, we compared neurotransmitter system profiles between the insular zones and their corresponding coactivated brain-wide systems (Fig. 7b). These profiles were highly similar (*mean Pearson's r=0.66; range: 0.35–0.91*). For example, positive associations between domain-general insular zones and CB1, 5-HT1b, mGluR5, and MOR was also present in their coactivated brain-wide systems (e.g., anterior PFC, TPJp, aMCC).

Off-target correlations across different functional domains (e.g., between the aversive-selective insular zones and appetitive-selective brain-wide systems) were generally weaker than on-target correlations and were often negative. This correspondence was strongest for domain-general and aversive domains. Domain-general regions showed on-target similarity *r=0.88* (off-target range: *r=-0.78–0.43*) and aversive processes showed on-target similarity *r=0.91* (off-target range: *r=-0.37–0.27*). Pain showed the least correspondence, suggesting distinct neurotransmitter profiles for pain-selective insular zones compared to their extra-insular coactivated regions. The strongest cross-domain correspondence was that between pain-selective insular zones and aversive-selective coactivated zones, suggesting a possible substrate linking nociceptive representations in the insula and representations of negative emotion in other cerebral areas.

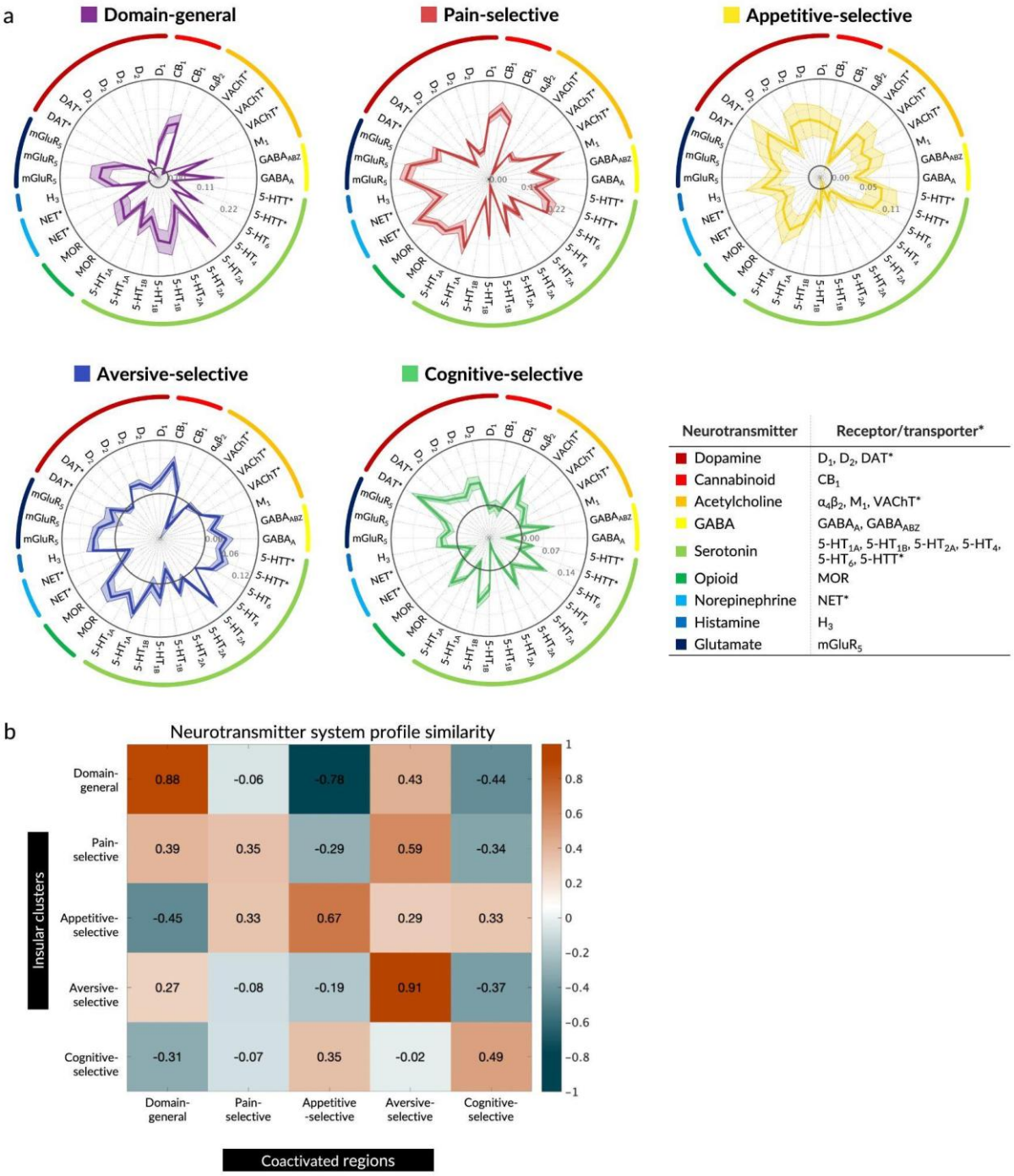

Figure 7. Neurotransmitter system profiles of insular zones. a, *Spatial similarity between the insular zones and 36 neurotransmitter maps from Neuromaps[74,99] with mean spatial similarity (center) and standard errors (error bars) estimated from 100 bootstrap samples. Black rings indicate zero correlation; values outside the ring are positive, and inside the ring are negative. Inset shows neurotransmitter systems and their corresponding receptors and transporters in the atlas.* ***b,***

Correlation between the insular zones and their extra-insular coactivated systems. Source data are provided as a Source Data file.

Discussion

The insula contains subregions associated with diverse cognitive, affective, and interoceptive processes, and its hypothesized role in integrating these streams may be fundamental for unified subjective experiences. However, spatially precise, empirical evidence characterizing functional convergence zones in the insula has been limited. Using large-scale fMRI data (n=540) systematically sampled across four functional domains combined with BFs, we evaluated both presence and absence of activation across domains. We identified a domain-general convergence zone in bilateral dAIns surrounded by domain-selective zones for pain, appetitive processes, aversive processes, and cognitive control. Each showed distinct meta-analytic functional profiles, brain-wide coactivation patterns, cytoarchitectonic organization, and neurotransmitter receptor distributions. We also validated these functional zones using four independent datasets (n=608), confirming both domain-general activation in convergence zones and functional selectivity in domain-selective zones.

We found an orderly progression from domain-selective zones in ventral (negative affect), posterior (pain and appetitive), and dorsal (cognitive) insular regions to the fully domain-general zones in dAIns, extending beyond previously proposed posterior-to-anterior progressions[38,39,100]. These findings support theories proposing hierarchical organization of convergence zones and spatial topography based on functional similarity[36,37], and align with theories of embodied cognition, emphasizing how the progressive integration of bodily signals enables goal-directed behavior and conscious awareness[34,35].

Our findings identified insular areas of functional convergence and selectivity with increased precision relative to previous work. The domain-general anterior insula heuristically defined by Craig[39] and in early meta-analyses[19] contains both domain-general and functionally selective zones for cognitive control, somatic pain, and/or non-somatic aversive processes in our analysis. While overlapping BOLD signals alone cannot establish functional convergence, multiple levels of evidence support this interpretation: (a) hierarchical progression from domain-selective to domain-general zones, (b) functional associations based on previous literature, (c) coactivated brain-wide systems, (d) cytoarchitectonic organization, and (e) neurotransmitter system profiles.

Our findings both confirm and extend Kurth et al.'s seminal meta-analysis[4]. While Kurth et al. identified partial overlap across domains in anterior-dorsal insula using coordinate-based methods, our image-based mega-analysis provides greater spatial precision, localizing convergence to specific regions in bilateral dorsal anterior insula. Furthermore, our approach enables us to differentiate domain-general from domain-selective zones and reveals a functional gradient from specialized processing in posterior/ventral regions to multi-domain integration in dorsal anterior insula—a nuanced organization not fully captured in previous work.

The patchy organization we observe aligns with high-resolution tract-tracing studies in non-human primates. Tract-tracing studies show that connections between prefrontal/cingulate cortex and macaque insula consistently form 'sharply delimited patches' that precisely coincide with

cytoarchitectonic boundaries[101]. This patchy organization, visible across neuroanatomical studies spanning decades[1,102,103] but previously overlooked, suggests that modular, patchy organization is a fundamental feature of insular architecture rather than statistical noise.

Functional associations using Neurosynth meta-analytic topic maps revealed that domain-general zones in dAIns were among the most functionally diverse (top 5%) across the brain, alongside aMCC, IFJ, and medial thalamus. Meta-analytic coactivation analysis further revealed high coactivation with other cortical convergence zones such as rlPFC, TPJp, and aMCC, which are situated at the transmodal end of unimodal-to-transmodal cortical gradients[78].

Coactivation patterns across the insular zones showed systematic topographical organization, with organized transitions between functional domains across cortical and subcortical regions. For example, in lateral frontal cortex, we observed an anterior-to-posterior hierarchy from domain-general rlPFC to cognitive control-related dlPFC to pain-related somatomotor regions. This is consistent with findings on prefrontal hierarchy, where anterior regions support more abstract, temporally extended processes and posterior regions support immediate task goals and actions[104–107]. In lateral temporal-parietal cortex, domain-general regions in TPJp were situated between cognitive control-related SPL and pain-related TPJa and S2. Similarly, domain-general regions in IFG were positioned between cognitive control-related premotor regions and anterior temporal regions (connected to medial temporal and hippocampal circuits) processing non-somatic aversive experiences. In the subcortex, a progression emerged from anterior striatal and thalamic zones specialized for cognitive control to posterior zones for pain, with appetitive processing localized to extreme posterior striatum, consistent with stable and long-term value encoding in non-human primates[108].

With respect to canonical resting-state networks, domain-general and domain-selective insular zones and their coactivated systems showed distinctive distribution patterns. While each domain showed stronger affiliation with some networks (e.g., aversive processes were most affiliated with default and limbic networks)—the functional zones we identified spanned multiple networks and did not align with them in a 1:1 fashion. This observation is consistent with findings that decoding models predicting affective experiences span multiple networks[109–112]. Although resting-state networks may relate to task-based patterns at a coarse level[113,114], tasks evoke reorganization of functional connections in ways not captured by static resting-state patterns[115–117], including alterations of brain-wide neuronal activity patterns by stimuli and activation of neuromodulatory nuclei[118–122]. This may explain why the insular zones and their coactivated systems identified here are not reducible to resting-state networks, but instead constitute a distinct way of understanding large-scale brain organization.

As with resting-state networks, our functional insular zones mapped onto cytoarchitecture to some degree, but cytoarchitectonic boundaries did not fully describe them. Domain-general convergence zones were located largely within cytoarchitectonic region Id6[23] in dAIns but our results also indicate functional heterogeneity within Id6, including pain and cognitive-selective zones in non-overlapping portions.

The observed cytoarchitectonic mappings were corroborated by evidence from intracranial studies, which provide more direct neural measurements (electrophysiology) and establish causal links to

behavior (stimulation). Domain-general and cognitive-selective zones were predominantly located in dysgranular areas Id6 and Id7, respectively, aligning with findings that dysgranular dAIns is key for transmodal processes such as arousal and cognitive control[20,101,123–130]. For example, Sabat et al.[129] identified a domain-general arousal hub in similar cytoarchitectonic regions to our cross-domain convergence zone, centered in Id7 but extending into Id6 and Id8. Intracranial electrophysiology and stimulation studies showed that Id6 showed primarily visceral sensations with anxiety/hypervigilance in a small subset of cases, whereas Id7 showed increased activity during task-related salience detection and no responses when stimulated[28]. Aversive-selective zones in Id10 align with known limbic system projections[128] and correspond to regions showing specific responses to negative emotional stimuli in electrophysiological recordings[131].

Pain-selective zones were a notable exception, spanning multiple cytoarchitectonic areas in ways that both align with and diverge from previous findings. Beyond Id6's role in vigilance discussed above, Duong et al.[28] found that Id6 stimulation evoked viscerоception, posterior insular areas Id2 and Ig2 evoked pain, and Id3 evoked somatosensation—consistent with other stimulation findings on somatic and visceral sensations[6,31,57,132,133]. This broad distribution may reflect both the importance of the insula for interoception and the multidimensional nature of pain, which involves a relatively unique combination of regions across the brain[82,134]. However, our findings diverge from established work showing that the posterior granular insula is a key region for somatosensory and nociceptive information[128]. Specifically, we did not observe pain-selective activity in Ig1 (bilateral), Ig2 (left), and Id2 (left) of dorsal posterior insula—regions where previous studies found pain-selective activity[54,55,135] and direct stimulation reliably evokes pain[29,56,127–129]. While right Ig2 and Id2 showed pain-selective activity, they were not the most strongly associated parcels with our pain-selective zones. This discrepancy likely reflects data harmonization constraints required for analyzing heterogeneous multi-study data: after evaluating several methods (see Methods: Data harmonization), we chose z-scoring, which affects detection of pain-selective responses in posterior insula due to pain's insula-wide activation. Additionally, somatotopic organization and lateralization may have contributed, as our dataset included varied stimulation sites that could obscure somatotopically mapped activity in posterior insula.

Neurotransmitter receptor and transporter binding patterns from Neuromaps[73,74] revealed distinct neurochemical profiles across insular zones. Similar patterns were also observed in their coactivated brain-wide systems. This supports the hypothesis that functional organization is guided by co-expression of neurotransmitter systems in functionally related areas, even without direct structural connections[73,139–142]. For instance, language-related areas show similar receptor distributions despite being anatomically dispersed[143], suggesting a common molecular basis for functionally related regions. Optogenetic and chemogenetic fMRI studies[144–150] provide corroborating evidence that manipulating neurotransmitter release from subcortical centers modulates functional connectivity among regions with shared receptor profiles.

One exception was that pain-selective insular zones showed higher neurochemical similarity to the extra-insular aversive processes system than to their own extra-insular pain system. This implies that pain-related neuromodulatory systems may be more region-specific within the insula, or that pain processing in the insula may not be exclusively nociceptive, but also involve pain-specific affective components, i.e., “pain” representations across nociceptive and vicarious pain, as recently observed in

mid-insula[112]. This may also reflect the multifaceted nature of pain, which elicits diverse emotional reactions (e.g., fear, anger) and motivates action policies (e.g., avoidance, escape).

These findings highlight the value of systematic multi-domain sampling in revealing both convergent and divergent patterns of insular functional organization and present an important direction for future research. Activity patterns related to broad constructs like “pain” or “cognitive control” can only be effectively identified by testing across distinct subdomains with varied stimuli and task designs[151–153]. While large-sample studies[154–158] enable investigation of how multiple psychological constructs are represented in the brain across large populations, reliance on single tasks to represent broad psychological constructs (e.g., an emotional face-matching task to study emotion) limits identification of generalizable representations. Characterizing generalizable neural representations requires systematic sampling across multiple implementations of each construct, as demonstrated here and in previous work[159].

Finally, the present study has several limitations that should be addressed in future research.

First, we selected a Bayes Factor threshold of 4.32:1 (corresponding to $q < 0.01$ *FDR* correction; moderate evidence by Bayesian standards), balancing sufficient evidence with practical considerations in detecting effects in neuroimaging data. Future studies with larger samples could employ higher thresholds to identify effects with even stronger evidence.

Second, more comprehensive sampling of each domain would be ideal, and testing the generality and functional specificity in different sets of studies would be valuable as person-level data become available. We have partially addressed this through validation with independent datasets ($n=608$), which confirmed the robustness of our findings. With sufficient person-level data, future studies could even test studies within subdomains as random effects. Such comprehensive datasets with systematically coded methodological variations would also shed light on how specific methodological variables impact activation patterns. Both advances, however, require systematic sharing of person-level activation maps across the field, extending current practices of reporting study-level coordinates and publishing study-level maps. Our approach here balances comprehensive sampling with practical constraints. With 9 studies per domain across 3 subdomains (540 participants total), our sampling exceeds comparable work[159] and the key strength lies in systematic sampling across different operationalizations of each domain, enabling identification of patterns that generalize across experimental paradigms. Furthermore, while our study systematically sampled four functional domains, several domains important to insular function remain to be examined—e.g., chemosensation such as smell and taste[58,59], heartbeat perception[51–53,160], non-pain somatic aversive experiences like breathlessness[161] and itch[162], autonomic arousal[160], inflammation and sickness[25,48–50], nausea[163], tussis[164], and others. Addressing this will require collaboration and sharing of multiple studies of sufficient size ($n \geqq 15$). We view this work as an important step toward understanding generalizable insular representations, while recognizing that future work can extend these findings with additional studies and paradigms.

Third, our psychological domain structure represents just one possible ontology for classifying studies[165–168]. The development and validation of ontologies is a complex and important research topic,

and there is no single “correct” solution. Future research with extended samples could empirically compare different candidate ontologies, working toward developing psychological categories better aligned with the functional architecture of the brain[167,169]. Our validation findings underscore this need: while confirming domain selectivity, they also revealed that tasks can activate multiple functional zones based on their component processes. The appetitive task[83] in our validation dataset elicited activation in both appetitive- and cognitive-selective zones, consistent with the task's cognitive demands—maintaining stimulus-reward mappings and sustaining inhibitory control during anticipatory delays—in addition to reward anticipation. This also highlights the iterative nature of brain-behavior mapping: task categorization influences identification of neural patterns, while neural results inform understanding of task components.

Fourth, we acknowledge that the insula exhibits considerable inter-individual variability in sulcal and gyral morphology. Our analyses identify group-level organization using template-based normalization to MNI space, mapping function onto anatomical features (gyri and sulci) at the group level. Future studies using precision neuroimaging approaches with within-person tasks could examine how anatomical variability influences functional localization and how closely domain-general and domain-selective regions map onto individual anatomical features.

Fifth, our cytoarchitectonic mapping relied on maximum probability maps from the Julich-Brain atlas, where each voxel is assigned to the area with the highest probability. This approach simplifies the inherent uncertainty in these assignments, particularly at borders between areas. Future studies could address this by using probabilistic approaches that preserve uncertainty information or by examining structure-function relationships at the individual subject level. We hope our study inspires future work to expand this approach and address these outstanding long-term goals.

Lastly, our analysis focuses primarily on activation patterns and does not extensively consider information carried by deactivation. While aggregating individual-level contrast images allows for observation of deactivation patterns that can provide valuable insights, interpreting these patterns presents significant challenges, as their underlying mechanisms are less well understood than those of activations. The relationship between BOLD signal decreases and neural activity may vary across brain regions, involving interactions between neural activity, neurovascular coupling, and hemodynamics[170–172]. Beyond this regional variability, BOLD decreases can reflect various neural processes, from inhibition of task-irrelevant activity to resource reallocation or shifts between functional modes[173,174]. Additionally, the choice of baseline condition significantly affects observed deactivation patterns, complicating cross-study comparisons. Given these complexities and the activation-based nature of our subsequent multi-level characterization analyses, we focused our primary Bayes Factor analysis on activation patterns. However, recognizing the potential importance of deactivation, we have included deactivation-based results in Supplementary Fig. 10 for reference. We encourage future studies to further investigate deactivation patterns for various brain functions in and beyond the insula.

Overall, this study provides strong empirical evidence for a fundamental organizing principle in the insula: the coexistence of functionally convergent and selective zones within a brain region long hypothesized to be crucial in integrating diverse information streams. Through systematic sampling across four functional domains and rigorous Bayes Factor analysis of both presence and absence of

activation, we reveal a gradient of convergence from domain-selective zones to a multi-domain convergence zone in bilateral dAIns, combining spatial coverage, precision, and functional diversity beyond previous approaches. Our multi-level characterization demonstrates that these functional zones are distinguished by specific patterns of cytoarchitecture, coactivation with other brain regions, and neurotransmitter distribution—providing evidence beyond mere overlap of BOLD signals that these represent distinct functional units. These results reconcile previous work by demonstrating how functional specialization and information convergence coexist within the insula's hierarchical organization, suggesting a potential role for this architecture in integrating diverse information streams to support unified subjective experiences and the construction of the sense of self.

Methods

Study design

This study uses a construct-validation approach, building upon previous research by Kragel et al.[159] and Van Oudenhove et al.[175], to explore domain-general and domain-selective representations of four functional domains in the insula: somatic pain, non-somatic appetitive processes, non-somatic aversive processes, and cognitive control. This approach aims to identify brain regions that consistently respond to a particular psychological construct (e.g., pain) across multiple experimental manipulations and studies, ensuring that the voxels identified as domain-general and domain-selective are not driven by specific experimental conditions or study-specific factors, but rather represent the underlying latent construct (for further details on the rationale of this approach, see refs.[159,175]).

Specifically, we systematically sampled participant-level fMRI activation maps from the Affective Neuroimaging Consortium (www.anic.science) database across the four domains above. Each domain includes three subdomains representing different experimental manipulations that engage processes within that domain. Pain domain includes responses to thermal, mechanical, and visceral stimulation; appetitive processes domain includes responses to food, drug, and sexual images; aversive processes domain includes responses to negative images, aversive sounds, and negative social interactions; and cognitive control domain includes responses during working memory, response inhibition, and attention switching tasks. For each subdomain, we included three independent studies using similar experimental manipulations, with 15 randomly sampled participants per study (total *k=36* study contrasts, *n=540*). This hierarchical and balanced design allows us to dissociate insula sub-areas that are selective for a specific domain and those that generalize across all four domains. See Supplementary Table 4 for a full list of studies included in the current dataset.

The current study was a mega-analysis of multiple independent studies. Participants were recruited independently for each study and informed consent was provided by all subjects in accordance with local ethics and institutional review boards. Descriptions of ethics approvals, image acquisition, and demographics are described briefly for all studies in Supplementary Table 4 and in full detail in the corresponding references (see also the Life Sciences Reporting Summary).

Data harmonization

To address potential differences in data scaling across studies, we employed a two-part analytic strategy capturing both global and local functional properties: (1) we analyze global insular activation to identify domain differences in overall engagement using mean activation values, and (2) we analyze relative local patterns after normalization to identify regions preferentially engaged by specific domains. This dual approach is necessary because some domains may produce widespread activation that could mask more subtle selective patterns in other domains.

To implement this strategy, we first resampled all data into a reference space (Study 1[176]) and analyzed the mean activation values normalized by each study's average voxelwise between-subject SD to assess differences in whole-insula activation between domains, preserving information about global activation patterns before normalization.

Next, we applied within-subject z-score normalization across voxels within the insula to examine relative local patterns. By analyzing patterns of values across voxels instead of absolute intensities, this approach accounts for idiosyncrasies in the scale of activity across studies, influenced by factors including differences in acquisition, preprocessing, voxel size, contrast weights, and other nuisance factors. This implies that local activity estimates are lower in images with more overall activations across the insula, leading to more conservative results, as domain convergence and selectivity analyses are performed on the relative activation maps.

We chose z-scoring after considering several alternative harmonization methods including ComBat[177], L2 normalization, and standard deviation normalization. These alternatives were either not applicable due to the nested relationship between scanning parameters and tasks, or did not significantly improve harmonization (see Supplementary Methods for detailed discussion of harmonization approaches and their limitations). Similar normalization procedures are common in multivariate pattern analysis in fMRI and in machine learning and multivariate statistics more broadly (e.g., in profile analysis)[178–180]. Here, it allows us to focus on relative differences in brain patterns across the four mental constructs while minimizing the impact of study-specific factors.

Multiclass support vector machine classifier

We trained multi-class linear Support Vector Machine (SVM) classifiers with 5-fold cross-validation for hyperparameter optimization (box constraint). The classifiers were trained to discriminate each domain from the others (one vs. all scheme) using two studies per subdomain for training and a third study as an independent test set for domain and subdomain-level evaluations (e.g., pain from all other domains, thermal pain from all other subdomains). To estimate out-of-study generalization error, we systematically sampled different studies for training and test sets by leaving a different study out in each subdomain for each model, training 100 models in total with splits stratified by subdomain, and reported the average performance on the test sets (see Supplementary Fig. 11 for a schematic description of study selection).

Bayes Factors

We calculated Bayes Factors (BFs) at the voxel level using Bayes Factor one-sample t-test with the Jeffrey-Zellner-Siow prior (JZS, Cauchy distribution on effect size; ref.[65]) to identify voxels in the insula exhibiting domain-general or domain-selective activation patterns. For each domain, we aggregated data across all three subdomains, yielding n=135 samples per domain (3 subdomains × 3 studies × 15 participants). BF directly compares the probability of the data under two competing hypotheses: the alternative hypothesis (an effect exists) versus the null hypothesis (no effect).

First, the Bayes Factor for a one-sample t-test (with n=135 per domain, aggregating across 3 subdomains × 3 studies × 15 participants) is calculated as follows (Equation 1):

$$B_{01} = \frac{\left(1+\frac{t^2}{\nu}\right)^{-(\nu+1)/2}}{\int_0^\infty (1+Ng)^{-1/2}\left(1+\frac{t^2}{(1+Ng)\,\nu}\right)^{-(\nu+1)/2} (2\pi)^{-1/2}\, g^{-3/2}\, e^{-1/(2g)}\, dg} \quad (1)$$

where t is the t-statistic, N is the sample size, ν is the degrees of freedom ($N-1$), and r is the scale factor (set to 0.707, indicating a moderate expected effect size; refs.[65,98]).

We set thresholds at *BF>4.32* for an effect and *BF<0.23* (an inverse of 4.32) for no effect, corresponding to 4.32:1 odds. This decision was supported by previous literature suggesting that Bayes Factors with JZS between 3 and 10 are considered moderate-level evidence[181–183]. These thresholds were chosen to ensure the identification of effects and null effects, minimizing the potential for false positives while maintaining sensitivity to true effects.

Voxels were considered activated only when showing both *BF>4.32* and positive t-statistics. The spatial extent and configuration of functional zones remained stable across a range of thresholds (Supplementary Fig. 12). Evidence for no activation included cases of either evidence for no effect (*BF<4.32* with either positive or negative t-statistics) or evidence for deactivation effect (*BF>4.32* with negative t-statistics). By conjunction of BFs across all domains, domain-general voxels required activation across all domains, while domain-selective voxels required activation in their designated domain and evidence for no activation in other domains. Specifically, domain-general voxels were defined as those with *BF>4.32* and *t>0* across all domains. Domain-selective voxels were defined as those with 1) *BF>4.32* and *t>0* for the designated domain, and 2) *BF<0.23* or *BF>4.32* and *t<0* for the other domains.

Anatomical definition of insula

For our primary analyses, we defined the insula based on established anatomical landmarks, including the three short gyri of the anterior insula (anterior, middle, and posterior short gyri), the two long gyri of the posterior insula (anterior and posterior long gyri), and the anterior inferior cortex, bounded by the peri-insula sulcus that separates the insula from surrounding opercula. Given ongoing debates about insular boundaries and functional connectivity with adjacent opercular regions, we conducted supplementary analyses using an expanded anatomical definition. This expanded mask included the

insula proper plus adjacent opercular regions (OP3, OP5, OP7, and OP9) from 2 different atlases: HCP-MMP1.0[184] from the Human Connectome Project (HCP)[155] and Julich-Brain Cytoarchitectonic Atlas[23,68]. This tested whether our main findings depend on specific anatomical definitions (see Supplementary Methods and Supplementary Fig. 7).

Validation with independent datasets

To validate the identified functional zones, we tested activations in each zone using independent validation datasets selected from the ANiC database (after our primary dataset was finalized) and from open data repositories (e.g., Human Connectome Project (HCP)[155]) when domain-specific data were unavailable in the database. We selected one study per domain known to robustly and selectively engage that domain: thermal pain stimulation for pain (*n=51*; high pain)[82], Monetary Incentive Delay task for appetitive processes (*n=32*; monetary reward anticipation)[83], viewing of negative images for aversive processes (*n=160*; viewing of negative images selected from the International Affective Picture System (IAPS))[84], and n-back working memory task from the HCP dataset for cognitive control (*n=365*, restricted to genetically unrelated participants; 2-back (place))[85]. See Supplementary Table 5 for detailed study information.

Validation data underwent identical quality control procedures and preprocessing pipelines as the primary datasets. We analyzed global activation patterns by comparing the mean/SD values across domains to test whether domain differences in overall insular activation replicated. We then extracted mean activation values from the five functional zones identified in our primary analysis (one domain-general zone and four domain-selective zones). For domain-selective zones, we assessed selectivity by comparing activation in the target domain against pooled off-target domains. For domain-general zones, we tested whether each domain showed significant activation above zero.

Neurosynth functional decoding

We examined spatial correlations between the identified insular zones and two types of meta-analytic maps: 525 term and 50 topic association test maps that show voxels preferentially associated with studies related to particular psychological terms or topics. Topic maps were streamlined from a set of 100 topics (“vs-topics-100”) that were extracted using Latent Dirichlet Allocation (LDA) from abstracts of all articles in the Neurosynth database as of July, 2015 (11,406 articles), after excluding non-psychologically relevant topics. We used standardized point-biserial correlations to calculate spatial correlations between our identified insular zones and these two types of meta-analytic maps for topics and terms. Correlation coefficients were z-scored within each zone to examine the relative strength of correlations across topics for each zone. We report topics showing standardized correlation>1 and the top 10 highest and lowest correlating terms for each insular zone. See Supplementary Table 2 for a full list of Neurosynth topic maps used in the current analysis.

Neurosynth functional diversity analysis

To assess functional diversity across brain regions, we used the uniformity test maps from the same set of 50 topics, which show voxels consistently activated across studies associated with each topic. For each brain voxel, we calculated the proportion of topics showing significant activation. Voxels were

then ranked brain-wide based on this proportion to quantify their functional diversity across psychological topics.

Coactivation between the insula and other brain areas

We performed a meta-analytic coactivation analysis using activation coordinates from 27,072 studies registered in the Neurosynth repository as of April, 2022. We created meta-analytic binary activation maps using Multi-level kernel density Analysis (MKDA; ref.[185]) with a 4-mm smoothing kernel. In these maps, a voxel was coded as active for a study if the reported peak coordinate was within 4-mm of the given voxel. Using these meta-analytic activation maps, we calculated point-biserial correlations between each domain-general and domain-selective insular zone and each voxel in the cortical and subcortical regions of the whole brain, excluding the insula. The resulting correlations were thresholded at *FDR-corrected q<0.001* and cluster size>100 voxels. Voxels above the threshold were assigned to one of the insular zones based on which zone showed the maximum correlation, provided that the maximum correlation with one of the insular zones was at least 10% higher than the next highest correlation.

To examine the relationship between the coactivated regions and seven resting-state networks (combined from refs.[87–89]), we calculated the percentage of voxels in the thresholded coactivated regions that overlapped with each of the seven resting-state networks in the cortical, subcortical, and cerebellar regions. A supplementary analysis using unthresholded coactivation maps is provided in Supplementary Fig. 13.

Cytoarchitectonic profiling

To determine the best matching cytoarchitectonic parcel for each insular zone, we calculated spatial overlap between each insular zone and each atlas parcel from the Julich-Brain Cytoarchitectonic Atlas[23,68] (see Fig. 6) using the Dice Coefficient (DC), a measure ranging from 0 (no intersection) to 1 (complete intersection). This atlas includes 16 distinct parcels in the insula based on their common cytoarchitectonic characteristics (granular, dysgranular, and agranular). We selected parcels with a DC higher than 0.1 to report and note which group each insular zone is predominantly associated with.

Neurotransmitter system profiling

We used a comprehensive receptor and transporter binding map atlas (Neuromaps[73,74]) that contains 40 PET-derived binding maps covering 19 neurotransmitter receptors and transporters and 9 systems in over 1,200 healthy individuals. The atlas includes maps for the following receptors and transporters (transporters indicated with *): α4β2, M1, VAChT* (acetylcholine); CB1 (cannabinoid); D1, D2, D3, DAT* (dopamine); GABAA/BZ (GABA); mGluR5, NMDA (glutamate); H3 (histamine); NET (norepinephrine); MOR (opioid); 5-HT1a, 5-HT1b, 5-HT2a, 5-HT4, 5-HT6, 5-HTT* (serotonin). Here we used 36 images after removing 4 images due to issues found during implementation.

We calculated point-biserial correlations between each insular zone and each receptor and transporter map in the atlas. Higher correlations indicate the relatively greater density of a given neurotransmitter receptor/transporter. To evaluate the significance and error variability of associations, we bootstrapped

each domain-general and selective insular map for 100 iterations. For each iteration, we resampled individual contrast maps and regenerated four insular maps for each domain based on these bootstrap samples. Spatial correlations were then calculated between each bootstrapped insular map and each PET binding map, reporting the mean and standard deviation of these spatial correlations across the 100 bootstrap samples as an estimate of the standard error. For the representativeness of the results, we only interpret the results where 1) there is more than one study on the same neurotransmitter receptor or transporter, and 2) the results from all studies on the same neurotransmitter receptor or transporter are in agreement. We made exceptions for cases showing meaningful associations based on previous literature. We applied the same approach to the coactivated extra-insular regions of each insular zone. For each insular zone, we computed Pearson's correlations between its neurotransmitter receptor profile (pattern of receptor densities across different systems) and the receptor profile of its corresponding coactivated regions to test for shared patterns of receptor/transporter distributions.

Data availability

The fMRI data from the main-analysis studies 1, 2, 4, 5, 7, 8, 19, 20, 22, 23, 25, 26, 28, 29, 31, and 32 are available at https://doi.org/10.6084/m9.figshare.24033402.v2. Data from studies 3 and 6 are available at https://neurovault.org/collections/8707/. Data from the validation dataset for cognitive control (n-back working memory task) are available from the Human Connectome Project database. The remaining datasets are available upon request from the corresponding authors of the individual studies. The Neurosynth dataset is available at https://github.com/canlab/Neuroimaging_Pattern_Masks/tree/master/neurosynth, the cytoarchitecture maps at https://github.com/canlab/Neuroimaging_Pattern_Masks/tree/master/Atlases_and_parcellations/2020_JulichBrain_v3.0.3, and the neurotransmitter receptor/transporter maps at https://github.com/canlab/Neuroimaging_Pattern_Masks/tree/master/Atlases_and_parcellations/2022_Hansen_PET_tracer_maps. Source data are provided with this paper.

Code availability

Matlab code for implementing all analyses is available at https://github.com/canlab/ and https://github.com/mijinjkwon/proj_insula_anic.

References

1. Mesulam, M.-M. & Mufson, E. J. Insula of the old world monkey. III: Efferent cortical output and comments on function. *J. Comp. Neurol.* **212**, 38–52 (1982).
2. Mufson, E. J. & Mesulam, M.-M. Insula of the old world monkey. II: Afferent cortical input and comments on the claustrum. *J. Comp. Neurol.* **212**, 23–37 (1982).
3. Augustine, J. R. Circuitry and functional aspects of the insular lobe in primates including humans. *Brain Res. Rev.* **22**, 229–244 (1996).
4. Kurth, F., Zilles, K., Fox, P. T., Laird, A. R. & Eickhoff, S. B. A link between the systems: functional differentiation and integration within the human insula revealed by meta-analysis. *Brain Struct. Funct.* **214**, 519–534 (2010).
5. Nieuwenhuys, R. Chapter 7 - The insular cortex: A review. in *Progress in Brain Research* (eds Hofman, M. A. & Falk, D.) vol. 195 123–163 (Elsevier, 2012).
6. Stephani, C., Vaca, G. F.-B., MacIunas, R., Koubeissi, M. Z. & Luders, H. Functional neuroanatomy of the insular lobe. *Brain Struct. Funct.* https://doi.org/10.1007/S00429-010-0296-3 (2011) doi:10.1007/S00429-010-0296-3.
7. Türe, U., Yaşargil, D. C., Al-Mefty, O. & Yaşargil, M. G. Topographic anatomy of the insular region. *J. Neurosurg.* **90**, 720–733 (1999).
8. Centanni, S. W., Janes, A. C., Haggerty, D. L., Atwood, B. & Hopf, F. W. Better living through understanding the insula: Why subregions can make all the difference. *Neuropharmacology* **198**, 108765 (2021).
9. Cerliani, L. *et al.* Probabilistic tractography recovers a rostrocaudal trajectory of connectivity variability in the human insular cortex. *Hum. Brain Mapp.* **33**, 2005–2034 (2012).
10. Cloutman, L. L., Binney, R. J., Drakesmith, M., Parker, G. J. M. & Lambon Ralph, M. A. The variation of function across the human insula mirrors its patterns of structural connectivity: Evidence from in vivo probabilistic tractography. *NeuroImage* **59**, 3514–3521 (2012).

11. Ghaziri, J. *et al.* The Corticocortical Structural Connectivity of the Human Insula. *Cereb. Cortex* **27**, 1216–1228 (2017).
12. Ghaziri, J. *et al.* Subcortical structural connectivity of insular subregions. *Sci. Rep.* **8**, 8596 (2018).
13. Jakab, A., Molnár, P. P., Bogner, P., Béres, M. & Berényi, E. L. Connectivity-based parcellation reveals interhemispheric differences in the insula. *Brain Topogr.* **25**, 264–271 (2012).
14. Mesulam, M.-M. & Mufson, E. J. The Insula of Reil in Man and Monkey. in *Association and Auditory Cortices* (eds Peters, A. & Jones, E. G.) 179–226 (Springer US, Boston, MA, 1985). doi:10.1007/978-1-4757-9619-3_5.
15. Nomi, J. S., Schettini, E., Broce, I., Dick, A. S. & Uddin, L. Q. Structural Connections of Functionally Defined Human Insular Subdivisions. *Cereb. Cortex* **28**, 3445–3456 (2018).
16. Deen, B., Pitskel, N. B. & Pelphrey, K. A. Three Systems of Insular Functional Connectivity Identified with Cluster Analysis. *Cereb. Cortex* **21**, 1498–1506 (2011).
17. Cauda, F. *et al.* Meta-analytic clustering of the insular cortex. Characterizing the meta-analytic connectivity of the insula when involved in active tasks. *NeuroImage* https://doi.org/10.1016/J.NEUROIMAGE.2012.04.012 (2012) doi:10.1016/J.NEUROIMAGE.2012.04.012.
18. Kelly, C. *et al.* A convergent functional architecture of the insula emerges across imaging modalities. *NeuroImage* **61**, 1129–1142 (2012).
19. Chang, L. J., Yarkoni, T., Khaw, M. W. & Sanfey, A. G. Decoding the Role of the Insula in Human Cognition: Functional Parcellation and Large-Scale Reverse Inference. *Cereb. Cortex* **23**, 739–749 (2013).
20. Uddin, L. Q., Kinnison, J., Pessoa, L. & Anderson, M. L. Beyond the Tripartite Cognition–Emotion–Interoception Model of the Human Insular Cortex. *J. Cogn. Neurosci.* **26**, 16–27 (2014).
21. Nomi, J. S. *et al.* Dynamic functional network connectivity reveals unique and overlapping profiles of insula subdivisions. *Hum. Brain Mapp.* **37**, 1770–1787 (2016).

22. Tian, Y. & Zalesky, A. Characterizing the functional connectivity diversity of the insula cortex: Subregions, diversity curves and behavior. *NeuroImage* **183**, 716–733 (2018).

23. Quabs, J. *et al.* Cytoarchitecture, probability maps and segregation of the human insula. *NeuroImage* **260**, 119453 (2022).

24. Dalley, J. W., Cardinal, R. N. & Robbins, T. W. Prefrontal executive and cognitive functions in rodents: neural and neurochemical substrates. *Neurosci. Biobehav. Rev.* **28**, 771–784 (2004).

25. Koren, T. *et al.* Insular cortex neurons encode and retrieve specific immune responses. *Cell* **184**, 5902-5915.e17 (2021).

26. Qadir, H. *et al.* Structural Connectivity of the Anterior Cingulate Cortex, Claustrum, and the Anterior Insula of the Mouse. *Front. Neuroanat.* **12**, (2018).

27. Tsai, P.-J. *et al.* Converging Structural and Functional Evidence for a Rat Salience Network. *Biol. Psychiatry* **88**, 867–878 (2020).

28. Duong, A. *et al.* Subjective states induced by intracranial electrical stimulation matches the cytoarchitectonic organization of the human insula. *Brain Stimulat.* **16**, 1653–1665 (2023).

29. Liberati, G. *et al.* Insular responses to transient painful and non-painful thermal and mechanical spinothalamic stimuli recorded using intracerebral EEG. *Sci. Rep.* **10**, 22319 (2020).

30. Mazzola, L., Mauguière, F. & Isnard, J. Electrical Stimulations of the Human Insula: Their Contribution to the Ictal Semiology of Insular Seizures. *J. Clin. Neurophysiol. Off. Publ. Am. Electroencephalogr. Soc.* **34**, 307–314 (2017).

31. Mazzola, L., Mauguière, F. & Isnard, J. Functional mapping of the human insula: Data from electrical stimulations. *Rev. Neurol. (Paris)* **175**, 150–156 (2019).

32. Picard, F., Bossaerts, P. & Bartolomei, F. Epilepsy and Ecstatic Experiences: The Role of the Insula. *Brain Sci.* **11**, 1384 (2021).

33. Rachidi, I. *et al.* The Insula: A Stimulating Island of the Brain. *Brain Sci.* **11**, 1533 (2021).

34. Barrett, L. F. & Simmons, W. K. Interoceptive predictions in the brain. *Nat. Rev. Neurosci.* **16**,

419–429 (2015).

35. Seth, A. K. Interoceptive inference, emotion, and the embodied self. *Trends Cogn. Sci.* **17**, 565–573 (2013).
36. Damasio, A. R. The Brain Binds Entities and Events by Multiregional Activation from Convergence Zones. *Neural Comput.* **1**, 123–132 (1989).
37. Simmons, W. K. & Barsalou, L. W. The Similarity-in-Topography Principle: Reconciling Theories of Conceptual Deficits. *Cogn. Neuropsychol.* **20**, 451 (2003).
38. Craig, A. D. How do you feel? Interoception: the sense of the physiological condition of the body. *Nat. Rev. Neurosci.* **3**, 655–666 (2002).
39. Craig, A. D. How do you feel — now? The anterior insula and human awareness. *Nat. Rev. Neurosci.* **10**, 59–70 (2009).
40. Varela, F. J., Thompson, E. & Rosch, E. *The Embodied Mind: Cognitive Science and Human Experience*. xx, 308 (The MIT Press, Cambridge, MA, US, 1991).
41. Wilson, M. Six views of embodied cognition. *Psychon. Bull. Rev.* **9**, 625–636 (2002).
42. Yarkoni, T., Poldrack, R. A., Nichols, T. E., Van Essen, D. C. & Wager, T. D. Large-scale automated synthesis of human functional neuroimaging data. *Nat. Methods* **8**, 665–670 (2011).
43. Honey, C. J. *et al.* Slow Cortical Dynamics and the Accumulation of Information over Long Timescales. *Neuron* **76**, 423–434 (2012).
44. Jain, S. *et al.* Interpretable multi-timescale models for predicting fMRI responses to continuous natural speech. in *Advances in Neural Information Processing Systems* vol. 33 13738–13749 (Curran Associates, Inc., 2020).
45. Menon, V. & Uddin, L. Q. Saliency, switching, attention and control: a network model of insula function. *Brain Struct. Funct.* **214**, 655–667 (2010).
46. Mayer, E. A., Naliboff, B. D. & Craig, A. D. B. Neuroimaging of the Brain-Gut Axis: From Basic Understanding to Treatment of Functional GI Disorders. *Gastroenterology* **131**, 1925–1942

(2006).

47. Van Oudenhove, L., Coen, S. J. & Aziz, Q. Functional brain imaging of gastrointestinal sensation in health and disease. *World J. Gastroenterol. WJG* **13**, 3438–3445 (2007).
48. Eisenberger, N. I., Moieni, M., Inagaki, T. K., Muscatell, K. A. & Irwin, M. R. In Sickness and in Health: The Co-Regulation of Inflammation and Social Behavior. *Neuropsychopharmacology* **42**, 242–253 (2017).
49. Rolls, A. Immunoception: the insular cortex perspective. *Cell. Mol. Immunol.* **20**, 1270–1276 (2023).
50. Tracey, K. J. The inflammatory reflex. *Nature* **420**, 853–859 (2002).
51. Critchley, H. D., Wiens, S., Rotshtein, P., Öhman, A. & Dolan, R. J. Neural systems supporting interoceptive awareness. *Nat. Neurosci.* **7**, 189–195 (2004).
52. Garfinkel, S. N., Seth, A. K., Barrett, A. B., Suzuki, K. & Critchley, H. D. Knowing your own heart: Distinguishing interoceptive accuracy from interoceptive awareness. *Biol. Psychol.* **104**, 65–74 (2015).
53. Hassanpour, M. S. *et al.* The Insular Cortex Dynamically Maps Changes in Cardiorespiratory Interoception. *Neuropsychopharmacology* **43**, 426–434 (2018).
54. Brooks, J. C. W. & Tracey, I. The insula: A multidimensional integration site for pain. *Pain* **128**, 1–2 (2007).
55. Labrakakis, C. The Role of the Insular Cortex in Pain. *Int. J. Mol. Sci.* **24**, 5736 (2023).
56. Mazzola, L., Isnard, J., Peyron, R. & Mauguière, F. Stimulation of the human cortex and the experience of pain: Wilder Penfield's observations revisited. *Brain* **135**, 631–640 (2012).
57. Ostrowsky, K. *et al.* Representation of pain and somatic sensation in the human insula: a study of responses to direct electrical cortical stimulation. *Cereb. Cortex* https://doi.org/10.1093/CERCOR/12.4.376 (2002) doi:10.1093/CERCOR/12.4.376.
58. Veldhuizen, M. G., Nachtigal, D., Teulings, L., Gitelman, D. R. & Small, D. M. The Insular Taste

Cortex Contributes to Odor Quality Coding. *Front. Hum. Neurosci.* **4**, (2010).

59. Small, D. M. Taste representation in the human insula. *Brain Struct. Funct.* **214**, 551–561 (2010).
60. Allman, J. M. *et al.* The von Economo neurons in frontoinsular and anterior cingulate cortex in great apes and humans. *Brain Struct. Funct.* https://doi.org/10.1007/S00429-010-0254-0 (2010) doi:10.1007/S00429-010-0254-0.
61. Evrard, H. C., Forro, T. & Logothetis, N. K. Von Economo Neurons in the Anterior Insula of the Macaque Monkey. *Neuron* https://doi.org/10.1016/J.NEURON.2012.03.003 (2012) doi:10.1016/J.NEURON.2012.03.003.
62. Hong, Y.-W., Yoo, Y., Han, J., Wager, T. D. & Woo, C.-W. False-positive neuroimaging: Undisclosed flexibility in testing spatial hypotheses allows presenting anything as a replicated finding. *NeuroImage* **195**, 384–395 (2019).
63. Salimi-Khorshidi, G., Smith, S. M., Keltner, J. R., Wager, T. D. & Nichols, T. E. Meta-analysis of neuroimaging data: A comparison of image-based and coordinate-based pooling of studies. *NeuroImage* **45**, 810–823 (2009).
64. Cronbach, L. J. & Meehl, P. E. Construct validity in psychological tests. *Psychol. Bull.* **52**, 281–302 (1955).
65. Rouder, J. N., Speckman, P. L., Sun, D., Morey, R. D. & Iverson, G. Bayesian t tests for accepting and rejecting the null hypothesis. *Psychon. Bull. Rev.* **16**, 225–237 (2009).
66. Kober, H. *et al.* Functional grouping and cortical–subcortical interactions in emotion: A meta-analysis of neuroimaging studies. *NeuroImage* **42**, 998–1031 (2008).
67. Laird, A. R. *et al.* Networks of task co-activations. *NeuroImage* **80**, 505–514 (2013).
68. Amunts, K., Mohlberg, H., Bludau, S. & Zilles, K. Julich-Brain: A 3D probabilistic atlas of the human brain's cytoarchitecture. *Science* **369**, 988–992 (2020).
69. Hein, M., Mohlberg, H., Bludau, S., Quabs, J. & Amunts, K. Probabilistic cytoarchitectonic map of Area Ia3 (Insula) (v4.0). EBRAINS https://doi.org/10.25493/QS00-PJ9 (2021).

70. Hein, M., Mohlberg, H., Bludau, S., Quabs, J. & Amunts, K. Probabilistic cytoarchitectonic map of Area Ia2 (Insula) (v4.0). EBRAINS https://doi.org/10.25493/BMNK-B8F (2021).

71. Hein, M., Mohlberg, H., Bludau, S., Quabs, J. & Amunts, K. Probabilistic cytoarchitectonic map of Area Id9 (Insula) (v4.0). EBRAINS https://doi.org/10.25493/JMCR-ZNQ (2021).

72. Kurth, F. *et al.* Cytoarchitecture and probabilistic maps of the human posterior insular cortex. *Cereb. Cortex* https://doi.org/10.1093/CERCOR/BHP208 (2010) doi:10.1093/CERCOR/BHP208.

73. Hansen, J. Y. *et al.* Mapping neurotransmitter systems to the structural and functional organization of the human neocortex. *Nat. Neurosci.* https://doi.org/10.1038/s41593-022-01186-3 (2022) doi:10.1038/s41593-022-01186-3.

74. Markello, R. D. *et al.* neuromaps: structural and functional interpretation of brain maps. *Nat. Methods* 1–8 (2022) doi:10.1038/s41592-022-01625-w.

75. Decot, H. K. *et al.* Coordination of Brain-Wide Activity Dynamics by Dopaminergic Neurons. *Neuropsychopharmacology* **42**, 615–627 (2017).

76. Bolt, T. *et al.* Autonomic physiological coupling of the global fMRI signal. *Nat. Neurosci.* **28**, 1327–1335 (2025).

77. Faillenot, I., Heckemann, R. A., Frot, M. & Hammers, A. Macroanatomy and 3D probabilistic atlas of the human insula. *NeuroImage* **150**, 88–98 (2017).

78. Margulies, D. S. *et al.* Situating the default-mode network along a principal gradient of macroscale cortical organization. *Proc. Natl. Acad. Sci.* **113**, 12574–12579 (2016).

79. Garcia-Larrea, L. *et al.* Operculo-insular pain (parasylvian pain): a distinct central pain syndrome. *Brain* **133**, 2528–2539 (2010).

80. Segerdahl, A. R., Mezue, M., Okell, T. W., Farrar, J. T. & Tracey, I. The dorsal posterior insula subserves a fundamental role in human pain. *Nat. Neurosci.* https://doi.org/10.1038/NN.3969 (2015) doi:10.1038/NN.3969.

81. Quabs, J., Bittner, N. & Caspers, S. Structural Connectivity Differences Reflect Microstructural

Heterogeneity of the Human Insular Cortex. *Hum. Brain Mapp.* **46**, e70231 (2025).

82. Woo, C.-W. *et al.* Separate neural representations for physical pain and social rejection. *Nat. Commun.* **5**, 5380 (2014).
83. MacNiven, K. H. *et al.* Association of Neural Responses to Drug Cues With Subsequent Relapse to Stimulant Use. *JAMA Netw. Open* **1**, e186466 (2018).
84. Gianaros, P. J. *et al.* Affective brain patterns as multivariate neural correlates of cardiovascular disease risk. *Soc. Cogn. Affect. Neurosci.* **15**, 1034–1045 (2020).
85. Barch, D. M. *et al.* Function in the human connectome: Task-fMRI and individual differences in behavior. *NeuroImage* **80**, 169–189 (2013).
86. Knutson, B., Adams, C. M., Fong, G. W. & Hommer, D. Anticipation of Increasing Monetary Reward Selectively Recruits Nucleus Accumbens. *J. Neurosci.* **21**, RC159–RC159 (2001).
87. Buckner, R. L., Krienen, F. M., Castellanos, A., Diaz, J. C. & Yeo, B. T. T. The organization of the human cerebellum estimated by intrinsic functional connectivity. *J. Neurophysiol.* **106**, 2322–2345 (2011).
88. Choi, E. Y., Yeo, B. T. T. & Buckner, R. L. The organization of the human striatum estimated by intrinsic functional connectivity. *J. Neurophysiol.* **108**, 2242–2263 (2012).
89. Yeo, B. T. *et al.* The organization of the human cerebral cortex estimated by intrinsic functional connectivity. *J. Neurophysiol.* **106**, 1125–1165 (2011).
90. Kragel, P. & Wager, T. D. Reproducible, Generalizable Brain Models of Affective Processes. in *Emotion in the Mind and Body* (eds Neta, M. & Haas, I. J.) 221–263 (Springer International Publishing, Cham, 2019). doi:10.1007/978-3-030-27473-3_8.
91. Wager, T. D. *et al.* An fMRI-Based Neurologic Signature of Physical Pain. *N. Engl. J. Med.* **368**, 1388–1397 (2013).
92. Satpute, A. B. *et al.* Involvement of Sensory Regions in Affective Experience: A Meta-Analysis. *Front. Psychol.* **6**, (2015).

93. Čeko, M., Kragel, P. A., Woo, C.-W., López-Solà, M. & Wager, T. D. Common and stimulus-type-specific brain representations of negative affect. *Nat. Neurosci.* **25**, 760–770 (2022).

94. Kragel, P. A., Reddan, M. C., LaBar, K. S. & Wager, T. D. Emotion schemas are embedded in the human visual system. *Sci. Adv.* 16 (2019).

95. Gluth, S., Rieskamp, J. & Büchel, C. Deciding when to decide: time-variant sequential sampling models explain the emergence of value-based decisions in the human brain. *J. Neurosci. Off. J. Soc. Neurosci.* **32**, 10686–10698 (2012).

96. Hutcherson, C. A. & Tusche, A. Evidence accumulation, not 'self-control', explains dorsolateral prefrontal activation during normative choice. *eLife* **11**, e65661 (2022).

97. Pauli, W. M., O'Reilly, R. C., Yarkoni, T. & Wager, T. D. Regional specialization within the human striatum for diverse psychological functions. *Proc. Natl. Acad. Sci.* **113**, 1907–1912 (2016).

98. Bo, K. *et al.* A systems identification approach using Bayes factors to deconstruct the brain bases of emotion regulation. *Nat. Neurosci.* 1–13 (2024) doi:10.1038/s41593-024-01605-7.

99. Hansen, J. Y. *et al.* Mapping gene transcription and neurocognition across human neocortex. *Nat. Hum. Behav.* **5**, 1240–1250 (2021).

100. Kuehn, E., Mueller, K., Lohmann, G. & Schuetz-Bosbach, S. Interoceptive awareness changes the posterior insula functional connectivity profile. *Brain Struct. Funct.* **221**, 1555–1571 (2016).

101. Krockenberger, M. S., Saleh-Mattesich, T. O. & Evrard, H. C. Cytoarchitectonic and connection stripes in the dysgranular insular cortex in the macaque monkey. *J. Comp. Neurol.* **531**, 2019–2043 (2023).

102. Selemon, L. D. & Goldman-Rakic, P. S. Common cortical and subcortical targets of the dorsolateral prefrontal and posterior parietal cortices in the rhesus monkey: evidence for a distributed neural network subserving spatially guided behavior. *J. Neurosci.* **8**, 4049–4068 (1988).

103. Burton, H., Fabri, M. & Alloway, K. Cortical areas within the lateral sulcus connected to cutaneous

representations in areas 3b and 1: A revised interpretation of the second somatosensory area in macaque monkeys. *J. Comp. Neurol.* **355**, 539–562 (1995).

104. Badre, D. & D'Esposito, M. Functional Magnetic Resonance Imaging Evidence for a Hierarchical Organization of the Prefrontal Cortex. *J. Cogn. Neurosci.* **19**, 2082–2099 (2007).
105. Christoff, K., Keramatian, K., Gordon, A. M., Smith, R. & Mädler, B. Prefrontal organization of cognitive control according to levels of abstraction. *Brain Res.* **1286**, 94–105 (2009).
106. Dixon, M. L., Fox, K. C. R. & Christoff, K. Evidence for rostro-caudal functional organization in multiple brain areas related to goal-directed behavior. *Brain Res.* **1572**, 26–39 (2014).
107. Koechlin, E., Ody, C. & Kouneiher, F. The Architecture of Cognitive Control in the Human Prefrontal Cortex. *Science* **302**, 1181–1185 (2003).
108. Kim, H. F. & Hikosaka, O. Distinct Basal Ganglia Circuits Controlling Behaviors Guided by Flexible and Stable Values. *Neuron* **79**, 1001–1010 (2013).
109. Chang, L. J., Gianaros, P. J., Manuck, S. B., Krishnan, A. & Wager, T. D. A Sensitive and Specific Neural Signature for Picture-Induced Negative Affect. *PLOS Biol.* **13**, e1002180 (2015).
110. Kragel, P. A., Koban, L., Barrett, L. F. & Wager, T. D. Representation, Pattern Information, and Brain Signatures: From Neurons to Neuroimaging. *Neuron* **99**, 257–273 (2018).
111. van't Hof, S. R. *et al.* The Brain Activation-Based Sexual Image Classifier (BASIC): A Sensitive and Specific fMRI Activity Pattern for Sexual Image Processing. *Cereb. Cortex N. Y. N 1991* **32**, 3014–3030 (2022).
112. Zhou, F. *et al.* A distributed fMRI-based signature for the subjective experience of fear. *Nat. Commun.* **12**, 6643 (2021).
113. Smith, S. M. *et al.* Correspondence of the brain's functional architecture during activation and rest. *Proc. Natl. Acad. Sci.* **106**, 13040–13045 (2009).
114. Tavor, I. *et al.* Task-free MRI predicts individual differences in brain activity during task performance. *Science* **352**, 216–220 (2016).

115. Finn, E. S. Is it time to put rest to rest? *Trends Cogn. Sci.* **25**, 1021–1032 (2021).

116. Greene, A. S., Gao, S., Noble, S., Scheinost, D. & Constable, R. T. How Tasks Change Whole-Brain Functional Organization to Reveal Brain-Phenotype Relationships. *Cell Rep.* **32**, (2020).

117. Zheng, W. *et al.* Pain-Evoked Reorganization in Functional Brain Networks. *Cereb. Cortex* **30**, 2804–2822 (2020).

118. Allen, W. E. *et al.* Thirst regulates motivated behavior through modulation of brainwide neural population dynamics. *Science* **364**, eaav3932 (2019).

119. Briggs, F., Mangun, G. R. & Usrey, W. M. Attention enhances synaptic efficacy and the signal-to-noise ratio in neural circuits. *Nature* **499**, 476–480 (2013).

120. Jung, W. B., Jiang, H., Lee, S. & Kim, S.-G. Dissection of brain-wide resting-state and functional somatosensory circuits by fMRI with optogenetic silencing. *Proc. Natl. Acad. Sci.* **119**, e2113313119 (2022).

121. Leong, A. T. L. *et al.* Long-range projections coordinate distributed brain-wide neural activity with a specific spatiotemporal profile. *Proc. Natl. Acad. Sci.* **113**, E8306–E8315 (2016).

122. Tu, W., Ma, Z. & Zhang, N. Brain network reorganization after targeted attack at a hub region. *NeuroImage* **237**, 118219 (2021).

123. Adamic, E. M., Teed, A. R., Avery, J. A., Cruz, F. de la & Khalsa, S. S. Hemispheric divergence of interoceptive processing across psychiatric disorders. *eLife* **13**, (2024).

124. Adolfi, F. *et al.* Convergence of interoception, emotion, and social cognition: A twofold fMRI meta-analysis and lesion approach. *Cortex* **88**, 124–142 (2017).

125. Bastuji, H., Frot, M., Perchet, C., Hagiwara, K. & Garcia-Larrea, L. Convergence of sensory and limbic noxious input into the anterior insula and the emergence of pain from nociception. *Sci. Rep.* **8**, 13360 (2018).

126. Evrard, H. C. The Organization of the Primate Insular Cortex. *Front. Neuroanat.* **13**, (2019).

127. Garfinkel, S. N. & Critchley, H. D. Interoception, emotion and brain: new insights link internal

physiology to social behaviour. Commentary on: *Soc. Cogn. Affect. Neurosci.* **8**, 231–234 (2013).

128. Uddin, L. Q., Nomi, J. S., Hebert-Seropian, B., Ghaziri, J. & Boucher, O. Structure and function of the human insula. *J. Clin. Neurophysiol. Off. Publ. Am. Electroencephalogr. Soc.* **34**, 300–306 (2017).
129. Sabat, M., de Dampierre, C. & Tallon-Baudry, C. Evidence for domain-general arousal from semantic and neuroimaging meta-analyses reconciles opposing views on arousal. *Proc. Natl. Acad. Sci.* **122**, e2413808122 (2025).
130. Grodzinsky, Y. *et al.* Logical negation mapped onto the brain. *Brain Struct. Funct.* **225**, 19–31 (2020).
131. Yih, J., Beam, D. E., Fox, K. C. R. & Parvizi, J. Intensity of affective experience is modulated by magnitude of intracranial electrical stimulation in human orbitofrontal, cingulate and insular cortices. *Soc. Cogn. Affect. Neurosci.* **14**, 339–351 (2019).
132. Afif, A., Minotti, L., Kahane, P. & Hoffmann, D. Anatomofunctional organization of the insular cortex: A study using intracerebral electrical stimulation in epileptic patients. *Epilepsia* https://doi.org/10.1111/J.1528-1167.2010.02755.X (2010) doi:10.1111/J.1528-1167.2010.02755.X.
133. Soulier, H. *et al.* Visceral and emotional responses to direct electrical stimulations of the cortex. *Ann. Clin. Transl. Neurol.* **10**, 5–17 (2023).
134. Woo, C.-W. *et al.* Quantifying cerebral contributions to pain beyond nociception. *Nat. Commun.* **8**, 14211 (2017).
135. Segerdahl, A. R., Mezue, M., Okell, T. W., Farrar, J. T. & Tracey, I. The dorsal posterior insula subserves a fundamental role in human pain. *Nat. Neurosci.* https://doi.org/10.1038/NN.3969 (2015) doi:10.1038/NN.3969.
136. Frot, M., Magnin, M., Mauguière, F. & Garcia-Larrea, L. Human SII and Posterior Insula Differently Encode Thermal Laser Stimuli. *Cereb. Cortex* **17**, 610–620 (2007).

137. Mazzola, L., Isnard, J. & Mauguière, F. Somatosensory and pain responses to stimulation of the second somatosensory area (SII) in humans. A comparison with SI and insular responses. *Cereb. Cortex* https://doi.org/10.1093/CERCOR/BHJ038 (2006) doi:10.1093/CERCOR/BHJ038.

138. Mazzola, L., Isnard, J., Peyron, R., Guénot, M. & Mauguière, F. Somatotopic organization of pain responses to direct electrical stimulation of the human insular cortex. *Pain* https://doi.org/10.1016/J.PAIN.2009.07.014 (2009) doi:10.1016/J.PAIN.2009.07.014.

139. Goulas, A. *et al.* The natural axis of transmitter receptor distribution in the human cerebral cortex. *Proc. Natl. Acad. Sci.* **118**, e2020574118 (2021).

140. Palomero-Gallagher, N. & Zilles, K. Cortical layers: Cyto-, myelo-, receptor- and synaptic architecture in human cortical areas. *NeuroImage* **197**, 716–741 (2019).

141. Zachlod, D., Palomero-Gallagher, N., Dickscheid, T. & Amunts, K. Mapping Cytoarchitectonics and Receptor Architectonics to Understand Brain Function and Connectivity. *Biol. Psychiatry* **93**, 471–479 (2023).

142. Suárez, L. E., Markello, R. D., Betzel, R. F. & Misic, B. Linking Structure and Function in Macroscale Brain Networks. *Trends Cogn. Sci.* **24**, 302–315 (2020).

143. Zilles, K., Bacha-Trams, M., Palomero-Gallagher, N., Amunts, K. & Friederici, A. D. Common molecular basis of the sentence comprehension network revealed by neurotransmitter receptor fingerprints. *Cortex* **63**, 79–89 (2015).

144. Ferenczi, E. A. *et al.* Prefrontal cortical regulation of brainwide circuit dynamics and reward-related behavior. *Science* **351**, aac9698 (2016).

145. Giorgi, A. *et al.* Brain-wide Mapping of Endogenous Serotonergic Transmission via Chemogenetic fMRI. *Cell Rep.* **21**, 910–918 (2017).

146. Grimm, C. *et al.* Locus Coeruleus firing patterns selectively modulate brain activity and dynamics. 2022.08.29.505672 Preprint at https://doi.org/10.1101/2022.08.29.505672 (2022).

147. Hamada, H. T. *et al.* Optogenetic activation of dorsal raphe serotonin neurons induces brain-wide

activation. *Nat. Commun.* **15**, 4152 (2024).

148. Ioanas, H.-I., Saab, B. J. & Rudin, M. Whole-brain opto-fMRI map of mouse VTA dopaminergic activation reflects structural projections with small but significant deviations. *Transl. Psychiatry* **12**, 1–10 (2022).
149. Lohani, S., Poplawsky, A. J., Kim, S.-G. & Moghaddam, B. Unexpected global impact of VTA dopamine neuron activation as measured by opto-fMRI. *Mol. Psychiatry* **22**, 585–594 (2017).
150. Turchi, J. *et al.* The Basal Forebrain Regulates Global Resting-State fMRI Fluctuations. *Neuron* **97**, 940-952.e4 (2018).
151. Gustavson, D. E. *et al.* Executive functions and substance use: Relations in late adolescence and early adulthood. *J. Abnorm. Psychol.* **126**, 257–270 (2017).
152. Miyake, A., Friedman, N. P., Rettinger, D. A., Shah, P. & Hegarty, M. How are visuospatial working memory, executive functioning, and spatial abilities related? A latent-variable analysis. *J. Exp. Psychol. Gen.* **130**, 621–640 (2001).
153. Reineberg, A. E., Banich, M. T., Wager, T. D. & Friedman, N. P. Context-specific activations are a hallmark of the neural basis of individual differences in general executive function. *NeuroImage* **249**, 118845 (2022).
154. Casey, B. J. *et al.* The Adolescent Brain Cognitive Development (ABCD) study: Imaging acquisition across 21 sites. *Dev. Cogn. Neurosci.* **32**, 43–54 (2018).
155. Van Essen, D. C. *et al.* The Human Connectome Project: A data acquisition perspective. *NeuroImage* **62**, 2222–2231 (2012).
156. Miller, K. L. *et al.* Multimodal population brain imaging in the UK Biobank prospective epidemiological study. *Nat. Neurosci.* **19**, 1523–1536 (2016).
157. Shafto, M. A. *et al.* The Cambridge Centre for Ageing and Neuroscience (Cam-CAN) study protocol: a cross-sectional, lifespan, multidisciplinary examination of healthy cognitive ageing. *BMC Neurol.* **14**, 204 (2014).

158. Berardi, G. *et al.* Multi-Site Observational Study to Assess Biomarkers for Susceptibility or Resilience to Chronic Pain: The Acute to Chronic Pain Signatures (A2CPS) Study Protocol. *Front. Med.* **9**, (2022).

159. Kragel, P. A. *et al.* Generalizable representations of pain, cognitive control, and negative emotion in medial frontal cortex. *Nat. Neurosci.* **21**, 283–289 (2018).

160. Hassanpour, M. S. *et al.* How the heart speaks to the brain: neural activity during cardiorespiratory interoceptive stimulation. *Philos. Trans. R. Soc. B Biol. Sci.* **371**, 20160017 (2016).

161. Faull, O. K., Hayen, A. & Pattinson, K. T. S. Breathlessness and the body: Neuroimaging clues for the inferential leap. *Cortex* **95**, 211–221 (2017).

162. Ross, S. E. Pain and itch: insights into the neural circuits of aversive somatosensation in health and disease. *Curr. Opin. Neurobiol.* **21**, 880–887 (2011).

163. Napadow, V. *et al.* The Brain Circuitry Underlying the Temporal Evolution of Nausea in Humans. *Cereb. Cortex N. Y. NY* **23**, 806–813 (2013).

164. Farrell, M. J. & Mazzone, S. B. Sensations and regional brain responses evoked by tussive stimulation of the airways. *Respir. Physiol. Neurobiol.* **204**, 58–63 (2014).

165. Bolt, T. *et al.* Ontological Dimensions of Cognitive-Neural Mappings. *Neuroinformatics* **18**, 451–463 (2020).

166. Insel, T. *et al.* Research Domain Criteria (RDoC): Toward a New Classification Framework for Research on Mental Disorders. *Am. J. Psychiatry* **167**, 748–751 (2010).

167. Poldrack, R. A. & Yarkoni, T. From Brain Maps to Cognitive Ontologies: Informatics and the Search for Mental Structure. *Annu. Rev. Psychol.* **67**, 587–612 (2016).

168. Turner, J. A. & Laird, A. R. The Cognitive Paradigm Ontology: Design and Application. *Neuroinformatics* **10**, 57–66 (2012).

169. Lindquist, K. A., Wager, T. D., Kober, H., Bliss-Moreau, E. & Barrett, L. F. The brain basis of

emotion: A meta-analytic review. *Behav. Brain Sci.* **35**, 121–143 (2012).

170. Hayes, D. J. & Huxtable, A. G. Interpreting Deactivations in Neuroimaging. *Front. Psychol.* **3**, 27 (2012).
171. Frankenstein, U. *et al.* Activation and deactivation in blood oxygenation level dependent functional magnetic resonance imaging. *Concepts Magn. Reson. Part A* **16A**, 63–70 (2003).
172. Mishra, A. M. *et al.* Where fMRI and Electrophysiology Agree to Disagree: Corticothalamic and Striatal Activity Patterns in the WAG/Rij Rat. *J. Neurosci.* **31**, 15053–15064 (2011).
173. Viviani, R., Dommes, L., Bosch, J. E. & Labek, K. Segregation, connectivity, and gradients of deactivation in neural correlates of evidence in social decision making. *NeuroImage* **223**, 117339 (2020).
174. Hasson, U., Nusbaum, H. C. & Small, S. L. Task-dependent organization of brain regions active during rest. *Proc. Natl. Acad. Sci.* **106**, 10841–10846 (2009).
175. Van Oudenhove, L. *et al.* Common and distinct neural representations of aversive somatic and visceral stimulation in healthy individuals. *Nat. Commun.* **11**, 5939 (2020).
176. Atlas, L. Y., Bolger, N., Lindquist, M. A. & Wager, T. D. Brain Mediators of Predictive Cue Effects on Perceived Pain. *J. Neurosci.* **30**, 12964–12977 (2010).
177. Johnson, W. E., Li, C. & Rabinovic, A. Adjusting batch effects in microarray expression data using empirical Bayes methods. *Biostatistics* **8**, 118–127 (2007).
178. Haxby, J. V., Connolly, A. C. & Guntupalli, J. S. Decoding Neural Representational Spaces Using Multivariate Pattern Analysis. *Annu. Rev. Neurosci.* **37**, 435–456 (2014).
179. Kriegeskorte, N., Mur, M. & Bandettini, P. Representational similarity analysis - connecting the branches of systems neuroscience. *Front. Syst. Neurosci.* **2**, (2008).
180. Misaki, M., Kim, Y., Bandettini, P. A. & Kriegeskorte, N. Comparison of multivariate classifiers and response normalizations for pattern-information fMRI. *NeuroImage* **53**, 103–118 (2010).
181. Jeffreys, H. *Theory of Probability*. (Clarendon Press, Oxford, England, 1939).

182. van Doorn, J. *et al.* The JASP guidelines for conducting and reporting a Bayesian analysis. *Psychon. Bull. Rev.* **28**, 813–826 (2021).

183. Kass, R. E. & Raftery, A. E. Bayes Factors. *J. Am. Stat. Assoc.* **90**, 773–795 (1995).

184. Glasser, M. F. *et al.* A multi-modal parcellation of human cerebral cortex. *Nature* **536**, 171–178 (2016).

185. Kober, H. & Wager, T. D. Meta-analysis of neuroimaging data. *WIREs Cogn. Sci.* **1**, 293–300 (2010).

Acknowledgements

The authors thank the members of the Cognitive and Affective Neuroscience lab for their valuable feedback throughout this project. We also thank Bethany Hunt, Melanie Kos, Charles Mazof, and Sreekar Kasturi for their help with data curation. This research was supported by funding from the National Institutes of Health (R37MH076136 and R01MH116026 to T.D.W.).

Author contribution

M.K. and T.D.W. designed the study. The Affective Neuroimaging Consortium members acquired and contributed neuroimaging data. M.K. conducted data analysis with contributions from K.B., R.B.-N., P.A.K., L.V.O., and T.D.W. M.K. and T.D.W. wrote the original draft. All authors provided feedback and revised the paper.

Competing interests

The authors declare no competing interests.

Figure legends/captions

Figure 1. Global insular activation and multi-class SVM classification across four functional domains. a, Global insular activation across four functional domains. Violin plots show the distribution of whole-insula activation values across participants (points; normalized by study-specific standard deviation). These values are removed when examining relative local patterns. All domains showed significant activation (all FDR-corrected $q<0.05$). Whole-insula activation was higher for pain than all other domains (all FDR-corrected $q<0.001$). **b,** Participant-level contrast images were z-scored for cross-study harmonization and subsequent analyses. Summary domain activation patterns (mean/SD) after normalization are shown here. **c,** Prediction accuracy for SVM classifiers trained to discriminate between domains using leave-one-study-out cross-validation. Accurate classification (see text) indicates separable, consistent neural representations for each domain. Source data are provided as a Source Data file.

Figure 2. Identifying domain-general and domain-selective insular zones using Bayes Factors. Bayes Factors (BFs) were calculated for each domain. BFs>1 indicate evidence favoring an effect, while BFs<1 indicate evidence favoring a null effect. **a,** An example map showing voxel-wise BFs for pain (red: favors effect; blue: favors null). Thresholds for sufficient evidence were set at 4.32 for effect (equivalent to FDR-corrected $q<0.01$) and 0.23 (the inverse of 4.32) for no effect. **b,** Definition of domain-general and domain-selective voxels. Voxels were considered activated only when BF>4.32 and t-statistics were positive, and not activated when BF<0.23 or BF>4.32 with negative t-statistics (i.e., significant deactivation). Domain-general voxels were defined as those showing activation in all domains. Domain-selective voxels showed activation in their designated domain and evidence favoring no activation in other domains.

Figure 3. Domain-general and domain-selective zones in the insula. a, Domain-general voxels (purple) were located in dorsal anterior insula, pain-selective voxels (red) in mid-posterior insula, appetitive-selective voxels (yellow) in mid-insula, aversive-selective voxels (blue) in ventral anterior

insula, and cognitive-selective voxels (green) in dorsal anterior insula, anterior and dorsal to domain-general zones. **b,** Spatial gradient of functional convergence in the insula. Darker colors indicate greater generalization across domains (from lightest = 1 to darkest = 4 domains) and therefore higher functional convergence. Volumetric data were projected onto insular cutaway surfaces for visualization.

Figure 4. Meta-analytic functional decoding of domain-general and domain-selective insular zones using Neurosynth. a, Topic-level decoding. Heatmap shows point-biserial correlations between domain-general and domain-selective zones and psychological topics registered in Neurosynth, z-scored across topics (Z(r)). Topics shown (x-axis) have Z(r)>1 for at least one domain (see Supplementary Fig. 9 for complete topic heatmap). **b,** Term-level decoding. Each subplot shows the top 10 highest and lowest correlating terms for each insular zone, selected from 525 psychological terms. da: Dopamine. Source data are provided as a Source Data file.

Figure 5. Brain-wide coactivation patterns and resting-state network affiliations of domain-general and domain-selective insular zones. a, Meta-analytic coactivation patterns between insular zones and extra-insular regions. Coactivated voxels outside of the insula are assigned to the maximally correlated insular zone, requiring that maximum correlation to be at least 10% higher than the next highest correlation. aMCC: anterior midcingulate cortex; dlPFC: dorsolateral prefrontal cortex; IFJ: inferior frontal junction; IPS: intraparietal sulcus; SPL: superior parietal lobule; M1: primary motor cortex; NAc: nucleus accumbens; OFC: orbitofrontal cortex; pACC: pregenual anterior cingulate cortex; pMCC: posterior midcingulate cortex; rlPFC: rostrolateral prefrontal cortex; S1: primary somatosensory cortex; S2: secondary somatosensory cortex; SMA: supplementary motor area; TPJa: anterior temporoparietal junction; TPJp: posterior temporoparietal junction; vlPFC: ventrolateral prefrontal cortex; vmPFC: ventromedial prefrontal cortex; VPL: ventral posterolateral nucleus; VPM: ventral posteromedial nucleus. **b,** Distribution of coactivated regions across seven resting-state networks[87–89]. Bar graph shows the percentage of coactivated voxels (FDR q<0.001) overlapping with each network across cortical, subcortical, and brainstem regions. Source data are provided as a Source Data file.

Figure 6. Cytoarchitectonic profiles of insular zones. For each functional zone, only the best matching cytoarchitectonic parcels are shown from the Julich-Brain Cytoarchitectonic Atlas[23,68] (32 parcels across left and right insula). Inset illustrates the full cytoarchitectonic parcellation of the insula as defined by Quabs et al.[23] using the most up-to-date atlas.

Figure 7. Neurotransmitter system profiles of insular zones. a, Spatial similarity between the insular zones and 36 neurotransmitter maps from Neuromaps[74,99 99] with mean spatial similarity (center) and standard errors (error bars) estimated from 100 bootstrap samples. Black rings indicate zero correlation; values outside the ring are positive, and inside the ring are negative. Inset shows neurotransmitter systems and their corresponding receptors and transporters in the atlas. **b,** Correlation between the insular zones and their extra-insular coactivated systems. Source data are provided as a Source Data file.

The Affective Neuroimaging Consortium

Yoni K. Ashar[7], Lauren Atlas[8,9,10], Lisa Feldman Barrett[11,12], Benjamin Becker[13], Luke Chang[1], Luana Colloca[14], Christopher G. Davey[15], Sigrid Elsenbruch[16,17], Miquel A. Fullana[18,19], Ben J. Harrison[15], Olivia K. Harrison[20,21], Alec Jamieson[15], Christian Keysers[22,23], Brian Knutson[24], Leonie Koban[25,26], Hedy Kober[27,28], Kevin S. LaBar[29], Claus Lamm[30], Martin Lindquist[31], Tina Lonsdorf[32,33], Marina Lopez-Sola[34,35,36], Elizabeth Reynolds Losin[37], Yina Ma[38], Christian J. Merz[39], Lauri Nummenmaa[40,41], Kyle Pattinson[42], Pierre Rainville[43,44], Marianne Reddan[45], Rebecca Saxe[46,47], Daniela Schiller[48,49], Alexander J. Shackman[50,51,52], Dana Small[53,54,55], Carles Soriano-Mas[56,57,58], Rudolf Stark[59,60,61], Choong-Wan Woo[62,63,64,65], Fadel Zeidan[66], Feng Zhou[67]

**Affiliations 1–6 are from the main author list. Consortium-specific affiliations start at 7.*

[7] Division of General Internal Medicine, University of Colorado Anschutz Medical Campus, Aurora, CO, United States

[8] National Center for Complementary and Integrative Health, National Institute of Health, Bethesda, MD, United States

[9] National Institute of Mental Health, National Institute of Health, Bethesda, MD, United States

[10] National Institute on Drug Abuse, National Institute of Health, Baltimore, MD, United States

[11] Department of Psychology, College of Science, Northeastern University, Boston, MA, United States

[12] Department of Psychiatry and the Athinoula A. Martinos Center for Biomedical Imaging, Massachusetts General Hospital, Boston, MA, United States

[13] Department of Psychology, The University of Hong Kong, Hong Kong, China

[14] Department of Pain and Translational Symptom Science, School of Nursing, University of Maryland, Baltimore, MD, United States

[15] Department of Psychiatry, The University of Melbourne, Melbourne, Australia

[16] Department of Medical Psychology and Medical Sociology, Center for Medical Psychology and Translational Neurosciences, Ruhr University Bochum, Bochum, Germany

[17] Department of Neurology, Center for Translational and Behavioral Neuroscience (C-TNBS), University Hospital Essen, University of Duisburg-Essen, Essen, Germany

[18] Institut d'Investigacions Biomèdiques August Pi i Sunyer (IDIBAPS), Barcelona, Spain

[19] Adult Psychiatry and Psychology Department, Institute of Neurosciences, Hospital Clinic, Barcelona, Spain

[20] Department of Psychology, University of Otago, Dunedin, New Zealand

[21] Translational Neuromodeling Unit, University of Zurich and ETH Zurich, Zurich, Switzerland

[22] The Netherlands Institute for Neuroscience, KNAW research institute, Amsterdam, The Netherlands

[23] Department of Psychology, University of Amsterdam, Amsterdam, The Netherlands

[24] Department of Psychology, Stanford University, Stanford, CA, United States

[25] Lyon Neuroscience Research Center (CRNL), CNRS, INSERM, Université Claude Bernard Lyon 1, Bron, France

[26] Le Vinatier Psychiatrie Universitaire Lyon Métropole, Bron, France

[27] Department of Psychology, University of California Berkeley, Berkeley, CA, United States

[28] Department of Psychiatry, Yale University, New Haven, CT, United States

[29] Department of Psychology and Neuroscience, Duke University, Durham, NC, United States

[30] Department of Cognition, Emotion, and Methods in Psychology, Faculty of Psychology, University of Vienna, Vienna, Austria

[31] Department of Biostatistics, Johns Hopkins Bloomberg School of Public Health, Baltimore, MD, United States

[32] Biological Psychology and Cognitive Neuroscience, Bielefeld University, Bielefeld, Germany

[33] Institute for Systems Neuroscience, University Medical Center Hamburg Eppendorf, Hamburg, Germany

[34] Serra Hunter Programme, Department of Medicine, School of Medicine and Health Sciences, University of Barcelona, Barcelona, Spain

[35] Institute of Neuroscience, University of Barcelona, Barcelona, Spain

[36] Institut d'Investigacions Mèdiques August Pi i Sunyer, Barcelona, Spain

[37] Department of Biobehavioral Health, Pennsylvania State University, University Park, PA, United States

[38] State Key Laboratory of Cognitive Neuroscience and Learning IDG/McGovern Institute for Brain Research, Beijing Normal University, Beijing, China

[39] Department of Cognitive Psychology, Institute of Cognitive Neuroscience, Faculty of Psychology, Ruhr University Bochum, Bochum, Germany

[40] Turku PET Centre and Turku University Hospital, Turku, Finland

[41] Department of Psychology, University of Turku, Turku, Finland

[42] Nuffield Department of Clin. Neurosciences, University of Oxford, Oxford, United Kingdom

[43] Department of Stomatology, Université de Montréal, Montréal, Canada

[44] Research Center of the Montreal Geriatric University Institute, Montréal, Canada

[45] School of Psychology and Neuroscience, Center for Cognitive Neuroimaging, University of Glasgow, Glasgow, United Kingdom

[46] Department of Brain and Cognitive Sciences, Massachusetts Institute of Technology, Cambridge, MA, United States

[47] McGovern Institute for Brain Research, Massachusetts Institute of Technology, Cambridge, MA, United States

[48] Department of Psychiatry, Department of Neuroscience, Icahn School of Medicine, Mount Sinai, New York, NY, United States

[49] Friedman Brain Institute, Icahn School of Medicine, Mount Sinai, New York, NY, United States

[50] Department of Psychology, University of Maryland, College Park, MD, United States

[51] Neuroscience and Cognitive Science Program, University of Maryland, College Park, MD, United States

[52] Maryland Neuroimaging Center, University of Maryland, College Park, MD, United States
[53] Department of Neurology and Neurosurgery, Department of Medicine, and Department of Psychology, McGill University, Montréal, Canada
[54] Research Institute of the McGill University Health Centre, Montréal, Canada
[55] Modern Diet and Physiology Research Center (MDPRC), Montréal, Canada
[56] Department of Psychiatry, Bellvitge University Hosp., Bellvitge Biomed. Institute-IDIBELL, Barcelona, Spain
[57] CIBERSAM, Madrid, Spain
[58] Department of Social Psychology and Quantitative Psychology, Institute of Neurosciences, University of Barcelona, Spain
[59] Department of Psychotherapy and Systems Neuroscience, Justus-Liebig-University Giessen, Giessen, Germany
[60] Bender Institute of Neuroimaging, Justus-Liebig-University Giessen, Giessen, Germany
[61] Center of Mind, Brain, and Behavior, Universities of Marburg and Giessen, Giessen, Germany
[62] Center for Neuroscience Imaging Research, Institute for Basic Science, Suwon, Republic of Korea
[63] Department of Biomedical Engineering, Sungkyunkwan University, Suwon, Republic of Korea
[64] Department of Intelligent Precision Healthcare Convergence, Sungkyunkwan University, Suwon, Republic of Korea
[65] Department of Brain Science and Engineering, Sungkyunkwan University, Suwon, Republic of Korea
[66] Department of Anesthesiology, University of California San Diego, La Jolla, CA, United States
[67] Faculty of Psychology, Southwest University, Chongqing, China

Editor's Summary: Bayesian fMRI mega-analysis reveals structured insular topography, with domain-selective zones with distinct neurobiological properties for pain, appetitive, aversive, and cognitive control processing progressively converging in dorsal anterior insula, providing a potential neural basis for unified subjective experiences.

Peer review information: *Nature Communications* thanks Jordi Manuello, Julian Quabs, and the other, anonymous, reviewer(s) for their contribution to the peer review of this work. A peer review file is available.

Supplementary Information

Convergent and selective representations of pain, appetitive processes, aversive processes, and cognitive control in the insula

Mijin Kwon[1*], Ke Bo[1], Rotem Botvinik-Nezer[1,2], Philip A. Kragel[3,4], Lukas Van Oudenhove[5], Tor D. Wager[1*], The Affective Neuroimaging Consortium[6]

[1] Department of Psychological and Brain Sciences, Dartmouth College, Hanover, NH, United States

[2] Department of Psychology, The Hebrew University of Jerusalem, Jerusalem, Israel

[3] Department of Psychology, Emory University, Atlanta, GA, United States

[4] Department of Psychiatry and Behavioral Sciences, Emory University, Atlanta, GA, United States

[5] Laboratory for Brain-Gut Axis Studies (LaBGAS), Translational Research in Gastrointestinal Disorders (TARGID), Department of Chronic Diseases and Metabolism (CHROMETA), University of Leuven, Leuven, Belgium

[6] Group author

* Corresponding authors

Correspondence to:

Tor D. Wager
Diana L. Taylor Distinguished Professor
Presidential Cluster in Neuroscience and
Department of Psychological and Brain Sciences
Dartmouth College
Email: tor.d.wager@dartmouth.edu

Mijin Kwon
Department of Psychological and Brain Sciences
Dartmouth College
Email: mijin.kwon.gr@dartmouth.edu

Supplementary Methods

Data harmonization and normalization

When analyzing data aggregated from multiple studies across various functional domains, it is crucial to account for two types of variability or biases to accurately identify functionally convergent and selective areas in the insula. Here we refer to these two as 1) study-wide variability and 2) functional domain-wide variability. Study-wide variability is primarily a technical issue, while domain-wide variability reflects both biological and technical/methodological differences between domains.

Study-wide variability: Data from different studies and sites are inevitably measured on different scales due to variable factors during data acquisition and analysis. These factors include scanner, acquisition, and analysis variables, such as field strength, TR, TE, acquired voxel size, flip angle, choice of baseline state, stimulus timing, physiological noise removal and filtering choices, scaling of the hemodynamic response function(s) used, model regressors and contrast weights, choice to analyze percent signal change, method for converting to percent signal change, choice to resample voxels, and contrast scaling across multiple runs.

Domain-wide variability: The magnitude of brain activity associated with each functional domain differs. For example, in our dataset, painful stimuli generate more pronounced (higher activation) and widespread activity across the brain, including the insula, compared to the other domains we examined. These differences reflect both biological factors (e.g., pain's engagement of arousal and salience systems) and technical/methodological factors (e.g., differences in task design, stimulus parameters, and implementation across domains). While the biological differences are meaningful signals reflecting how domains genuinely differ in their neural engagement, they create analytical challenges when identifying domain-selective regions. Without proper data harmonization to account for these differences in signal levels, it would be challenging to identify functionally selective areas for other domains.

Consideration of other data harmonization and normalization methods

To address these issues, we explored a range of data harmonization and normalization methods, including ComBat[1], L2 normalization, normalization with standard deviation as a norm, and z-scoring. ComBat has been successfully applied in various neuroimaging modalities, such as DTI[2], cortical thickness[3], volumetric T1[4], functional connectivity[5,6], and task-based fMRI[6]. However, ComBat was not applicable in our case due to the nested relationship between sites/scanning parameters and task/study. L2 normalization and normalization with standard deviation as a norm did not significantly improve data harmonization compared to raw data. Therefore, we decided to analyze relative patterns after applying z-scoring normalization at the image level across voxels to account for site, scanner, and inter-study variability while still finding meaningful differences in activation patterns within the insula between the included functional domains. Although this approach may result in the loss of some informative signals, such as pain-related activity in the posterior insula, it enables the identification of local coding patterns for each domain.

Supplementary analysis with expanded insula boundaries

Given the close functional connectivity between insular cortex and adjacent opercular regions, we tested whether our findings depend on specific anatomical boundary definitions. We repeated our main Bayes Factor analysis to identify domain-general and domain-selective zones with an expanded mask that included both insula proper and adjacent opercular regions. The expanded mask was constructed using parcels from two complementary atlases: HCP-MMP1.0[7] and Julich-Brain Cytoarchitectonic Atlas[8]. For the Julich-Brain Atlas, we selected cytoarchitectonically-defined opercular areas OP3, OP5, OP7, and OP9. For HCP-MMP1.0, since this atlas does not contain the same opercular parcels, we identified anatomically corresponding regions based on spatial proximity. The following parcels were selected from each atlas:

1. **Julich-Brain Cytoarchitectonic Atlas**:
    - Insular parcels: Ig1, Ig2, Ig3, Id1, Id2, Id3, Id4, Id6, Id7, Id8, Id9, Id10, Ia1, Ia2 (bilateral)
    - Opercular parcels: OP3, OP5, OP7, OP9 (bilateral)
2. **HCP-MMP1.0 Atlas**:
    - Insular parcels: 52, PI, Ig, PoI1, PoI2, MI, AVI, AAIC, Pir (bilateral)
    - Opercular parcels: FOP2, FOP3, FOP4, FOP5 (bilateral)

Results from this expanded analysis are presented in Supplementary Fig. 7. We reported results only from the analysis using the parcels from the Julich-Brain Cytoarchitectonic Atlas in the main results, but Supplementary Fig. 7 includes results from both atlases for comparison, demonstrating consistent findings across different parcellation schemes.

Supplementary Figures

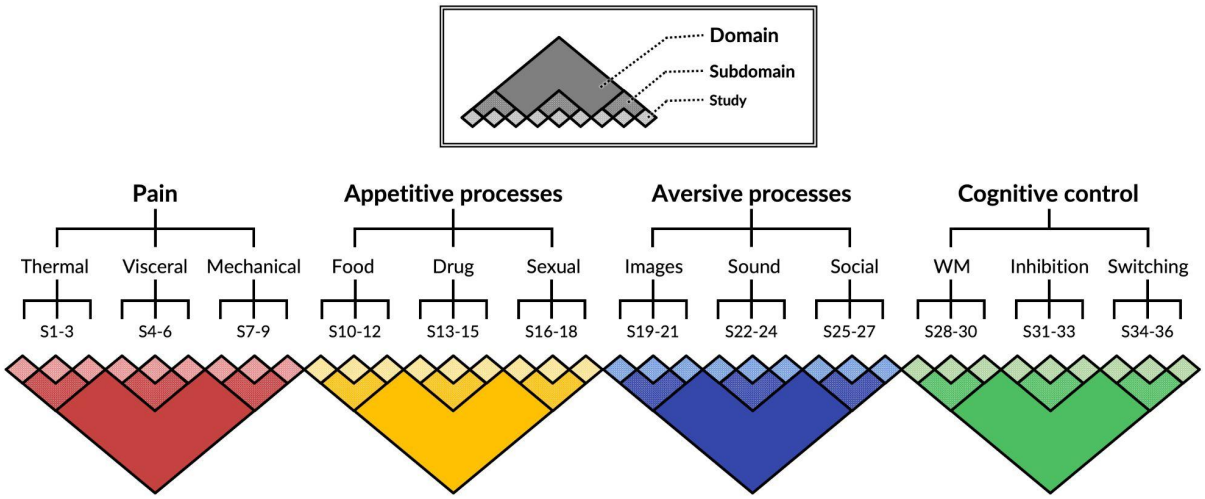

Supplementary Fig. 1

Multi-study data structure. Dataset used in the current study consists of 15 participants from each of 36 fMRI studies systematically sampled across four functional domains closely linked to insular function: somatic pain, non-somatic appetitive processes, non-somatic aversive processes, and cognitive control. Each functional domain comprises three subdomains representing different experimental paradigms within that domain, with three studies per subdomain to ensure representativeness and generalizability. Pain domain includes thermal (thermal stimulation), mechanical (mechanical stimulation), and visceral (visceral stimulation) subdomains. Appetitive processes domain includes food (food images), drug (drug images), and sexual (sexual images) subdomains. Aversive processes domain includes images (negative images), sound (aversive sounds), and social (negative social interactions) subdomains. Cognitive control domain includes WM (working memory), inhibition (response inhibition), and switching (attention switching) subdomains.

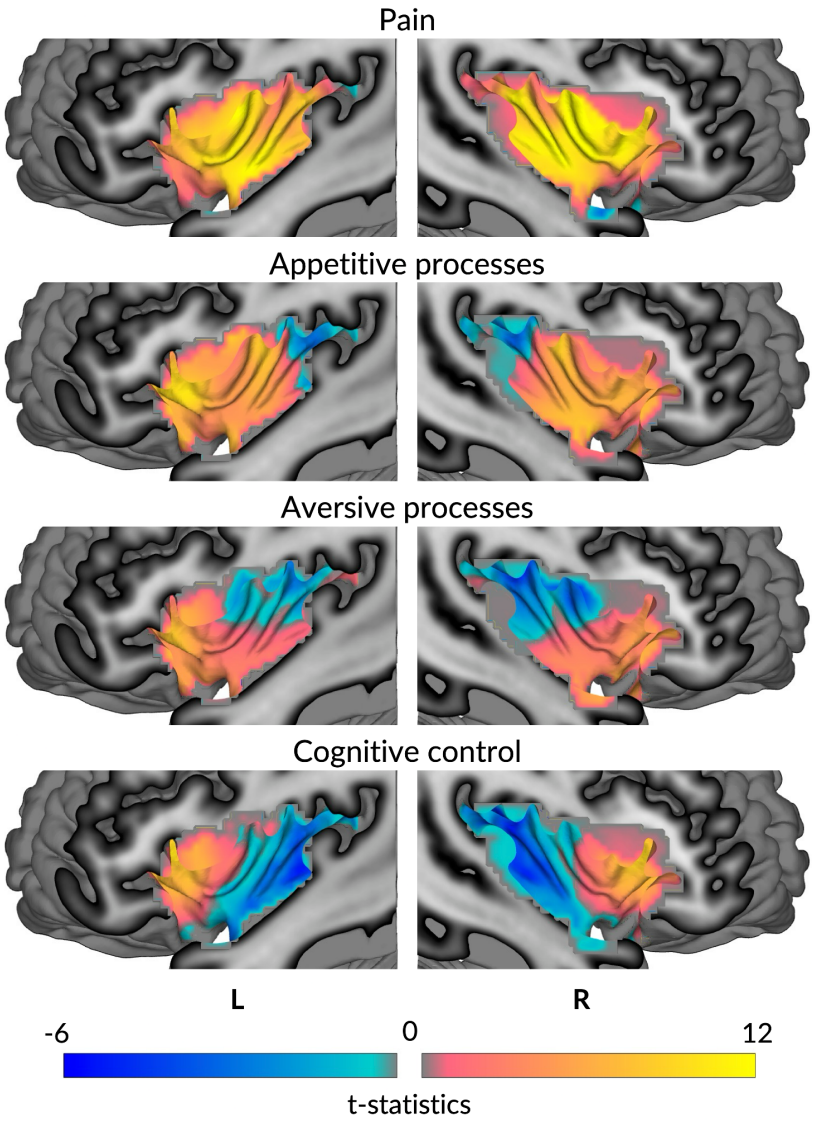

Supplementary Fig. 2

Domain-level t-statistic maps (unthresholded) for global insular activation across domains. Statistical parametric maps showing t-values from one-sample t-tests (n=135 per domain) for mean activation values normalized by each study's average voxel-wise between-subject SD to account for differences in signal scale across studies. Pain shows stronger and more widespread activation throughout the insula compared to other domains. Color scale represents t-statistic values.

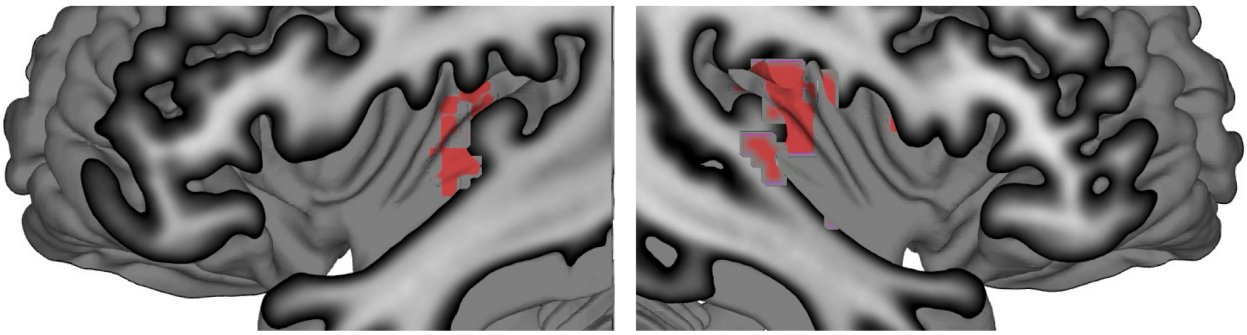

Supplementary Fig. 3

L2 normalization reveals pain-selective regions in posterior insula. Domain-selective zones identified using L2 normalization, which scales activation patterns to unit length without mean centering. In contrast to z-scoring normalization (used in the main analysis), which standardizes both mean and variance across voxels, L2 normalization maintains the sign and spatial distribution of activation patterns. This reveals pain-selective zones in the posterior insula that were obscured in the main analysis, confirming that pain-related signals are present in posterior regions but are masked in our primary analysis due to pain's significantly higher whole-insula activation compared to other domains.

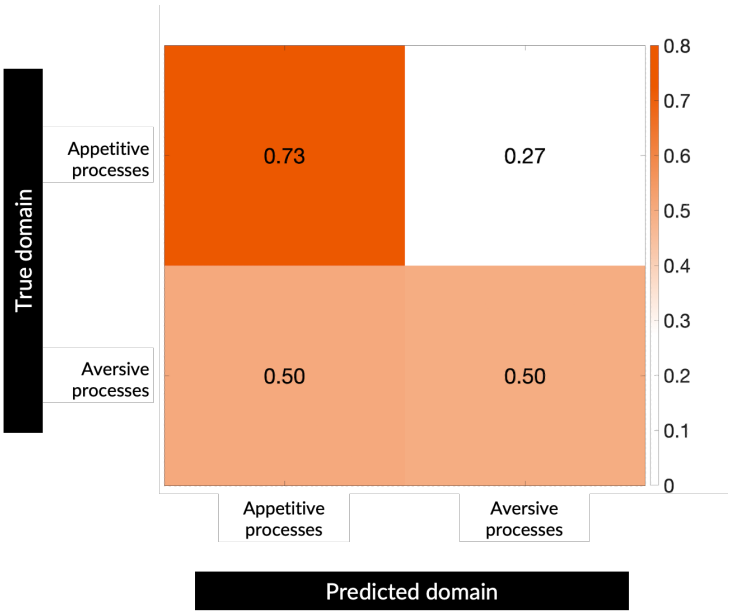

Supplementary Fig. 4

Pairwise classification between appetitive and aversive processes. To further investigate the multiclass classification patterns observed in Fig. 2b, we trained binary SVM classifiers specifically between appetitive and aversive processes. When classifying appetitive processes, accuracy was above chance (73%), but when classifying aversive processes, accuracy was at chance level (50%). This pattern suggests that while appetitive processes have distinct neural representations, aversive processes share substantial neural patterns with a subset of appetitive processes or potentially greater heterogeneity in their neural representations, which may result in more conservative results in identifying aversive-selective zones.

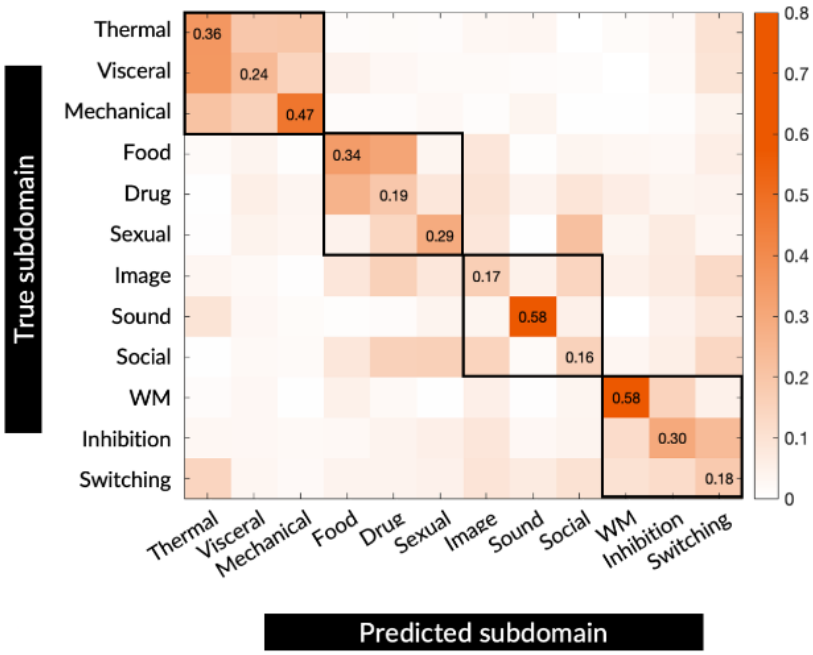

Supplementary Fig. 5

Subdomain classification using insular activation patterns. Confusion matrix shows prediction accuracies for multiclass SVM classifiers trained to discriminate between 12 subdomains (3 per domain) using the same leave-one-study-out scheme as domain classification (see Methods for details). Classifiers performed above chance (8.3%) for all subdomains (mean=32.11%, range: 15.6% for aversive social interaction to 57.8% for working memory), with mechanical pain, aversive sound, and working memory showing higher discriminability compared to other subdomains.

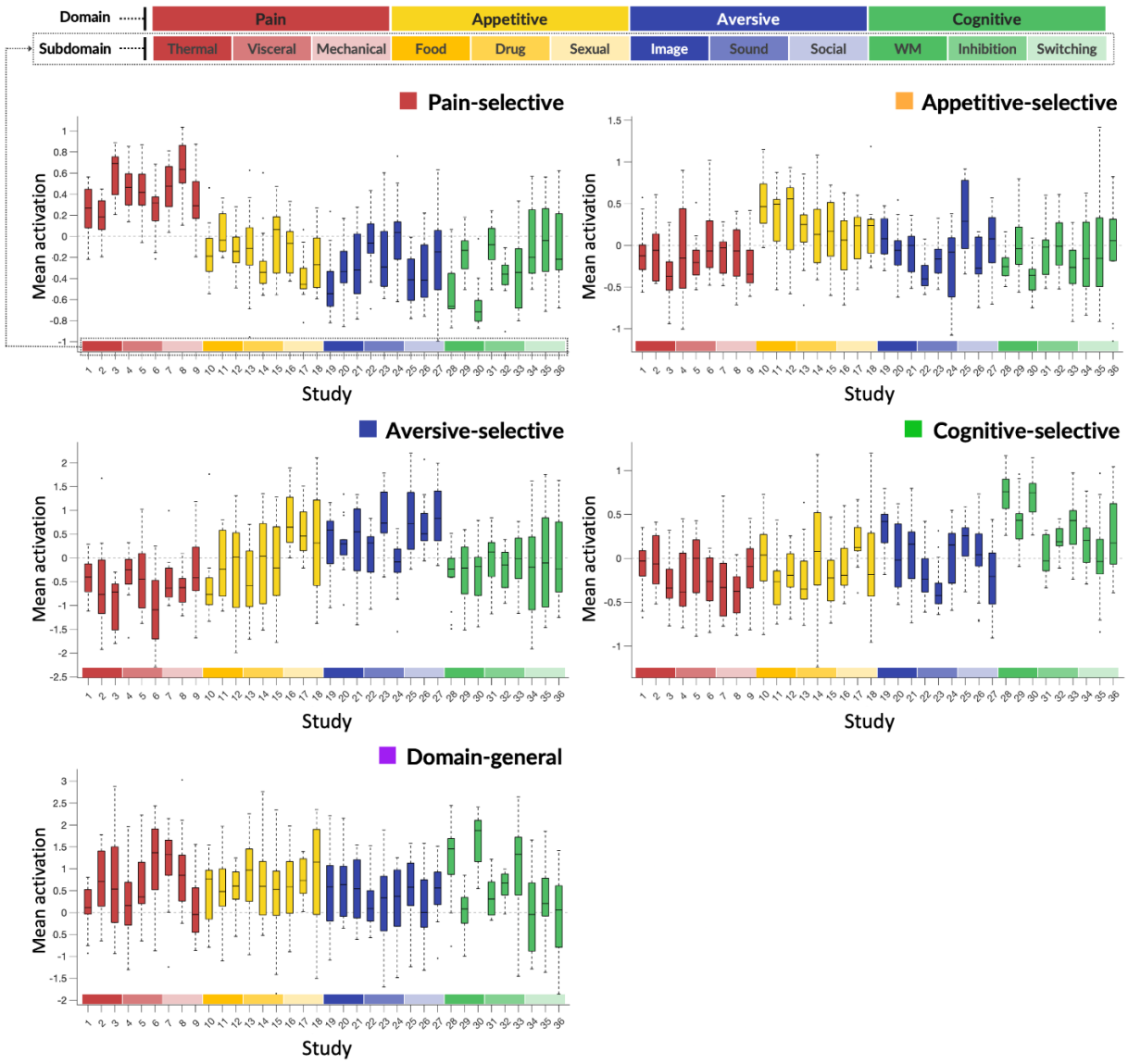

Supplementary Fig. 6

Activation profiles of insular zones. Mean z-scored contrast coefficients for domain-general and domain-selective zones across all 36 individual studies, grouped by domains and subdomains. Zones were identified using Bayes Factor analysis at the domain level (aggregating across all studies within each domain); this figure displays the activation values from these domain-defined zones separated by individual study to show consistency of activation profiles across studies and subdomains. Domain-general zones show high activation across all domains, while domain-selective zones show high activation for their designated domain and low/no activation for other domains. These patterns are consistent across studies and subdomains within each domain with few exceptions. The centerline shows the median; box edges represent first (25th percentile) and third (75th percentile) quartiles, with the box length showing the interquartile range (IQR, middle 50% of data). Whiskers extend to the most extreme values within 1.5 × IQR from the box edges, and points beyond the whiskers indicate outliers. Source data are provided as a Source Data file.

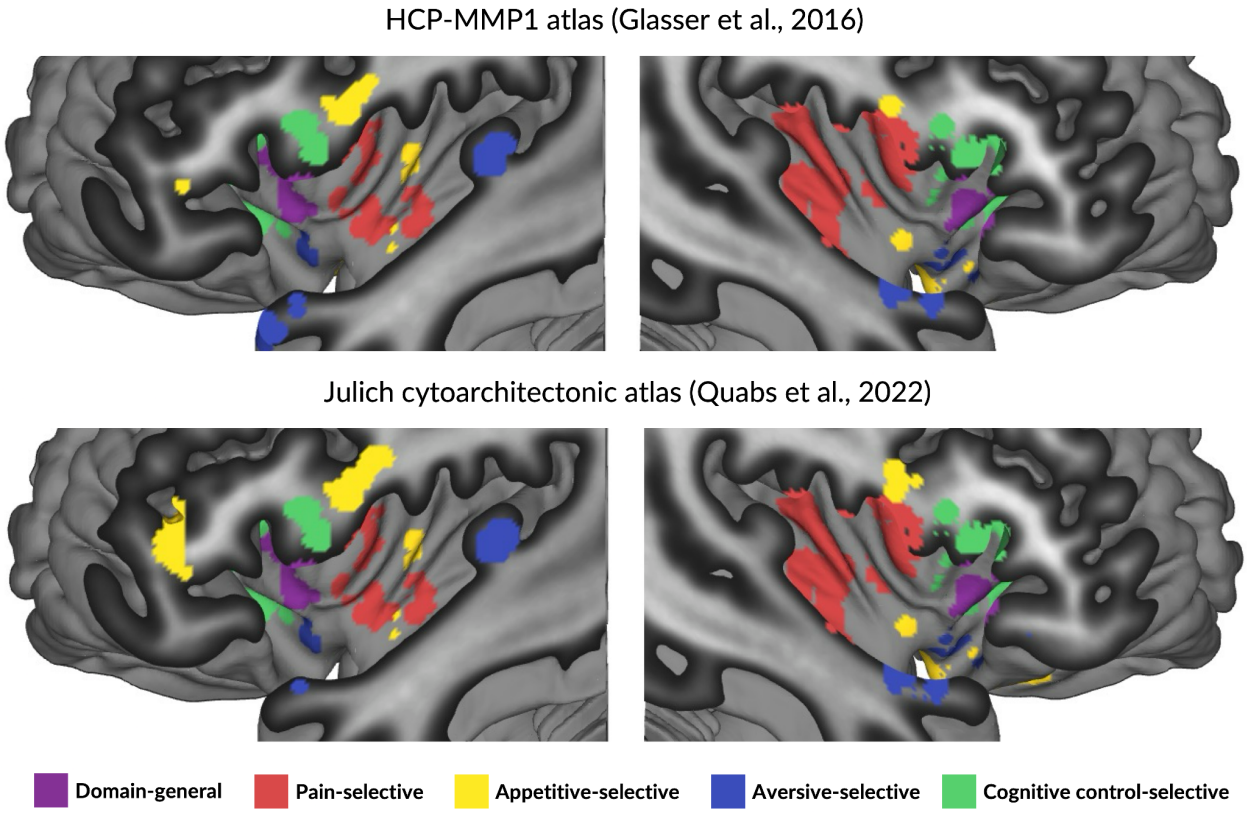

Supplementary Fig. 7

Domain-general and domain-selective zones using expanded anatomical definition including opercular regions. Analysis using masks that include both insula proper and adjacent opercular regions from Julich-Brain Cytoarchitectonic Atlas (top) and HCP-MMP1.0 Atlas (bottom). This analysis revealed similar domain-general and domain-selective patterns in opercular areas with known structural connections to the insula[9]. For example, pain-selective activation appeared primarily in OP5 and domain-general activation was found in OP7 and OP9, consistent with their connectivity to mid-posterior and dorsal anterior insula.

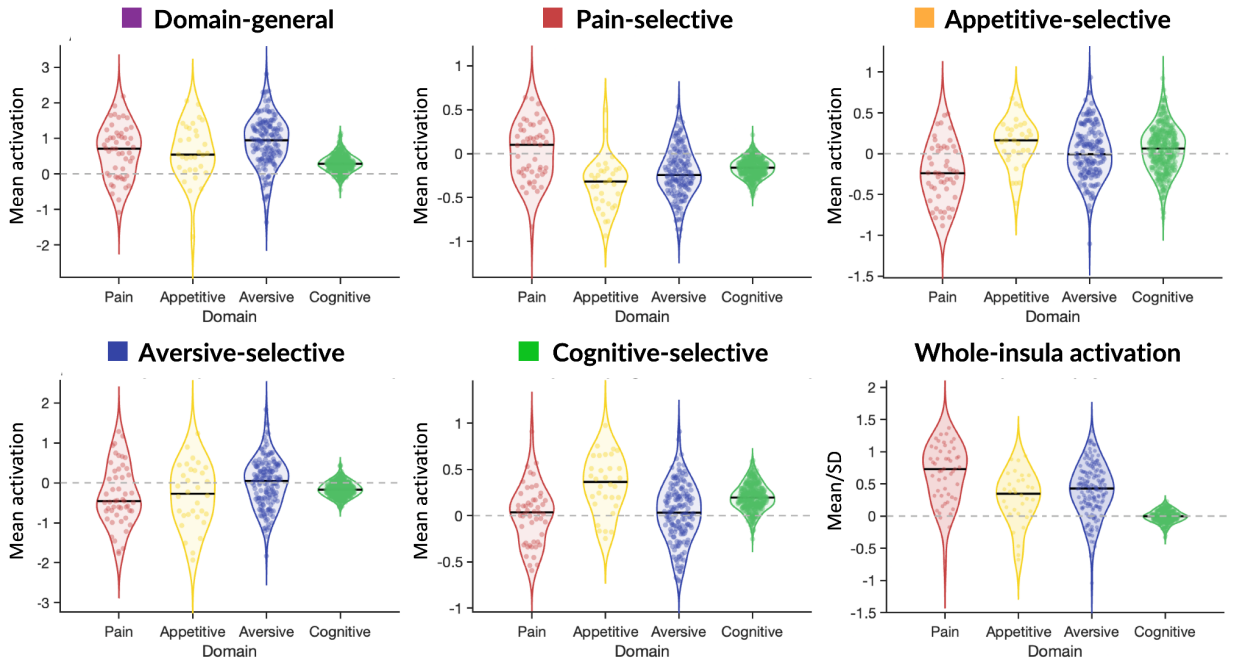

Supplementary Fig. 8

Validation of insular zones using independent datasets. Activation profiles from independent validation datasets (n=608) for the five identified functional zones. First five panels show mean activation within domain-general, pain-selective, appetitive-selective, aversive-selective, and cognitive-selective zones. The bottom last panel shows global insula activation (mean/SD) across domains in the validation datasets. Source data are provided as a Source Data file.

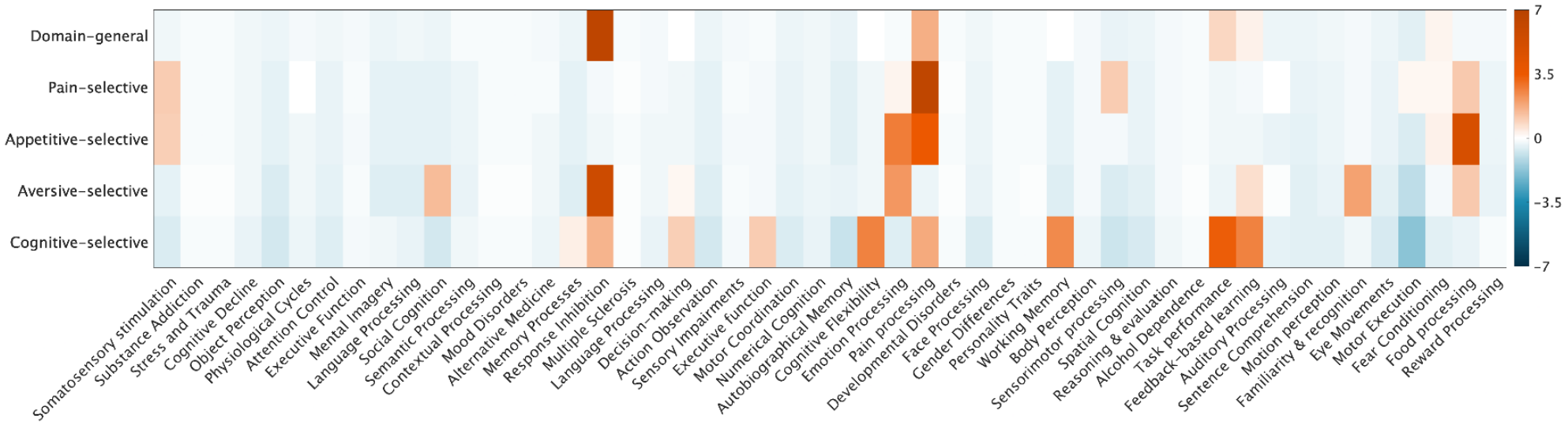

Supplementary Fig. 9

Complete topic-level decoding of insular zones using Neurosynth. Heatmap shows standardized point-biserial correlations between domain-general and domain-selective insular zones and all 50 psychological topic maps.

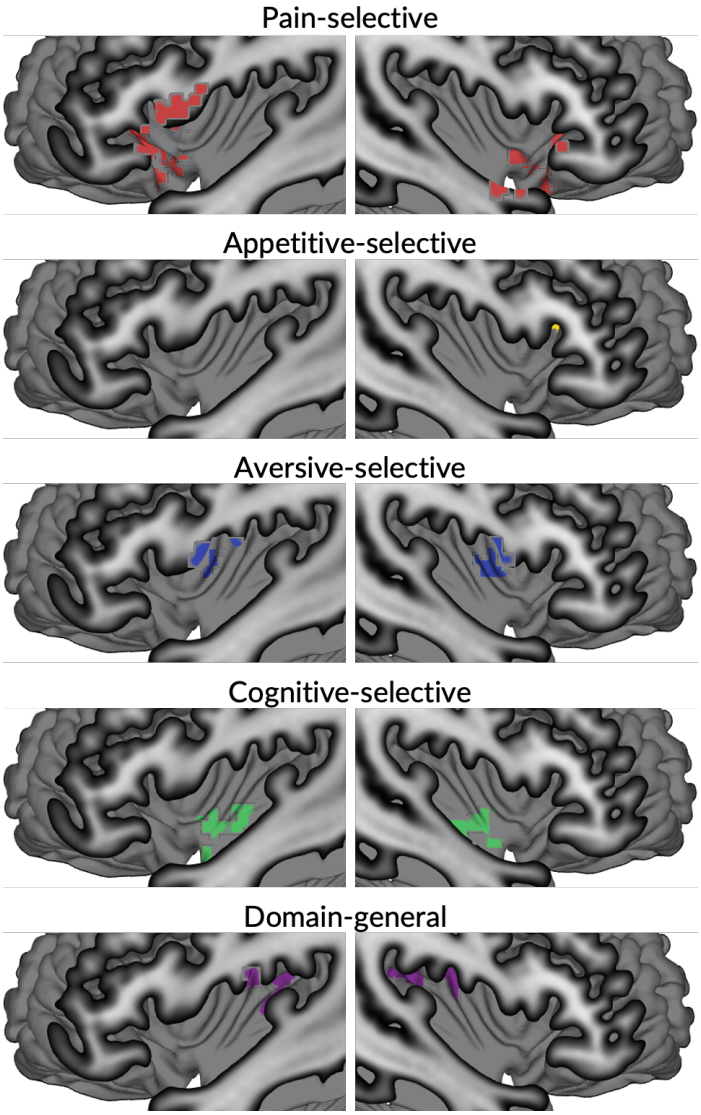

Supplementary Fig. 10

Deactivation-based functional zones in the insula. Domain-general zones identified from deactivation patterns were predominantly located in the posterior-most portion of the insula. Domain-selective deactivation zones showed distinct distributions: pain-selective in dorsal and ventral anterior insula, appetitive-selective in left dorsal anterior insula, aversive-selective in dorsal mid insula, and cognitive control-selective in ventral mid insula.

1. Study selection and stratification (Repeated for all domains)

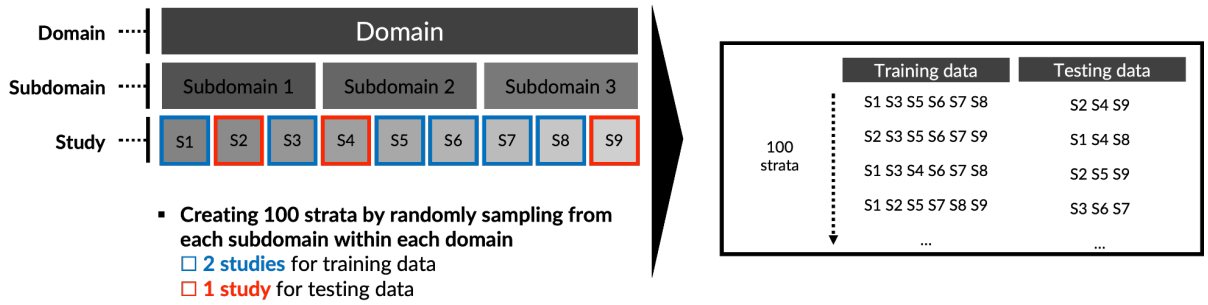

2. Model training and testing

Training

- Multiclass support vector machine (linear) with fitcecoc function
- One-vs-all scheme
- Hyperparameter optimization (lambda*) with 5-fold cross validation and max 5 evaluations (* *Regularization parameter inversely related to to the box constraint (C)*)

→ **Train 100 models with selected training datasets**

Training on held-out data

- Calculating average prediction accuracy across 100 models
- Testing significance of each domain using binomial distribution (normal approximation due to large sample size)
- Applying Bonferroni correction for multiple comparisons correction

Supplementary Fig. 11

Schematic description of study selection and training and testing of multi-class Support Vector Machine (SVM) model. Part 1 shows study selection and stratification for one example domain. Each domain comprises three subdomains with three studies each (9 studies total per domain). For each iteration, one study per subdomain is held out as the test set (red border), while the remaining two serve as training data (blue border), ensuring the classifier is tested on entirely independent studies. Different held-out combinations are systematically sampled across 100 iterations. Part 2 shows the training and testing procedure. Training data from all four domains are used to fit a multi-class linear SVM with a one-vs-all scheme and 5-fold cross-validation for hyperparameter optimization (box constraint). The trained classifier is then applied to the held-out studies to predict domain labels. Classification accuracy is averaged across all 100 test sets to estimate out-of-study generalization performance.

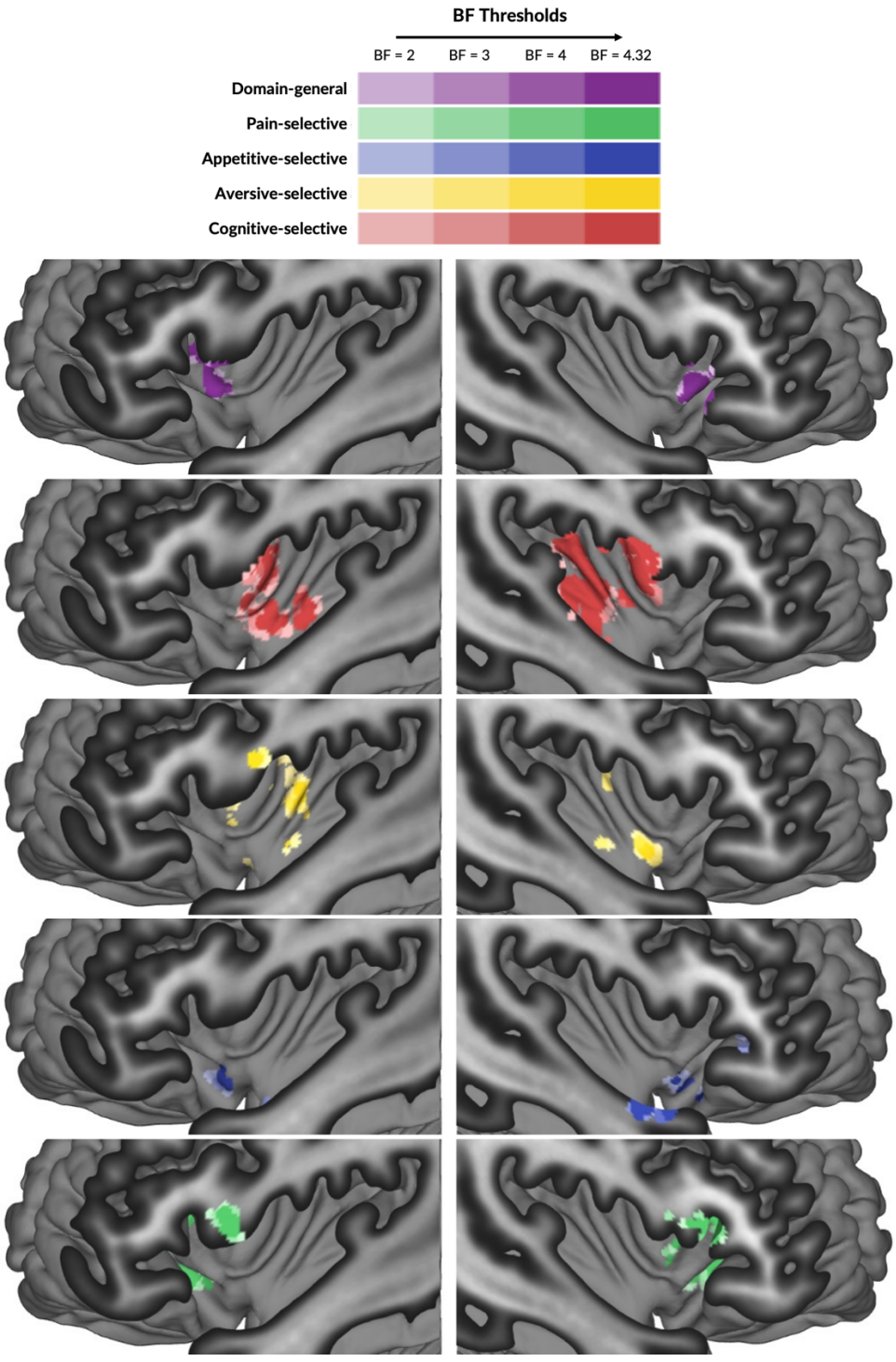

Supplementary Fig. 12

Domain-general and domain-selective zones at different Bayes Factor thresholds (BF = 2, 3, 4, and 4.32). Each row of the figure and color legend shows a different zone type: domain-general (purple), pain-selective (red), appetitive-selective (yellow), aversive-selective (blue), and cognitive control-selective (green). Left and right columns show left and right hemispheres,

respectively. Color intensity indicates the BF threshold at which each voxel survives, with lighter shades corresponding to lower thresholds and darker shades to higher thresholds from BF = 2 (lowest) to 4.32 (highest, the threshold used in the main analysis). Voxels surviving higher thresholds are spatial subsets of those at lower thresholds. The spatial extent and overall configuration of functional zones remain stable across thresholds, indicating that the identified zones are robust to the choice of BF threshold.

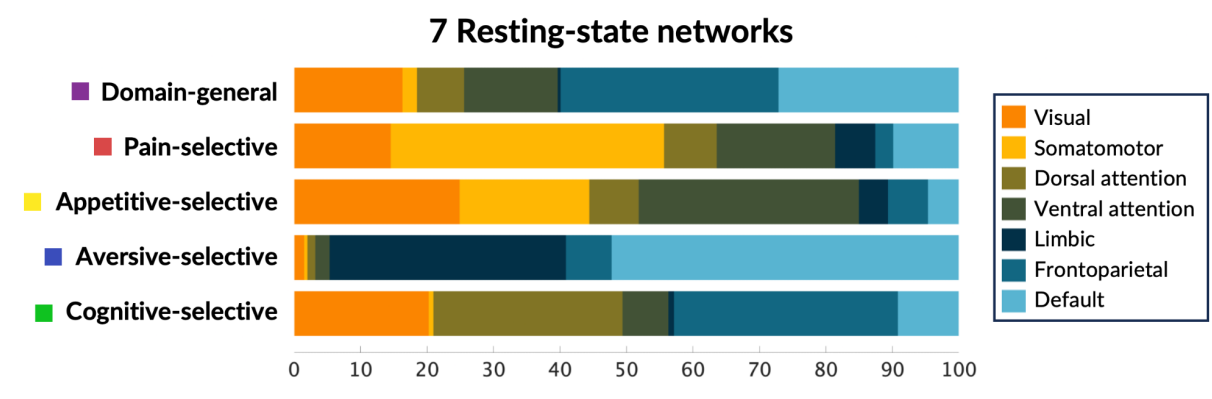

Supplementary Fig. 13

Resting-state network affiliations using unthresholded coactivation maps. This analysis shows network affiliations including subthreshold coactivated voxels, complementing the thresholded analysis in Fig. 5b. Source data are provided as a Source Data file.

Supplementary Tables

Supplementary Table 1

Domain-selective and domain-general insular clusters. Cluster information including center coordinates in standard MNI (Montreal Neurological Institute) space and parcellation labels using three existing atlases[7,8,10]

Insular cluster	L/R	Number of voxels	MNI Coordinates			Mean Bayes factors	Parcellations		
			X	Y	Z		7	10	8
Pain-selective	L	98	-40	2	2	22.80 [3.08, 97.98]	Ctx_PoI2_L	Posterior short gyrus (left)	L_Area_Id6
	R	222	38	-6	2		Ctx_PoI2_R	Anterior long gyrus (right)	R_Area_Op5
Appetitive-selective	L	9	-38	-8	2	6.88 [3.04,14.10]	Ctx_PoI2_L	Anterior long gyrus (left)	L_Area_Id5
	R	5	34	-12	-8		Ctx_PoI1_R	Posterior long gyrus (right)	R_Area_Ia3
Aversive-selective	L	33	-38	12	-16	10.12 [2.99, 25.73]	Ctx_AAIC_L	Anterior inferior gyrus (left)	L_Area_Id10
	R	42	36	14	-14		Ctx_AAIC_R	Anterior inferior gyrus (right)	R_Area_TI
Cognitive-selective	L	58	-28	20	8	15.46 [2.96, 51.72]	Ctx_FOP4_L	Anterior short gyrus (left)	L_Area_Id7
	R	84	30	20	4		Ctx_AVI_R	Anterior short gyrus (right)	R_Area_Id6
Domain-general	L	55	-42	16	-2	24.60 [3.13, 68.94] (Pain) 26.40 [2.98, 61.20] (Appetitive) 11.25 [3.00, 26.22] (Aversive) 20.70 [3.29, 56.28] (Cognitive)	Ctx_MI_L	Anterior short gyrus (left)	L_Area_Id6
	R	65	44	18	-4		Ctx_44_R	Anterior inferior gyrus (right)	R_Area_Id8'

Supplementary Table 2

Neurosynth topic maps selected for the current study and their correlations with each domain-general and domain-selective insular zone

Topic label	Domain-selective and domain-general insular zones					Neurosynth Topic ID
	Pain-selective	Appetitive-selective	Aversive-selective	Cognitive-selective	Domain-general	
Somatosensory Stimulation	1.0425	1.0072	-0.3993	-0.5538	-0.2708	0
Substance Addiction	-0.1215	-0.1551	-0.0977	-0.1420	-0.1541	2
Stress and Trauma	-0.1194	-0.1531	-0.0945	-0.1377	-0.1529	4
Cognitive Decline	-0.2390	-0.2606	-0.2701	-0.3774	-0.2204	5
Object Perception	-0.3890	-0.3947	-0.5712	-0.6783	-0.3045	6
Physiological Cycles	-0.0137	-0.2308	-0.2214	-0.3109	-0.2017	7
Attention Control	-0.3467	-0.3574	-0.4281	-0.4966	-0.2244	9
Executive Function	-0.1460	-0.1770	-0.1335	-0.1910	-0.1679	13
Mental Imagery	-0.3938	-0.3861	-0.4971	-0.2657	-0.3077	14
Language Processing	-0.4150	-0.4049	-0.5280	-0.3580	-0.2688	15
Social Cognition	-0.3836	-0.3900	1.3726	-0.6613	-0.3015	17
Semantic Processing	-0.2892	-0.3057	-0.3373	-0.2522	-0.1610	20
Contextual Processing	-0.1155	-0.1497	-0.0889	-0.1300	-0.1508	21
Mood Disorders	-0.1161	-0.1502	-0.0897	-0.1311	-0.1511	22
Alternative Medicine	-0.1163	-0.2323	-0.2238	-0.3142	-0.2026	23
Memory Processes	-0.4258	-0.4058	-0.5440	0.3508	-0.3257	24
Response Inhibition	-0.2176	-0.2414	5.5929	1.5550	6.5496	25
Multiple Sclerosis	-0.1042	-0.1395	-0.0723	-0.1073	-0.1444	30
Language Processing (2)	-0.2166	-0.2427	-0.2408	-0.3374	-0.2027	32
Decision-making	-0.2214	-0.2448	0.1886	0.9870	-0.0404	34
Action Observation	-0.3908	-0.3970	-0.4927	-0.6813	-0.3059	40
Sensory Impairments	-0.1578	-0.1876	-0.1509	-0.2147	-0.1746	46
Executive Function (2)	-0.1857	-0.2149	-0.1954	1.0597	-0.1109	49
Motor Coordination	-0.3480	-0.3589	-0.4304	-0.5963	-0.2820	51
Numerical Cognition	-0.2428	-0.2640	-0.2755	-0.3779	-0.2225	52

Autobiographical Memory	-0.4722	-0.4702	-0.3787	-0.8443	-0.3683	56
Cognitive Flexibility	-0.2249	-0.2479	-0.2493	2.6202	0.0488	58
Emotion Processing	0.2267	2.7119	2.1519	-0.5264	-0.1547	60
Pain Processing	6.5060	3.5111	-0.2935	1.7713	1.6717	61
Developmental Disorders	-0.1082	-0.1430	-0.0781	-0.1153	-0.1466	62
Face Processing	-0.3056	-0.3192	-0.3676	-0.5723	-0.2579	65
Gender Differences	-0.1306	-0.1599	-0.1110	-0.1602	-0.1593	66
Personality Traits	-0.1103	-0.1450	-0.0812	-0.1195	-0.1478	67
Working Memory	-0.4072	-0.4117	-0.5167	2.4255	-0.0402	68
Body Perception	-0.1919	-0.2182	-0.2009	-0.2829	-0.1938	70
Sensorimotor Processing	1.0622	-0.1656	-0.5678	-0.7829	-0.3348	72
Spatial Cognition	-0.3599	-0.3692	-0.4474	-0.6150	-0.2885	75
Reasoning & Evaluation	-0.1808	-0.2083	-0.1846	-0.2607	-0.1876	77
Alcohol Dependence	-0.1240	-0.1573	-0.1013	-0.1470	-0.1555	81
Task Performance	-0.2436	-0.2647	-0.2767	3.3536	0.8578	82
Feedback-based Learning	-0.2169	-0.2407	0.7106	2.6108	0.2978	85
Auditory Processing	-0.0534	-0.3679	-0.0616	-0.4330	-0.2877	86
Sentence Comprehension	-0.3753	-0.3831	-0.4516	-0.4684	-0.2941	87
Motion Perception	-0.2930	-0.3092	-0.3493	-0.4855	-0.2508	88
Familiarity & Recognition	-0.1762	-0.2041	1.9528	-0.2515	-0.1849	90
Eye Movements	-0.3571	-0.3667	-0.4432	-0.6138	-0.2869	93
Motor Execution	0.1785	-0.5495	-1.0050	-1.7706	-0.4728	95
Fear Conditioning	0.1967	0.3050	-0.2151	-0.4761	0.2336	97
Food Processing	1.1238	4.9280	1.1365	-0.3482	-0.2116	98
Reward Processing	-0.2900	-0.3177	-0.3428	-0.1450	-0.1861	99

Supplementary Table 3

List of highly matching cytoarchitectonic parcels for each insular zone

Insular cluster	L/R	Parcel	Dice coefficient	Cytoarchitectonic feature
Pain-selective	L	Id6 (L)	0.260	Dysgranular, Dorsal anterior
		Id3 (L)	0.160	Dysgranular, Dorsal anterior
		Id5 (L)	0.120	Agranular-dysgranular, Inferior posterior
	R	Id6 (R)	0.190	Dysgranular, Dorsal anterior
		Id3 (R)	0.160	Granular-dysgranular, Posterior
		Id2 (R)	0.150	Granular-dysgranular, Posterior
		Ig2 (R)	0.120	Granular-dysgranular, Posterior
Appetitive-selective	L	Id5 (L)	0.200	Agranular-dysgranular, Inferior
	R	Ia3 (R)	0.110	Agranular, Ventral anterior cluster
Aversive-selective	L	Id10 (L)	0.170	Agranular, Ventral anterior
	R	Id10 (R)	0.170	Agranular, Ventral anterior
		Id9 (R)	0.140	Agranular, Ventral anterior
Cognitive-selective	L	Id7 (L)	0.260	Dysgranular, Dorsal anterior
		Id6 (L)	0.120	Dysgranular, Dorsal anterior
	R	Id6 (R)	0.210	Agranular, Ventral anterior
		Id8 (R)	0.160	Dysgranular, Dorsal anterior
		Id7 (R)	0.150	Dysgranular, Dorsal anterior
		Id10 (R)	0.100	Agranular, Ventral anterior
Domain-general	L	Id6 (L)	0.260	Dysgranular, Dorsal anterior
	R	Id8 (R)	0.160	Agranular, Ventral anterior

Supplementary Table 4

Study info for main analysis

Study #	Domain	Subdomain	Publication	N	Contrasts	Stimulus/ Paradigm	Experimental design	Stimulus dynamics	N (female)	Mean Age	IRB/Ethics Approval Committee	MRI System
1	Pain	Thermal	Atlas et al. (2010)[11]	15	High vs low pain	Thermal stimulation	Event-related	10s duration (1.5s ramp up, 7s plateau, 1.5s ramp down); individually calibrated	19 (9)	25.5	Columbia University	1.5T GE Signa TwinSpeed Excite HD
2	Pain	Thermal	Wager et al. (2013)[12]	15	49.3° C vs baseline	Thermal stimulation	Event-related	10s duration; 44.3-49.3°C in 1°C increments	33 (22)	27.9	Columbia University	1.5T GE Signa TwinSpeed Excite HD
3	Pain	Thermal	Krishnan et al. (2016)[13]	15	High pain (48 degree) vs baseline	Thermal stimulation	Event-related	11s duration (2s ramp-up, 7s plateau, 2s ramp-down); 46, 47, 48°C fixed temperatures	28 (10)	25.2	University of Colorado Boulder	3T Siemens Tim Trio
4	Pain	Visceral	Kano et al. (2017)[14]	15	Distension vs baseline	Rectal distention	Event-related	18s distension (approximately 5s inflation, approximately 10s at threshold); individually calibrated	29 (15)	22.5	Tohoku University School of Medicine	3T Siemens TrioTIM
5	Pain	Visceral	Rubio et al. (2015)[15]	15	Distension vs baseline	Rectal distention	Block	18s distension (approximately 5s inflation, 13s at threshold); individually calibrated	15 (9)	24*	Comité de Protection des Personnes Sud Est V, France	3T Philips Achieva TX

6	Pain	Visceral	Coen et al. (2011)[16]	15	Distension vs rest	Esophageal pain	Event-related	1s phasic distension at pain tolerance threshold; individually calibrated	31 (16)	30	King's College London, UK	3T GE Signa Excite II
7	Pain	Mechanical	Kragel et al. (2018)[17]	15	7 kg/cm2 vs baseline	Pressure Stimulation	Event-related	10s duration; 7 kg/cm² to thumbnail	15 (4)	26.9	University of Colorado Boulder	3T Siemens TrioTIM
8	Pain	Mechanical	Čeko et al. (2022)[18]	15	4, 5, 6 and 7 kg/cm2 vs baseline	Pressure Stimulation	Event-related	10s duration; 4, 5, 6, 7 kg/cm² to thumbnail	15 (8)	24.2	University of Colorado Boulder	3T Siemens Prisma
9	Pain	Mechanical	Ashar et al. (Unpublished)	15	High vs low pressure	Pressure Stimulation	Event-related	6s duration; 4, 7 kg/cm² to thumbnail	141 (75)	41.7	University of Colorado Boulder	3T Siemens Prisma
10	Appetitive Processes	Food	Koban et al. (2023)[19]	15	Food cue vs. baseline (HC*)	Craving regulation with food cues	Event-related	6s image presentation	22 (9)	26.4	Columbia University	1.5T GE Signa TwinSpeed Excite HD
11	Appetitive Processes	Food	Koban et al. (2023)[19]	15	Food cue vs. baseline (HC*)	Craving regulation with food cues	Event-related	6s image presentation	18 (6)	42.1	Yale University	3T Siemens Magnetom Trio
12	Appetitive Processes	Food	Koban et al. (2023)[19]	15	Food cue vs. baseline (Smoker)	Craving regulation with food cues	Event-related	6s image presentation	21 (8)	26.8	Columbia University	1.5T GE Signa TwinSpeed Excite HD
13	Appetitive Processes	Drug	Koban et al. (2023)[19]	15	Drug cue vs. baseline (Drinker)	Craving regulation with drug cues	Event-related	6s image presentation	17 (7)	33.4	Yale University	3T Siemens Tim Trio
14	Appetitive Processes	Drug	Koban et al. (2023)[19]	15	Drug cue vs. baseline (Cocaine user)	Craving regulation with drug cues (cocaine)	Event-related	6s image presentation	21 (3)	43.5	Yale University	3T Siemens Magnetom Trio

15	Appetitive Processes	Drug	Koban et al. (2023)[19]	15	Drug cue vs. baseline (Smoker)	Craving regulation with drug cues (cigarette)	Event-related	6s image presentation	21 (8)	26.8	Columbia University	1.5T GE Signa TwinSpeed Excite HD
16	Appetitive Processes	Sexual	Wehrum et al. (2013)[20]	15	Sexual vs. neutral pictures	Sexually arousing images	Block design	3s per picture; 5 pictures per block	100 (50)	25.4	German Psychological Society	1.5T Siemens Symphony with quantum gradient system
17	Appetitive Processes	Sexual	Stark et al. (2019)[21]	15	Sexual video vs. baseline	Sexually arousing videos	Event-related	8s video presentation	70 (33)	25.7	German Psychological Society	3T Siemens Prisma
18	Appetitive Processes	Sexual	Kragel et al. (2019)[22]	15	Sexual images vs. baseline	Sexually arousing images from IAPS and GAPED	Event-related	4s image presentation	18 (10)	25	University of Colorado Boulder	3T Siemens Healthcare
19	Aversive Processes	Visual	Gianaros et al. (2014)[23]	15	Negative pictures vs baseline	Images from IAPS	Event-related	7s image presentation	183 (88)	42.7	University of Pittsburgh	1.5 and 3T GE Signa LX Horizon Echospeed ,
20	Aversive Processes	Visual	Yarkoni et al. (2011)[24]	15	Negative vs neutral pictures	Images from IAPS	Event-related	~10s image presentation (pooled from 5 studies)	108 (NR)	NR	Stanford University, Columbia University	1.5T GE Signa Twin Speed Excite HD scanner
21	Aversive Processes	Visual	Kober et al. (2019)[25]	15	Negative pictures vs baseline	Images from IAPS	Event-related	8s stimulus presentation	16 (5)	31.75	Columbia University	1.5T GE Signa Twin Speed Excite HD scanner
22	Aversive Processes	Auditory	Kragel et al. (2018)[17]	15	Unpleasant Sounds vs baseline	Sounds from IADS	Event-related	8s duration; sounds from IADS database	15 (7)	31.1	University of Colorado Boulder	3T Siemens Tim Trio

23	Aversive Processes	Auditory	Geuter et al. (2020)[26]; Kragel et al. (2018)[17]	15	Unpleasant Sounds vs baseline	Sounds from IADS	Event-related	8s duration; sounds from IADS database	15 (9)	24.4	University of Colorado Boulder	3T Siemens Tim Trio
24	Aversive Processes	Auditory	Ashar et al. (Unpublished)	15	Sound high vs. low in unpleasantness	Aversive sound (knife scraping on glass)	Event-related	6s duration; knife scraping sound at 2 intensity levels	141 (75)	41.7	University of Colorado Boulder	3T Siemens Prisma
25	Aversive Processes	Social	Kross et al. (2011)[27]	15	Images of ex-partner vs friend	Images of ex-partners	Event-related	15s image presentation	40 (21)	20.8	Columbia University	1.5T GE Signa TwinSpeed
26	Aversive Processes	Social	Krishnan et al. (2016)[13]	15	High pain images vs baseline	Images of others in pain	Event-related	11s image presentation	30 (12)	25.2	University of Colorado Boulder	3T Siemens Tim Trio
27	Aversive Processes	Social	Yu et al. (2020)[28]	15	Self-incorrect vs. baseline	Guilt from causing pain due to one's error	Event-related	3s feedback of performance	24 (11)	22	Peking University	3T Siemens Tesla Trio
28	Cognitive Control	WM	DeYoung et al. (2009)[29]	15	3-back blocks vs baseline	N-back (faces and words) task	Block	2s per stimulus	104 (59)	22.7	Washington University Medical Center	3T Siemens Allegra
29	Cognitive Control	WM	van Ast et al. (2016)[30]	15	N-back blocks vs baseline	N-back (words) task	Event-related	2s per stimulus	21 (10)	22.2	Columbia University	3T Philips Achieva
30	Cognitive Control	WM	Unpublished	15	Word event vs. fixation	Updating working memory task	Event-related	2s per stimulus	30 (16)	28.1	University of Colorado Boulder	3T Magnetom Trio
31	Cognitive Control	Inhibition	Aron et al. (2007)[31]	15	All trials vs baseline	Stop signal task	Event-related	~1s per stimulus	15 (5)	28.1	UCLA	3T Siemens Allegra
32	Cognitive Control	Inhibition	Xue et al. (2008)[32]	15	All trials vs baseline	Stop signal task	Event-related	~1s per stimulus	15 (9)	23.6	UCLA	3T Siemens Allegra
33	Cognitive Control	Inhibition	Unpublished	15	Antisaccade vs. fixation	Response inhibition task	Event-related	3.82s per stimulus (cue 2.32s, target 1.5s)	30 (16)	28.1	University of Colorado Boulder	3T MAGNETOM Trio

34	Cognitive Control	Switching	Unpublished	15	Switching vs. fixation	Set shifting task	Event-related	~3s	30 (16)	28.1	University of Colorado Boulder	3T MAGNETOM Trio
35	Cognitive Control	Switching	Wager et al. (2005)[33]	15	Switch vs. non-switch	Attention switching task (external)	Event-related	self-paced	39 (NR)	NR	University of Michigan	3T GE Signa
36	Cognitive Control	Switching	Wager et al. (2005)[33]	15	Switch vs. non-switch	Attention switching task (internal)	Event-related	self-paced	39 (NR)	NR	University of Michigan	3T GE Signa

** HC: healthy controls*

Supplementary Table 5

Study info for validation datasets

Domain	Publication	N*	Contrasts	Stimulus/ Paradigm	Experimental design	Stimulus dynamics	Mean Age	IRB/Ethics Approval Committee	MRI System
Pain	Woo et al. (2014)[34]	51	Heat pain vs warmth	Thermal stimulation	Event-related	15s duration (1.5s ramp up, 12s plateau, 1.5s ramp down); individually calibrated	20.8	Columbia University	1.5T GE Signa TwinSpeed Excite HD
Appetitive Process	MacNiven et al. (2018)[35]	32	Gain vs. no-gain anticipation	Monetary Incentive Delay (MID) task[36]	Event-related	cue, anticipation, target response, and outcome	32	Stanford University	3 Tesla GE Discover MR750
Aversive Process	Gianaros et al. (2020)[37]	160	Negative vs neutral images	Images from IAPS	Event-related	7s image presentation	39.7	University of Pittsburgh	3T Siemens Tim Trio
Cognitive control	Barch et al. (2013)[38]	365	2-back vs 0-back (place)	N-back (place) task	Block	2s per stimulus	28.7	N/A	Siemens 3T Connectome Skyra

** Represents the final number of participants included after preprocessing and quality control procedures.*

Supplementary References

1. Johnson, W. E., Li, C. & Rabinovic, A. Adjusting batch effects in microarray expression data using empirical Bayes methods. Biostatistics 8, 118–127 (2007).
2. Fortin, J.-P. et al. Harmonization of multi-site diffusion tensor imaging data. NeuroImage 161, 149–170 (2017).
3. Fortin, J.-P. et al. Harmonization of cortical thickness measurements across scanners and sites. NeuroImage 167, 104–120 (2018).
4. Pomponio, R. et al. Harmonization of large MRI datasets for the analysis of brain imaging patterns throughout the lifespan. NeuroImage 208, 116450 (2020).
5. Yu, M. et al. Statistical harmonization corrects site effects in functional connectivity measurements from multi-site fMRI data. Hum. Brain Mapp. 39, 4213–4227 (2018).
6. Nielson, D. M. et al. Detecting and harmonizing scanner differences in the ABCD study - annual release 1.0. 309260 Preprint at https://doi.org/10.1101/309260 (2018).
7. Glasser, M. F. et al. A multi-modal parcellation of human cerebral cortex. Nature 536, 171–178 (2016).
8. Quabs, J. et al. Cytoarchitecture, probability maps and segregation of the human insula. NeuroImage 260, 119453 (2022).
9. Quabs, J., Bittner, N. & Caspers, S. Structural Connectivity Differences Reflect Microstructural Heterogeneity of the Human Insular Cortex. Hum. Brain Mapp. 46, e70231 (2025).
10. Faillenot, I., Heckemann, R. A., Frot, M. & Hammers, A. Macroanatomy and 3D probabilistic atlas of the human insula. NeuroImage 150, 88–98 (2017).
11. Atlas, L. Y., Bolger, N., Lindquist, M. A. & Wager, T. D. Brain Mediators of Predictive Cue Effects on Perceived Pain. J. Neurosci. 30, 12964–12977 (2010).

12. Wager, T. D. et al. An fMRI-Based Neurologic Signature of Physical Pain. N. Engl. J. Med. 368, 1388–1397 (2013).
13. Krishnan, A. et al. Somatic and vicarious pain are represented by dissociable multivariate brain patterns. eLife 5, e15166 (2016).
14. Kano, M. et al. Influence of Uncertain Anticipation on Brain Responses to Aversive Rectal Distension in Patients With Irritable Bowel Syndrome. Psychosom. Med. 79, 988 (2017).
15. Rubio, A. et al. Uncertainty in anticipation of uncomfortable rectal distension is modulated by the autonomic nervous system — A fMRI study in healthy volunteers. NeuroImage 107, 10–22 (2015).
16. Coen, S. J. et al. Neuroticism Influences Brain Activity During the Experience of Visceral Pain. Gastroenterology 141, 909-917.e1 (2011).
17. Kragel, P. A. et al. Generalizable representations of pain, cognitive control, and negative emotion in medial frontal cortex. Nat. Neurosci. 21, 283–289 (2018).
18. Čeko, M., Kragel, P. A., Woo, C.-W., López-Solà, M. & Wager, T. D. Common and stimulus-type-specific brain representations of negative affect. Nat. Neurosci. 25, 760–770 (2022).
19. Koban, L., Wager, T. D. & Kober, H. A neuromarker for drug and food craving distinguishes drug users from non-users. Nat. Neurosci. 26, 316–325 (2023).
20. Wehrum, S. et al. Gender Commonalities and Differences in the Neural Processing of Visual Sexual Stimuli. J. Sex. Med. 10, 1328–1342 (2013).
21. Stark, R. et al. No Sex Difference Found: Cues of Sexual Stimuli Activate the Reward System in both Sexes. Neuroscience 416, 63–73 (2019).
22. Kragel, P. A., Reddan, M. C., LaBar, K. S. & Wager, T. D. Emotion schemas are embedded in the human visual system. Sci. Adv. 16 (2019).
23. Gianaros, P. J. et al. An Inflammatory Pathway Links Atherosclerotic Cardiovascular Disease Risk to Neural Activity Evoked by the Cognitive Regulation of Emotion. Biol. Psychiatry 75, 738–745 (2014).

24. Yarkoni, T., Poldrack, R. A., Nichols, T. E., Van Essen, D. C. & Wager, T. D. Large-scale automated synthesis of human functional neuroimaging data. Nat. Methods 8, 665–670 (2011).
25. Kober, H., Buhle, J., Weber, J., Ochsner, K. N. & Wager, T. D. Let it be: mindful acceptance down-regulates pain and negative emotion. Soc. Cogn. Affect. Neurosci. 14, 1147–1158 (2019).
26. Geuter, S. et al. Multiple Brain Networks Mediating Stimulus–Pain Relationships in Humans. Cereb. Cortex 30, 4204–4219 (2020).
27. Kross, E., Berman, M. G., Mischel, W., Smith, E. E. & Wager, T. D. Social rejection shares somatosensory representations with physical pain. Proc. Natl. Acad. Sci. 108, 6270–6275 (2011).
28. Yu, H. et al. A Generalizable Multivariate Brain Pattern for Interpersonal Guilt. Cereb. Cortex 30, 3558–3572 (2020).
29. DeYoung, C. G., Shamosh, N. A., Green, A. E., Braver, T. S. & Gray, J. R. Intellect as distinct from Openness: Differences revealed by fMRI of working memory. J. Pers. Soc. Psychol. 97, 883–892 (2009).
30. van Ast, V. A. et al. Brain Mechanisms of Social Threat Effects on Working Memory. Cereb. Cortex 26, 544–556 (2016).
31. Aron, A. R., Behrens, T. E., Smith, S., Frank, M. J. & Poldrack, R. A. Triangulating a Cognitive Control Network Using Diffusion-Weighted Magnetic Resonance Imaging (MRI) and Functional MRI. J. Neurosci. 27, 3743–3752 (2007).
32. Xue, G., Aron, A. R. & Poldrack, R. A. Common Neural Substrates for Inhibition of Spoken and Manual Responses. Cereb. Cortex 18, 1923–1932 (2008).
33. Wager, T. D., Jonides, J., Smith, E. E. & Nichols, T. E. Toward a taxonomy of attention shifting: individual differences in fMRI during multiple shift types. Cogn. Affect. Behav. Neurosci. https://doi.org/10.3758/CABN.5.2.127 (2005) doi:10.3758/CABN.5.2.127.

34. Woo, C.-W. et al. Separate neural representations for physical pain and social rejection. Nat. Commun. 5, 5380 (2014).
35. MacNiven, K. H. et al. Association of Neural Responses to Drug Cues With Subsequent Relapse to Stimulant Use. JAMA Netw. Open 1, e186466 (2018).
36. Knutson, B., Adams, C. M., Fong, G. W. & Hommer, D. Anticipation of Increasing Monetary Reward Selectively Recruits Nucleus Accumbens. J. Neurosci. 21, RC159–RC159 (2001).
37. Gianaros, P. J. et al. Affective brain patterns as multivariate neural correlates of cardiovascular disease risk. Soc. Cogn. Affect. Neurosci. 15, 1034–1045 (2020).
38. Barch, D. M. et al. Function in the human connectome: Task-fMRI and individual differences in behavior. NeuroImage 80, 169–189 (2013).

Full List of Members of The Affective Neuroimaging Consortium

Yoni K. Ashar: Division of General Internal Medicine, University of Colorado Anschutz Medical Campus, Aurora, CO, United States

Lauren Atlas: National Center for Complementary and Integrative Health, National Institute of Health, Bethesda, MD, United States; National Institute of Mental Health, National Institute of Health, Bethesda, MD, United States; National Institute on Drug Abuse, National Institute of Health, Baltimore, MD, United States

Lisa Feldman Barrett: Department of Psychology, College of Science, Northeastern University, Boston, MA, United States; Department of Psychiatry and the Athinoula A. Martinos Center for Biomedical Imaging, Massachusetts General Hospital, Boston, MA, United States

Benjamin Becker: Department of Psychology, The University of Hong Kong, Hong Kong, China

Luke Chang: Department of Psychological and Brain Sciences, Dartmouth College, Hanover, NH, United States

Luana Colloca: Department of Pain and Translational Symptom Science, School of Nursing, University of Maryland, Baltimore, MD, United States

Christopher G. Davey: Department of Psychiatry, The University of Melbourne, Melbourne, Australia

Sigrid Elsenbruch: Department of Medical Psychology and Medical Sociology, Center for Medical Psychology and Translational Neurosciences, Ruhr University Bochum, Bochum, Germany; Department of Neurology, Center for Translational and Behavioral Neuroscience (C-TNBS), University Hospital Essen, University of Duisburg-Essen, Essen, Germany

Miquel A. Fullana: Institut d'Investigacions Biomèdiques August Pi i Sunyer (IDIBAPS), Barcelona, Spain; Adult Psychiatry and Psychology Department, Institute of Neurosciences, Hospital Clinic, Barcelona, Spain

Valeria Gazzola: The Netherlands Institute for Neuroscience, KNAW research institute, Amsterdam, The Netherlands; Department of Psychology, University of Amsterdam, Amsterdam, The Netherlands

Ben J. Harrison: Department of Psychiatry, The University of Melbourne, Melbourne, Australia

Olivia K. Harrison: Department of Psychology, University of Otago, Dunedin, New Zealand; Translational Neuromodeling Unit, University of Zurich and ETH Zurich, Zurich, Switzerland

Alec Jamieson: Department of Psychiatry, The University of Melbourne, Melbourne, Australia

Christian Keysers: The Netherlands Institute for Neuroscience, KNAW research institute, Amsterdam, The Netherlands; Department of Psychology, University of Amsterdam, Amsterdam, The Netherlands

Brian Knutson: Department of Psychology, Stanford University, Stanford, CA, United States

Leonie Koban: Lyon Neuroscience Research Center (CRNL), CNRS, INSERM, Université Claude Bernard Lyon 1, Bron, France; Le Vinatier Psychiatrie Universitaire Lyon Métropole, Bron, France

Hedy Kober: Department of Psychology, University of California Berkeley, Berkeley, CA, United States; Department of Psychiatry, Yale University, New Haven, CT, United States

Kevin S. LaBar: Department of Psychology and Neuroscience, Duke University, Durham, NC, United States

Claus Lamm: Department of Cognition, Emotion, and Methods in Psychology, Faculty of Psychology, University of Vienna, Vienna, Austria

Martin Lindquist: Department of Biostatistics, Johns Hopkins Bloomberg School of Public Health, Baltimore, MD, United States

Tina Lonsdorf: Biological Psychology and Cognitive Neuroscience, Bielefeld University, Bielefeld, Germany; Institute for Systems Neuroscience, University Medical Center Hamburg Eppendorf, Hamburg, Germany

Marina Lopez-Sola: Serra Hunter Programme, Department of Medicine, School of Medicine and Health Sciences, University of Barcelona, Barcelona, Spain; Institute of Neuroscience, University of Barcelona, Barcelona, Spain; Institut d'Investigacions Mèdiques August Pi i Sunyer, Barcelona, Spain

Elizabeth Reynolds Losin: Department of Biobehavioral Health, Pennsylvania State University, University Park, PA, United States

Yina Ma: State Key Laboratory of Cognitive Neuroscience and Learning IDG/McGovern Institute for Brain Research, Beijing Normal University, Beijing, China

Christian J. Merz: Department of Cognitive Psychology, Institute of Cognitive Neuroscience, Faculty of Psychology, Ruhr University Bochum, Bochum, Germany

Hideki Mochizuki: Department of Dermatology and Cutaneous Surgery and Miami Itch Center, Miller School of Medicine, University of Miami, Miami, United States

Vitaly Napadow: Department of Physical Medicine and Rehabilitation, Spaulding Rehabilitation Hospital, Harvard Medical School, Charlestown, MA, United States; Athinoula A. Martinos Center for Biomedical Imaging, Massachusetts General Hospital, Harvard Medical School, Charlestown, MA, United States

Lauri Nummenmaa: Turku PET Centre and Turku University Hospital, Turku, Finland; Department of Psychology, University of Turku, Turku, Finland

Kyle Pattinson: Nuffield Department of Clin. Neurosciences, University of Oxford, Oxford, United Kingdom

Luiz Pessoa: Department of Psychology and Maryland Neuroimaging Center, University of Maryland, College Park, Maryland, United States; Department of Electrical and Computer Engineering, University of Maryland, College Park, Maryland, United States

Hilke Plassmann: INSEAD, Fontainebleau, France; Paris Brain Institute (ICM), Sorbonne University, Paris, France

Pierre Rainville: Department of Stomatology, Université de Montréal, Montréal, Canada; Research Center of the Montreal Geriatric University Institute, Montréal, Canada

Marianne Reddan: School of Psychology and Neuroscience, Center for Cognitive Neuroimaging, University of Glasgow, Glasgow, United Kingdom

Rebecca Saxe: Department of Brain and Cognitive Sciences, Massachusetts Institute of Technology, Cambridge, MA, United States; McGovern Institute for Brain Research, Massachusetts Institute of Technology, Cambridge, MA, United States

Daniela Schiller: Department of Psychiatry, Department of Neuroscience, Icahn School of Medicine, Mount Sinai, New York, NY, United States; Friedman Brain Institute, Icahn School of Medicine, Mount Sinai, New York, NY, United States

Alexander J. Shackman: Department of Psychology, University of Maryland, College Park, MD, United States; Neuroscience and Cognitive Science Program, University of Maryland, College Park, MD, United States; Maryland Neuroimaging Center, University of Maryland, College Park, MD, United States

Dana Small: Department of Neurology and Neurosurgery, Department of Medicine, and Department of Psychology, McGill University, Montréal, Canada; Research Institute of the McGill University Health Centre, Montréal, Canada; Modern Diet and Physiology Research Center (MDPRC), Montréal, Canada

Jason F. Smith: Department of Psychology, University of Maryland, College Park, MD, United States

Carles Soriano-Mas: Department of Psychiatry, Bellvitge University Hosp., Bellvitge Biomed. Institute-IDIBELL, Barcelona, Spain; CIBERSAM, Madrid, Spain; Department of Social Psychology and Quantitative Psychology, Institute of Neurosciences, University of Barcelona, Spain

Rudolf Stark: Department of Psychotherapy and Systems Neuroscience, Justus-Liebig-University Giessen, Giessen, Germany; Bender Institute of Neuroimaging, Justus-Liebig-University Giessen, Giessen, Germany; Center of Mind, Brain, and Behavior, Universities of Marburg and Giessen, Giessen, Germany

Bram Vervliet: Department of Brain and Cognition, KU Leuven, Leuven, Belgium; Leuven Brain Institute, KU Leuven, Leuven, Belgium

Choong-Wan Woo: Center for Neuroscience Imaging Research, Institute for Basic Science, Suwon, Republic of Korea; Department of Biomedical Engineering, Sungkyunkwan University, Suwon, Republic of Korea; Department of Intelligent Precision Healthcare Convergence, Sungkyunkwan University, Suwon, Republic of Korea; Department of Brain Science and Engineering, Sungkyunkwan University, Suwon, Republic of Korea

Fadel Zeidan: Department of Anesthesiology, University of California San Diego, La Jolla, CA, United States

Feng Zhou: Faculty of Psychology, Southwest University, Chongqing, China

nature portfolio

Corresponding author(s): Tor D. Wager & Mijin Kwon

Last updated by author(s): Mar 17, 2026

Reporting Summary

Nature Portfolio wishes to improve the reproducibility of the work that we publish. This form provides structure for consistency and transparency in reporting. For further information on Nature Portfolio policies, see our Editorial Policies and the Editorial Policy Checklist.

Statistics

For all statistical analyses, confirm that the following items are present in the figure legend, table legend, main text, or Methods section.

n/a	Confirmed	
☐	☒	The exact sample size (*n*) for each experimental group/condition, given as a discrete number and unit of measurement
☐	☒	A statement on whether measurements were taken from distinct samples or whether the same sample was measured repeatedly
☐	☒	The statistical test(s) used AND whether they are one- or two-sided *Only common tests should be described solely by name; describe more complex techniques in the Methods section.*
☒	☐	A description of all covariates tested
☐	☒	A description of any assumptions or corrections, such as tests of normality and adjustment for multiple comparisons
☐	☒	A full description of the statistical parameters including central tendency (e.g. means) or other basic estimates (e.g. regression coefficient) AND variation (e.g. standard deviation) or associated estimates of uncertainty (e.g. confidence intervals)
☐	☒	For null hypothesis testing, the test statistic (e.g. *F*, *t*, *r*) with confidence intervals, effect sizes, degrees of freedom and *P* value noted *Give P values as exact values whenever suitable.*
☐	☒	For Bayesian analysis, information on the choice of priors and Markov chain Monte Carlo settings
☒	☐	For hierarchical and complex designs, identification of the appropriate level for tests and full reporting of outcomes
☐	☒	Estimates of effect sizes (e.g. Cohen's *d*, Pearson's *r*), indicating how they were calculated

Our web collection on statistics for biologists contains articles on many of the points above.

Software and code

Policy information about availability of computer code

Data collection	Data collection methods varied across studies. Details are provided in the original publications listed in Supplementary Table 4 (main analysis) and Supplementary Table 5 (validation analysis).
Data analysis	Analysis was conducted using CANLab and SPM software implemented in MATLAB. Code for implementing all analyses is available at https://github.com/canlab/, https://github.com/mijinjkwon/proj_insula_anic, and www.fil.ion.ucl.ac.uk/spm/software/.

For manuscripts utilizing custom algorithms or software that are central to the research but not yet described in published literature, software must be made available to editors and reviewers. We strongly encourage code deposition in a community repository (e.g. GitHub). See the Nature Portfolio guidelines for submitting code & software for further information.

Data

Policy information about availability of data

All manuscripts must include a data availability statement. This statement should provide the following information, where applicable:

- Accession codes, unique identifiers, or web links for publicly available datasets
- A description of any restrictions on data availability
- For clinical datasets or third party data, please ensure that the statement adheres to our policy

The fMRI data from main-analysis studies 1, 2, 4, 5, 7, 8, 19, 20, 22, 23, 25, 26, 28, 29, 31, and 32 are available at https://doi.org/10.6084/m9.figshare.24033402.v2. Data from studies 3 and 6 are available at https://neurovault.org/collections/8707/. Data from the validation dataset for cognitive control (n-back working memory task) are available from the Human Connectome Project database (https://www.humanconnectome.org). The remaining main-analysis and validation datasets are

available upon request from the corresponding authors of the individual studies. The Neurosynth dataset used in the analyses is available at https://github.com/canlab/Neuroimaging_Pattern_Masks/tree/master/neurosynth, the cytoarchitecture maps at https://github.com/canlab/Neuroimaging_Pattern_Masks/tree/master/Atlases_and_parcellations/2020_JulichBrain_v3.0.3, and the neurotransmitter receptor/transporter maps at https://github.com/canlab/Neuroimaging_Pattern_Masks/tree/master/Atlases_and_parcellations/2022_Hansen_PET_tracer_maps.

Research involving human participants, their data, or biological material

Policy information about studies with human participants or human data. See also policy information about sex, gender (identity/presentation), and sexual orientation and race, ethnicity and racism.

Reporting on sex and gender	Sex, determined by self-report across all studies for 36 study contrasts in the main analysis and 4 in the validation analysis, is documented in Supplementary Table 4 and Supplementary Table 5, respectively. While the study included both male and female participants, it was not designed or powered to systematically examine sex differences in insular function, and therefore no sex-based analyses were performed. Gender information beyond binary sex was not uniformly collected across individual studies, precluding gender-based analyses.
Reporting on race, ethnicity, or other socially relevant groupings	Race, ethnicity, and other socially relevant grouping information was collected differently across the studies included in the main and validation analyses. The current study was not designed or powered to investigate differences among racial, ethnic, or other social groups in insular function, and therefore no analyses were performed examining these factors.
Population characteristics	Population characteristics are summarized in Supplementary Table 4 (main analysis) and Supplementary Table 5 (validation). Specific inclusion/exclusion criteria are detailed in the original publications.
Recruitment	Recruitment methods varied across studies and are detailed in the original publications. Our systematic sampling across multiple studies and sites helps mitigate potential study-specific recruitment biases.
Ethics oversight	Each study in the main analysis and validation analysis was approved by its respective institutional review board, as listed in Supplementary Table 4 and Supplementary Table 5, respectively.

Note that full information on the approval of the study protocol must also be provided in the manuscript.

Field-specific reporting

Please select the one below that is the best fit for your research. If you are not sure, read the appropriate sections before making your selection.

☒ Life sciences ☐ Behavioural & social sciences ☐ Ecological, evolutionary & environmental sciences

For a reference copy of the document with all sections, see nature.com/documents/nr-reporting-summary-flat.pdf

Life sciences study design

All studies must disclose on these points even when the disclosure is negative.

Sample size	The current analysis included 540 participants (15 participants sampled from 36 studies). Sample size determinations for individual studies are detailed in their original publications.
Data exclusions	No data were excluded from the analysis.
Replication	Direct replication was attempted by validating primary findings against independent datasets for each domain.
Randomization	As a mega-analysis of existing studies, this was not a randomized study. Contrasts were constructed within subjects to compare effects across studies. Participants were recruited independently for each study. Domain assignment was determined by the experimental manipulation used in each study (e.g., studies using thermal stimulation were assigned to the pain domain).
Blinding	Investigators were not blinded during data analysis but were unaware of group comparisons during original data collection.

Reporting for specific materials, systems and methods

We require information from authors about some types of materials, experimental systems and methods used in many studies. Here, indicate whether each material, system or method listed is relevant to your study. If you are not sure if a list item applies to your research, read the appropriate section before selecting a response.

Materials & experimental systems

n/a	Involved in the study
☒	☐ Antibodies
☒	☐ Eukaryotic cell lines
☒	☐ Palaeontology and archaeology
☒	☐ Animals and other organisms
☒	☐ Clinical data
☒	☐ Dual use research of concern
☒	☐ Plants

Methods

n/a	Involved in the study
☒	☐ ChIP-seq
☒	☐ Flow cytometry
☐	☒ MRI-based neuroimaging

Plants

Seed stocks	Not applicable to the current study
Novel plant genotypes	Not applicable to the current study
Authentication	Not applicable to the current study

Magnetic resonance imaging

Experimental design

Design type	Multiple experimental designs were used across 36 studies. Our approach aims to generalize across these methodological factors.
Design specifications	Trial number, stimulus duration, and scan length varied across studies. Details are provided in the original publications referenced in Supplementary Table 4.
Behavioral performance measures	Behavioral data were not included.

Acquisition

Imaging type(s)	BOLD fMRI
Field strength	1.5 and 3 Tesla
Sequence & imaging parameters	EPI (standard and multi-band) and spiral in-out sequences were used for data acquisition. Details are provided in the original publications listed in Supplementary Table 4.
Area of acquisition	Whole brain scans were used.

Diffusion MRI ☐ Used ☒ Not used

Preprocessing

Preprocessing software	Each study used different preprocessing pipeline and software. Details are provided in the original publications listed in Supplementary Table 4.
Normalization	Images were normalized to Montreal Neurological Institute (MNI) space using study-specific MNI templates.
Normalization template	The templates used depend on the study but all studies used MNI templates
Noise and artifact removal	Regression of motion parameters was performed in all studies.
Volume censoring	Outlier timepoints identified via Mahalanobis distance using a chi-square test were excluded in some studies.

Statistical modeling & inference

Model type and settings	Data used were all 2nd level contrast maps sampled from 36 studies and they were then evaluated by Bayes factor for the purpose of conjunction analysis to identify domain-general and domain-selective voxels.

Effect(s) tested

Bayes Factors were calculated for each functional domain to compare evidence for alternative and null hypotheses using JZS prior (Rouder et al., 2009). Thresholds were set at 4.32 for alternative and 0.23 (1/4.32) for null hypothesis, corresponding to FDR-corrected q < 0.01. Voxels were classified as activated when showing both BF > 4.32 and positive t-statistics. Evidence for no activation included cases of either BF < 0.23 or BF > 4.32 with negative t-statistics. With conjucntion analysis, voxels activated in all four domains were classified as domain-general, while voxels activated in one domain with evidence for no activation in other domains were classified as domain-selective.

Specify type of analysis: ☐ Whole brain ☐ ROI-based ☒ Both

Anatomical location(s) Insula

Statistic type for inference

Voxel-wise statics were used.

(See Eklund et al. 2016)

Correction

FDR correction

Models & analysis

n/a	Involved in the study
☒	☐ Functional and/or effective connectivity
☒	☐ Graph analysis
☒	☐ Multivariate modeling or predictive analysis